UNIVERSITA' DEGLI STUDI DI PISA

FACOLTA' DI INGEGNERIA

Corso di Laurea Specialistica in Ingegneria Aerospaziale

EcosimPro simulation of transient flow for rocket engine and test bench applications

RELATORI

Prof. Luca d'Agostino

TUTOR AZIENDALE

Dr. Richard Arnold

CANDIDATA

Maria Palma Celano

ANNO ACCADEMICO

2011-2012

TABLE OF CONTENTS

ABSTRACT

Storable propellant engine start-up is a complex phase which involves non-stationary hydraulic effects, two-phase flow. Each element of the engine, oxidizer and fuel lines, combustion chamber, has to be verified and qualified. For this purpose test facilities are an indispensable element for development and acceptance for space system, subsystem and components.

The partial failure of Ariane 5 flight No 510 on December 7 2001 called for the attention of liquid rocket propulsion engineers on the importance of the simulation of high frequency (HF) instabilities in propellant feed lines. The disturbances observed during the start-up of the flying engine were not triggered in any of the tests performed. As a consequence of the difference in the engine and test bench lines, transient phenomena result not predicable from a test campaign and so highly dangerous for engines performances and operation.

The knowledge of the flow characteristics in both the test benches and flying rocket stages is essential for future hardware design. Efforts have to be made for advancing the understanding of the transient flow behaviour in pipes for safe operation of the engine and for reducing the high costs and risks associated with tests. In this context, the development of tools for simulating the behaviour of flight-like feed systems by using non-flight-like test bench equipment are widespread.

In the present work a numerical investigation and evaluation of the critical fluid-system parameters is performed by means of the simulation and modeling software EcosimPro 4.4, based on C++ programming language. A hydraulic model of the test bench P2 in Lampoldhausen up to the test facility main valve is built up, as well as a simplified model of the Aestus engine. To validate and qualify the combined test bench-engine model, real on-ground test transients and steady-state results are compared with numerical results.

The numerical model has been successfully modified and adjusted and simulation results matched the measured values within acceptable ranges. Good agreement with steady-state-pressure, propellant mass flow rates behaviour and transient start-up in terms of water hammer peaks have been obtained. However, the water hammer frequencies have been not matched

accurately due to 1D-restrictions of the code and mainly to different characteristics of the simulated fluids.

Future efforts have to be done to improve the implementation of fluid property data bases implementation, especially for NTO (equilibrium condition between NO_2 and N_2O_4 depending on pressure and temperature) and for deeper understanding and investigation of possible influences of the content of pressurization gas content in the liquid fluid on the transient behaviour of the propellant feed system.

1. INTRODUCTION

Numerical investigation and evaluation of steady-state and transient fluid system parameters is a key problem for the verification and qualification of stage element of the engine. Flow characteristics of both test benches and applied rocket stages is essential for future hardware design. Efforts have to be done for advancing the understanding of flow behaviour in pipe transient for the safe operation of the engine and to reduce the high costs and risks linked to a pure testing. Following this trend, propulsion system modelling and use of test data from computer simulation as calibration data are widespread.

In particular the partial failure of Ariane 5 flight 510 in 07 December 2001 has drawn attention to the importance of the real feed lines simulation in high frequency (HF) instabilities, phenomena not observed in any of the tests performed, as a consequence of the difference in the engine and test bench lines. Attention has to be turn in the case of flow transient studies to the coupling of these two elements and to the evaluation of any difference in hydraulic lines configuration of test bench and feed line systems of the real thruster, due to the strong dependence of these phenomena on systems geometry.

The purpose of the present work is then the development of a numerical tool to simulate flight-like feed system behaviour by using non-flight-like test bench equipment. The numerical investigation would be used for the evaluation of critical fluid-system parameters. The physical modelling and simulation software chosen is EcosimPro 4.4.

The main steps followed in the present work are:

- The build-up of a hydraulic transient EcosimPro model of the P2 up to the test facility main valve
- The creation of a hydraulic transient EcosimPro simplified model of the Aestus engine for validation purposes
- The validation and qualification of the combined test bench-engine model by means of real on ground test results comparison
- The outcome of a preliminary sensitivity study of transient behaviour of the system.

2. ECOSIMPRO

2.1. Introduction

EcosimPro is a physical simulation modelling tool with an integrated visual environment that provides intuitive tools for simulating different kind of system.

The project developed by Empresarios Agrupados A.I.E initiated in the early ‘90s with funds from the European Space Agency (ESA) with the aim of creating simulation software to model Environmental Control and Life support System (ECLSS) for the European modulus (COLUMBUS) of the International Space Station (ISS) and for Hermes. The original objective was not to construct a generic tool but specific software for the ECLSS.

By now EcosimPro can be used to model a larger number of simple and complex physical systems. The software provides an object-oriented non casual approach towards creating reusable components libraries and powerful symbolic and numerical methods capable of processing complex systems represented by differential-algebraic equations (DAE) or ordinary-differential equations(ODE) and discrete events.

The multidisciplinary nature of this modelling tool led to its use in many other disciplines, including fluid mechanics, chemical processing, control, energy, propulsion and flight dynamics.

The EcosimPro general math capabilities are:

- Symbolic handling of equations (eg: derivation, etc.)
- Robust solvers for non-linear and DAE systems
- Math wizards for: defining boundary conditions, solving algebraic loops, reducing high-index DAE problems
- Mathematical algorithms based on graph theory to minimize the number of unknown variables and equations
- Discrete events handler to stop simulation when an event occurs.

2.2. EPSS, European Space Propulsion System Simulation

2.2.1. General overview and key concept

The EPSS software provides a collection of standard databases for the propellant, pressuring gases and other fluid simulation as a collection of components and functions for the spacecraft and launch vehicle propulsion system simulation to be used for analysis of concept definition, mission analysis, impact studies, investigation of anomalies and optimization, testing and pressuring gas/propellant loading.

The object oriented tool, with the propulsion library for example, allows the user to draw, and design at the same time, the propulsion system with components of that specific library with tanks, lines, orifices, thrusters and tees and enables both steady state and transient study. The user enhances the design with components from the thermal library (heaters, thermal conductance, radiators), control library (analogue/digital devices), electrical library, etc, to represent a functional propulsion system, e.g. fluid properties, pipe networking, including multi-phase fluid flow, two-phase two fluids tanks, non-adiabatic combustion chambers, chemistry, turbomachinery, etc.

The main features of this software are:

- Conservation equations for liquid, gas and two-phase flow regimes implemented,
- Fluid phase automatically calculated and a homogenous equilibrium model for a real fluid under two phase conditions with or without a non condensable gas (so that absorption/desorption is not considered),
- Flow inertia, inversion and gravity forces and high speed phenomena present,
- Concentrated and distributes load losses calculated,
- Heat transfer between fluid and the wall is modelled,
- Special components as check valve and pressure regulators available.

The EPSS software is structured in different areas summarized as followed.

A set of fluid property functions for the propellants, pressuring gases and ground fluids allowing for the calculation of real properties of the typical working fluids in propulsion systems.

A set EcosimPro libraries including: 1D Fluid Flow Library (to simulate cold gas flow, liquid flow and homogeneous equilibrium tow-phase flow, two fluid flow), Combustion Library (for chemical equilibrium of an arbitrary mixture of chemicals in transient and non-adiabatic conditions so that vaporization and global reaction times can be considered), Chemical Library, Tank Library, Turbo-machinery Library.

Every physical system can be described by means of the fundamental concepts presented in the following lines.

Component: basic simulation unit generated by EcosimPro Language (EL) represented by means of variables, differential-equations, topology and event- based behaviour, defined from a system library or by the user, containing a mathematical description of the real-world component. Two kinds of components are programmed: *abstract* and *operational components*. *Abstract component* describe some physical behaviour that does not represent a complete component, but that can be used as a base for others. These components contain the main formulation later used in the *operational components*. Within the component optional blocks can be included:

- PORTS interface with the environment outside the component and must be a type already declared
- DATA known data items of the component
- DECLS declaration of the local variables to the experiment
- OBJECTS the instances of classes used in this component
- TOPOLOGY aggregation of other components and their connections
- INIT initialization of the component
- DISCRETE discrete behaviour of the component
- CONTINUOUS continuous behaviour of the component
- OBJECTS declaration of the external objects defined with classes
- INIT initial value (i.e. starting value) assigned to the boundary variables
- BODY this block contains the sequential instruction which defines the experiment

Port connection type: set of variables to be interchanged in connections in order to join together more components to interface one or to shape a new one. The program in this sense is hierarchical: it allows creation of more complex components from other equipped with ports and to inherit behaviour from other components (tried and tested code from parent components can be reused).

Partition: associated mathematical model for the component defining the causality of the final model. It is the intermediate step between the component and the experiment.

*Experimen*t: representation of different simulation cases. It enables the definition of the initial conditions and the boundary conditions of the mathematical model and the desired solution (transient or steady state). Within the experiment four optional blocks can be included:

- DECLS declaration of the local variables to the experiment.
- OBJECTS declaration of the external objects defined with classes.
- INIT initial value (i.e. starting value) assigned to the boundary variables.
- BODY block that contains the sequential instruction which defines the experiment.

Libraries: general classification by disciplines of all components.

The EL is the basic language used in EcosimPro. This language has been developed to be used in modelling combined continuous-discrete physical systems. It is based on continuous modelling concepts, developed in the 1970's, and modern object-oriented techniques so that components can be inherited from one another and can be aggregated to create other more complex and modular components. EL allows mathematical modelling of complex structures by automatically solving systems of differential-algebraic equations, it can also generate reports, plots and other hard copies from within a classical sequential language and it has the ability to reuse C, FORTRAN and C++ classes.

Three different types of statements can be used in EL, depending on the context: sequential, continuous (the only one allowed in classical languages such as FORTRAN and C++) or discrete (only statements are allowed in event-oriented modelling).

- Sequential statements are used for initializations, functions and discrete event bodies which require a strict execution order. They are executed progressively and allow for the user to

control the flow of the program. They can be used in all sequential parts (BODY INIT). An example of these statements are WHILE, IF and FOR cycles.

- Continuous statements are used to express sets of differential-algebraic equations where the order in which they are written is important. They create the core where the continuous physical models are defined.
- Discrete statements are used to express events controlled by conditional statements which indicate when an event occurs. The basic statement is WHEN which declares an event by waiting for a condition to become true, at which point the associated code is executed.

The EL language creates the basic component and the Libraries are the mechanism used to organize design information and to provide other functionalities. A Library in EL is a set of items: components, port types, global variables, classes and functions which are related to the same area. They are the natural way to group components and functions.

After all the preliminary steps, the problem is formulated as a system of differential-algebraic equations (DAEs) written as follows:

$$F[t, y(t), y'(t)] = 0 \qquad (2.1)$$
$$y(t) = y_0$$

EcosimPro has a robust DAE solver called DASSL. It is useful to solve two general classes of problems: the ones for which $y'(t)$ is impossible to solve explicitly and the ones for which is possible to solve $y'(t)$ but it is impractical to do so. The underlying idea is to replace the derivative in (1) by a difference approximation and then to solve the resulting equation for the solution at the current time t_N using Newton's method. DASSL is not limited to approximate $y'(t)$ using the first order approximation, but it can also approximate the derivate using the *kth* order finite difference, where k is between 1 and 5. The order k and the time step are automatically chosen by this method at each step on the basis of the behaviour of the solution.

The iteration technique is a Newton-Raphson method, and the iteration matrix required in this case can be given as a Jacobian analytical subroutine or calculated as a Jacobian numerically using finite differences.

2.2.2. Modelling

The first step to create a model in EcosimPro is to create a Library by either using the EcosimPro Language (EL) or by reusing the already existing component and create the schematic that represent the physical system, combining together the different elements. The next step involves the generation of an associated mathematical model or partition, then creating an experiment for this partition. Finally, the simulation can start.

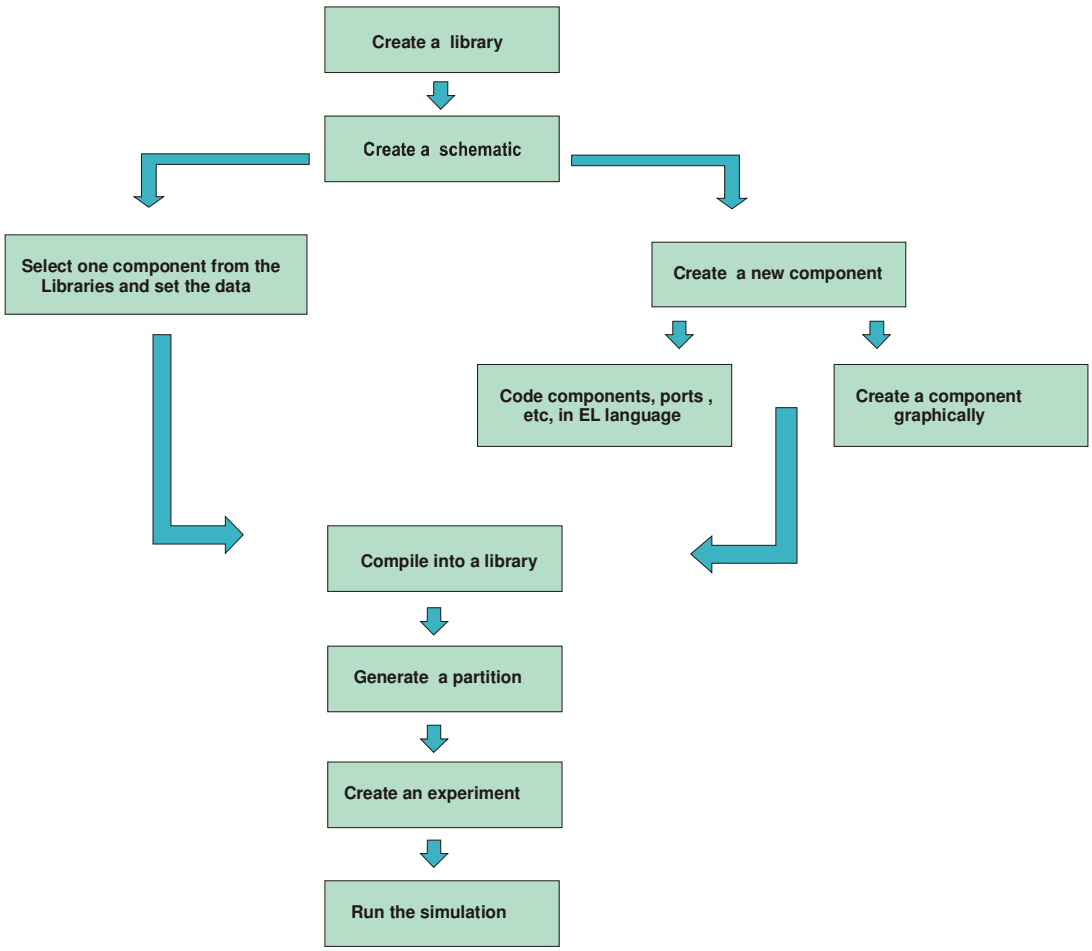

2.2.3. Libraries

FLUID PROPERTIES LIBRARY

Getting appropriate fluid properties is a matter of vital importance and the Fluid Properties Library provides a large collection of functions returning the value of fluid properties (or the complete thermodynamic state) and introducing relevant parameters such as temperature, pressure, internal energy, density, etc. Most of the common fluids used for rockets are available.

Fluids in EcosimPro are supported in different categories:

- *Perfect gas*: temperature dependent only transport and heat capacity properties obtained from CEA coefficients.
- *Simplified liquid*: non pressure dependent properties.
- *Real fluid*: density, sound speed, specific heat interpolated in external tables as function of the temperature and pressure, considering liquid conditions such as superheated, supercritical or two-phase). The mixture of real fluid with non-condensable gas is also allowed and the homogenous equilibrium model is used to calculate the properties (quality, void fraction...) in case of two-phase flow.

For real fluids properties, data tables provided with EPSS have been generated using three different methods:

- Running the NIST program: pressure is used as a parameter and temperature as the first independent variable. The tables cover the liquid, vapour and super-critical zones and can guarantee continuity between two-phase flow, vapour, liquid and super critical state.
- Using an EXCEL tool for some fluids such as MMH, UDMH not available with NIST program.
- The user can finally build his own property files.

The following methods are used for calculating fluid properties in the EXCEL tool. The density is calculated according to Peng-Robinson's state equation of state. The saturation pressure is assumed to be a polynomial or exponential adjustment of the temperature. The enthalpy and entropy properties are

based on the calculation of the non-ideal term $\left[\left(\frac{\partial p}{\partial T}\right)_V T - p\right]$ to be added to the $c_p(T)$ polynomial adjustment coefficient calculated at zero pressure (ideal gases) assuming:

$$C_V = A - R_g + BT + CT^2 + DT^3 \tag{2.2}$$

The Peng-Robinson equation is badly adapted to the NTO properties because of the fluid reactivity and the variable concentration of nitrogen oxides that must be considered in the gas phase. For this fluid, the gas properties are calculated by means of CEA equilibrium properties. Liquid properties are calculated using specific correlation for a semi-perfect liquid. The liquid table will give good results when temperature is below critical, and will have large errors when the critical temperature is approached.

Two main problems are faced. The first one refers to the difficulty to find reliable correlation for all properties of liquid N_2O_4 (NTO), which is directly linked to experimental study. The second one deals with the spontaneous decomposition that takes place as soon as N_2O_4 is in gaseous state (dissociation in NO_2 at ambient pressure and 400 K and a second dissociation at higher temperatures creating NO and O_2). Taking this phenomenon into account implies calculating the chemical equilibrium at every pressure and temperature of interest in the vapour and supercritical phase. This is done using the CEA code where reaction contribution to c_p and thermal conductivity are taken into account.

For perfect gas the thermodynamic state, as a function of ρ-T, is based on the classical perfect gas state equation. The energy calculations are based on the computation of the specific heat at constant pressure for ideal gases, as a function of the temperature only, by means of polynomial expression:

$$\frac{Cp}{R} = a_1 T^{-2} + a_2 T^{-1} + a_3 + a_4 T + a_5 T^2 + a_6 T^3 + a_7 T^4 \tag{2.3}$$

The functions giving the viscosity and the thermal conductivity, when data is available, are also based on polynomial expressions. Otherwise they are estimated with different methods.

For simplified liquid density, speed of sound and specific heat values are based on the tables read from the property file and are interpolated as function of the temperature only. Once the properties have been interpolated, the equation of state can be applied assuming constant compressibility with pressure:

$$\rho(P,T) = \rho(T)\lfloor 1 + \kappa(P - P_{REF})\rfloor \tag{2.4}$$

Viscosity and thermal conductivity are also interpolated from external data as a function of temperature:

$$Viscosity = v\ (T)$$

$$Conductivity = \lambda\ (T)$$

In case of a perfect gas-real liquid mixture, the homogeneous equilibrium model (HEM) of the mixture is calculated. One fluid must be a real fluid or a simplified liquid, the other a perfect non-condensable gas (NCG). The hypotheses done with this model are:

- NCG forms a homogenous mixture at uniform temperature with the real fluid
- NCG occupies the same volume as the Real Fluid according to Gibbs Dalton Law
- If NCG is present the Real Fluid vapour is saturated (relative humidity=1)
- NCG is insoluble in the liquid phase of the Real Fluid.

The heat capacity, viscosity and thermal conductivity are calculated as a mixture of a liquid and composed gas (vapour and NCG) .The mixture properties are a result of the weighing of the pure fluid with the mass fraction:

$$\begin{aligned} c_P &= x_{mix} c_{Pgas} + (1-x) c_{Pliq} \\ \mu_P &= x_{mix} \mu_{Pgas} + (1-x) \mu_{Pliq} \\ \lambda_P &= x_{mix} \lambda_{Pgas} + (1-x) \lambda_{Pliq} \end{aligned} \tag{2.5}$$

where x_{mix} is the mixture quality defined as the mass ratio of gas (vapour+ NCG).

The gas mixture transport properties and speed of sound are calculated. In the same way the speed of sound is specifically approximated as an equivalent two-phase mixture, where the vapour phase is a mixture of NCG with 100% humidity.

FLUID FLOW 1D LIBRARY

This Library is the EcosimPro library for 1D transient simulations of two-fluid, two-phase system. The main features of this library are:

- Conservation equations for liquid, gas and two-phase flow regimes.
- Automatic calculation of fluid phase (homogenous equilibrium model used to calculate a real fluid under two phase conditions with or without NCG)
- Flow inertia, inversion and gravity forces and high speed phenomena.
- Calculation of concentrated (valves) and distributed load (pipes) losses
- Inclusion of heat transfer between fluid and the wall.
- Special components such as check valves and pressure regulators.

In ESPSS fluid networks every component is a resistive or a capacitive component.

The *C* (capacitive) elements integrate the mass and the energy equations: they receive the flow variables (volumetric, mass and entropy flow) and deliver the state variables (pressure, density, velocity, chemical composition and enthalpy). These elements simulate a volume with several fluid ports. Ports that belong to *C* elements have a small dot in the middle of the arrow and need to be initialized in a different way according to the option chosen.

The simplest component belonging to this group is *Volume*. It represents an adiabatic volume with a given number of fluid ports and contains:

Mass conservation equation:

$$\frac{d\rho_{mix}}{dt}V + \rho_{mix}\frac{dV}{dt} = \sum m_j \tag{2.6}$$

Non condensable mass fraction (x_nc) conservation equation:

$$\frac{dx\_nc}{dt}V\rho_{mix} + x\_nc\left(\frac{d\rho_{mix}}{dt}V + \rho_{mix}\frac{dV}{dt}\right) = \sum m_{nc\,j} \tag{2.7}$$

Energy equation:

$$\frac{d\rho_{mix}}{dt}VE_{mix} + \rho_{mix}\frac{dV}{dt}E_{mix} + \frac{dE_{mix}}{dt}V\rho_{mix} = \sum(mH)_j + Q_{in} - P\frac{dV}{dt} \qquad (2.8)$$
$$E_{mix} = e + v^2/2$$

where *j* is the number of ports.

From the thermal point of view, the term Q_{in} permits the heat exchange of heat through a thermal port. The average velocity of the volume is required for the total energy conservation equations and for the evaluation of the friction forces and the wall heat transfer. For this calculation, volumes are considered to be made of two sides (1), (2), each one with a certain number of ports.

The average velocity is computed as follow:

$$v = \frac{m_{j,in} - m_{in,2}}{2\rho A} \qquad (2.9)$$

where the total mass flow rate entering the volume from the side (1) is:

$$m_{in,1} = \sum_{\forall portaiSide1} m_{j,in} \qquad (2.10)$$

from the side (2):

$$m_{in,2} = \sum_{\forall portaiSide2} m_{j,in} \qquad (2.11)$$

This average velocity will be transmitted to the ports and the effective port velocity will be:

$$v(j) = v\cos(\alpha) \qquad (2.12)$$

where α is the port angle.

Instead of simply adiabatic constant volume, it is also possible to have more complicated components like *Chamber* and *Cavity* that are generic variable volumes which also take into account the possibility of sonic limitation. The critical mass flow models phenomena such as compressible and sub-cooled choking and it is calculated at each port as a function of pressure, density and speed of sound of the lumped volume.

Nevertheless the pressure elevation due to the change in height of the fluid is evaluated as follows:

$$\Delta p(j) = \rho g(z_{top} - z_{jun,J}) \tag{2.13}$$

M (momentum) elements explicitly calculate the mass flow between *C* elements and work in the opposite way as a *C* component.

The basic resistive component is the Junction. It represents a concentrated load loss with sonic loss limitation where no mass accumulation and enthalpy flow is assumed.

This element contains the momentum conservation equation that dynamically calculates the mass flow (per unit area):

$$\begin{aligned}&(I_1 + I_2)(A\frac{dG}{dt} + \frac{dA}{dt}G) + Lv\frac{dG}{dt} = \\ &(P + 0.5\rho_{mix}v^2)_1 - (P + 0.5\rho_{mix}v^2)_2 - 0.5(\zeta + \zeta_{crit})\frac{G|G|}{\rho_{up}}\end{aligned} \tag{2.14}$$

where 1,2 indicate the inlet and the outlet port.

The mass flow rate *G* instead of *m* (=*GA*) is used for preventing a singularity in the system at the complete cross section closing (*A*=0).

The linearization of the quadratic term $G|G|$ in the momentum equation, when $G<G_{LAM,}$ takes in account that pressures losses are linear with laminar mass flow regimes.

The pressure drop coefficient will be automatically calculated from the orifice area and the adjacent connected flow areas assuming abrupt area changes as follows:

$$\begin{aligned}\zeta_f &= 0.002 + 0.5(1 - A_{th}/A_1) + (1 - A_{th}/A_2)^2 \\ \zeta_b &= 0.002 + 0.5(1 - A_{th}/A_2) + (1 - A_{th}/A_1)^2\end{aligned} \tag{2.15}$$

or can be an input of the user.

Valve and *Filter* components are built in the same way with a special arrangement of the momentum equation.

For the *Filter,* the mass flow, pressure and temperature at reference conditions are added:

$$(I_1 + I_2)\frac{dm}{dt} = (P)_1 - (P)_2 - \Delta P_{ref}\left(\frac{m}{m_{ref}}\right)^n \left(\frac{\mu}{\mu_{ref}}\right)^{2-n} \frac{\rho_{ref}}{\rho} \tag{2.16}$$

where n is the exponent of the mass flow in the pressure loss equation.

For the *Valve* the derivative of the valve area in the momentum equation will be calculated as follows:

$$\frac{dA}{dt} = \frac{A_{controlled} - A}{tau} \tag{2.17}$$

Where $A_{controlled}$ is the A_0 s_pos.signal and *tau* is the time constant of area change (s).

The signal will be a boundary to be specified in the *Experiment* file or controlled by a component of the Control Library.

Pipe and *Tube* components are built as an alternation of *Junctions* and *Volumes*. They simulate a cylindrical or rectangular area-varying non-uniform mesh 1D pipe or fluid vein.

The number of volumes in which the pipe is split into will be a parameter chosen by the user.

1D mass, energy and momentum equations, in transient regime, are incorporated so that all kind of flows (compressible or nearly incompressible flows, single or two components flow as well single or two-phase flow) can be simulated:

$$\frac{\partial \omega}{\partial t} + \frac{\partial f(\omega)}{\partial x} = \Omega(\omega)$$

$$\omega = A\begin{pmatrix} \rho \\ \rho x\_nc \\ \rho v \\ \rho E \end{pmatrix} \qquad \Omega(\omega) = \begin{pmatrix} -\rho A k_{wall}(\partial P/\partial t) \\ -\rho A k_{wall}(\partial P/\partial t) x\_nc \\ -0.5(\Delta\xi/\Delta x)\rho v|v| + \rho g A + P(dA/dx) \\ \Delta Q/\Delta x + \rho g v A \end{pmatrix} \tag{2.18}$$

$$f(\omega) = \begin{pmatrix} \rho v \\ \rho x\_ncv \\ \rho v^2 + P \\ \rho v(E + P/\rho) \end{pmatrix}$$

In the first equation it must be noted that the source term responsible for the wall compressibility effect of the mixture, fundamental for the simulation of phenomenon like water hammer.

The equivalent distributed friction ($\Delta\xi$) calculates the pressure drop coefficient and the friction factor, including laminar and turbulent regimes.

At each discretized volume, the non-derivate state variables (pressure, qualities and temperature) will be calculated using the state function. If it is present a NCG, the homogenous equilibrium model will also be applied.

The sonic flow per unit area $(\rho u)_{crit}$ is calculated at each pipe port as a function of the corresponding node pressure, density and speed of sound. The last one will be used to take into account the sonic flow limitation

Models of arbitrary piping networks are built by an alternating C-M arrangement of the two types of Fluid Flow 1D component. Then a special component called *Working Fluid* defines the working fluid in a loop so that all interconnected elements will have the same fluids. For the first main fluid every category is possible, for the second fluid only perfect gases are allowed. Simplified liquids are supposed to have a zero constant vapour pressure, then, using this kind of fluid, bubble formation should take place when the pressure reaches a negative value. *Pipe* and *Volume*, so all the capacitive components will in this case calculate the corresponding void fraction and the pressure peaks due to bubble collapse.

It has to be noted that initializing a model and choosing the appropriate boundaries is an important point: boundary components will determine *P, T,* ρ and the mass fraction at the model interfaces. The simplest way to do this is using the component *Vol_TM*. It represents time dependent (*TMD*) boundary conditions and its purpose is to establish the complete thermodynamic state of a fluid port by imposing two variables (*P-T, P-x, T-x..)* and the non-condensable mass fraction(*x_nc*).

TANKS LIBRARY

Tanks play a fundamental role in rocket engine and spacecraft feed and pressurization system, an important role that can be evaluated using the Tank Library. This Library accounts for transient simulation of rocket engine and spacecraft tanks. Every component belonging to this Library can be

connected with the FLUID FLOW 1D component with the aim of simulating a complete rocket engine cycle.

The most important features are the following:

- Gas, liquid and two-phase regimes modelled for ideal and real fluids. Mixtures of real fluid (two phase condition) with or without NCG are included.
- Correlation to calculate the heat transfer between the tank walls and the fluid cavities
- Bladder tank component, including bladder motion calculation is present.
- Single tanks 1D ,working with a pressuring gas and a liquid, are available including liquid level calculation (liquid and gas, heat exchange with the walls, mass and heat exchange at the liquid/gas interface).

This element allows for the calculation of the liquid level evolution assuming that the gas mixture (vapour plus NCG) is separated from the liquid and assuming liquid and gas phases at the same equilibrium temperature.

The mass, energy and momentum equations are basically the same present in the *Pipe* with additional moving grid terms corresponding to a variable volumes discretization:

$$\begin{aligned} &V_i\rho_i^{'} + V_i^{'}\rho_i = m_{jun,i-1} - m_{jun,i} + m_{dif,i-1} - m_{dif,i-1} + m_{fch,i-1} - m_{fch,i} \\ &(u'_i\,\rho_i + u_i\rho'_i)V_i + u_i\rho_i V'_i = (mh)_{jun,i-1} - (mh)_{jun,i} + q_{wall,i} + \lambda_{jun,i}(T_{i-1} - T_i)(A/L)_{jun,i} \end{aligned} \tag{2.19}$$

The diffusive mass flow at the exit of volume i is calculated as follows:

$$m_{dif,i} = (\mu/\rho)_{1-1/2}\left(\partial\rho \big/ \partial L\right)_{i-1/2} A_{jun,i} \tag{2.20}$$

The phase change (boiling or condensation) mass flow at the exit of the volume i is estimated as follows, when the temperature of the gas control volume is equal to or less than T_{sat_gas}:

$$m_{fich,i} = f_{turb}\,\rho_{sat\_liq,i} V_i (1 - x_i) \tag{2.21}$$

when the temperature of the liquid control volume is greater than or equal to T_{sat_liq} ,the boiling of the liquid volume is obtained as:

$$m_{fich,i} = f_{turb}\,\rho_{sat\_vap,i} V_i (x)_i \tag{2.22}$$

The number of fluid (gas and liquid) and thermal nodes have to be taken equal to one, if it is not necessary to calculate the thermal stratification in the tank.

The temperature variations in the wall and in the liquid and gas sides, are calculated along the vertical axis. Heat transfer and mass transfer at the liquid/gas interface as well at the wall interface are also taken into account.

The use of special components like *Sphere_ins* and *Cylinder_ins,* connected to the respective thermal ports of the *Tank*, model the insulation layer according to its conductance properties.

Most typical wall shapes, to model heat conductivity in walls and insulations, are present.

The gravity is only in one direction, top or bottom and the lateral acceleration is not included in the calculation. The liquid height of the tank is taken into account to calculate the liquid column pressure.

Other fundamental libraries present in EcosimPro are:

- The Turbo Machinery Library for the simulation of pumps, turbines and compressors.
- The Combustion Chamber Library for modelling of rocket engines
- The Control library that provides the custom items needed to represent analogue and digital control systems
- The Thermal library supplied with components to predict temperature distributions and heat flows in systems and devices using the thermal network method.

3. FLUID TRANSIENTS

3.1. Introduction

Flow in pipelines and channels are usually unsteady. A change from the steady state flow in a piping system occurs because of a change in boundary conditions.

There are many kinds of boundary conditions that may introduce transients. Common ones are changes in valves settings, starting and stopping of pumps, waves on a reservoir and unstable pump or fan characteristics. The changes in flow, acceleration and slow down of the fluid masses, can cause large pressure or depth fluctuations which can endanger the integrity of pipes. Such large fluctuations are the most dangerous events which the lines will be exposed to.

These pressure fluctuations are called pressure transients and the corresponding flow, *transient flow*. To describe unsteady flow the word *water hammer* is used synonymously, although it is customarily restricted to water.

Operation of spacecraft propulsion systems is regularly adversely faced with water hammer. The presence of very low pressure or vacuum conditions complicates the classically known water hammer, due to various phenomena such as cavitation, absorption and desorption of a pressurizing gas.

In the following chapter the water hammer phenomenon and the relevant factors influencing its behaviour are presented. In the last paragraph, an EcosimPro schematic for validation purposes is described.

3.2. Water hammer

3.2.1. Fluid transients flow concepts and basic differential water hammer equations

General overview

Water hammer mainly concerns with the generation, propagation and reflection of pressure waves in liquid filled pipe systems. Sudden shut-down of a pump or closure of a valve causes fluid transients which may involve large pressure variation, local and distributed cavity

formation, hydraulic and structural vibrations and excessive mass oscillation. Large pressure waves are transmitted through the system with the speed of sound, causing additional pressures in networks. These waves can have very steep front prone to excite the structural system.

In a solid body, a common practice for the analysis of a mass being acted on by a force is to consider the mass concentrated at its centroid. This technique can be applied to a mass of water as well. If the mass is very long and thin, as occurs in pipelines and channels, such an approach is not realistic. When a force is applied to a long mass, the force is propagated by wave action. The wave transmission takes a finite time interval and the entire mass involved does not experience the force at the same time.

An analysis that takes into account this phenomenon is called *elastic analysis,* whereas the method used for solid bodies is said to be *a rigid body analysis*. Thus the basic methods for the study of an unsteady flow are: the *rigid column theory* and *elastic theory*. In the former, the pipeline is considered rigid and does not deform under the pressure as well as the fluid, which is assumed to be incompressible. In the latter, both the elasticity of the fluid and of the pipe is taken into account.

The simplest and most representative fluid transient case to consider is a sudden valve closure at the end of a pipeline. The mass of fluid that was moving forward with velocity v_0 before the closure, builds up a high pressure shock wave due to the sudden stoppage. The water downstream the valve will attempt to continue flowing, creating a vacuum that may cause the pipe to collapse or implode. The more rapid the valve closure the more rapid is the change in momentum, hence greater is the additional pressure development.

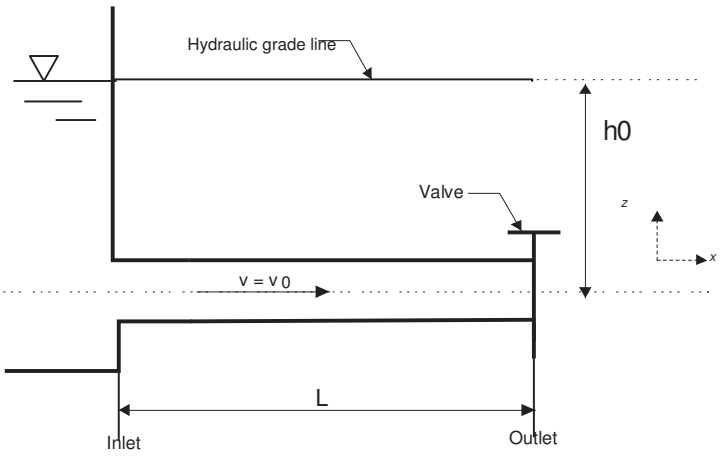

Figure 3.1. - Reservoir-Pipe-Valve system.

The complete cycle that results from an instantaneous closure of a valve is briefly presented. At the instant the valve closes, the fluid nearest the valve is compressed, brought to rest and the pipe wall is stretched. The process is repeated for the next layer of fluid. The fluid upstream, from the valve continues to move downstream with the same speed v_0 until the successive layers have been compressed back to the source. The high pressure moves upstream as a wave, bringing the fluid to rest as it passes, compressing it and expanding the pipe. When the wave reaches the upstream end all the fluid is stopped and it is under the extra head h. All the momentum has been lost and the kinetic energy has been transformed into elastic energy.

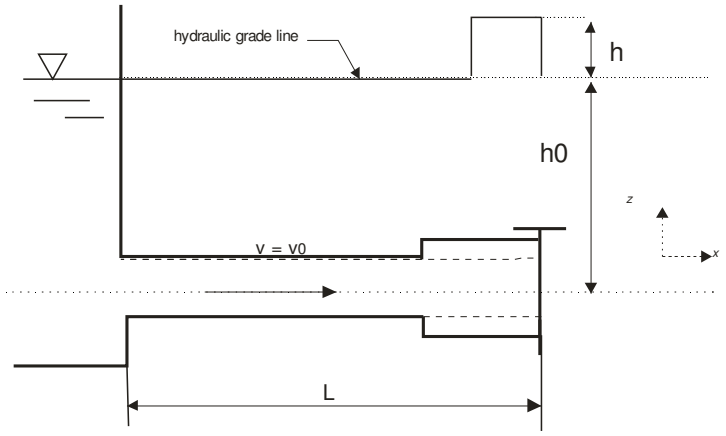

Figure 3.2 - Propagation of pressure wave at t=ε

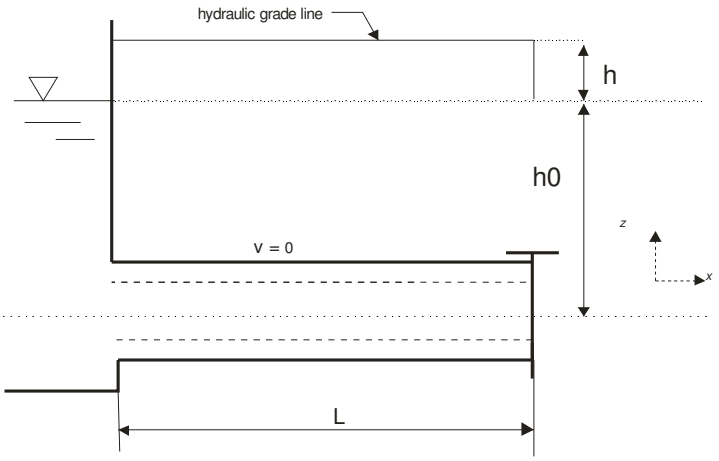

Figure 3.3 - Propagation of pressure wave at t= L/a

Since the reservoir pressure is unchanged, an unbalanced condition at the upstream end is present. The fluid starts to flow backward returning the pressure to initial value and the pipe wall in the initial configuration. Thus the flow proceeds at velocity v_0 in the backward direction. The unbalanced pressure energy is then converted into kinetic energy. This process of conversion travels downstream in the pipe with the speed of sound a. At the moment the wave arrives at the valve the pressure is again at the starting value and the velocity is everywhere v_0.

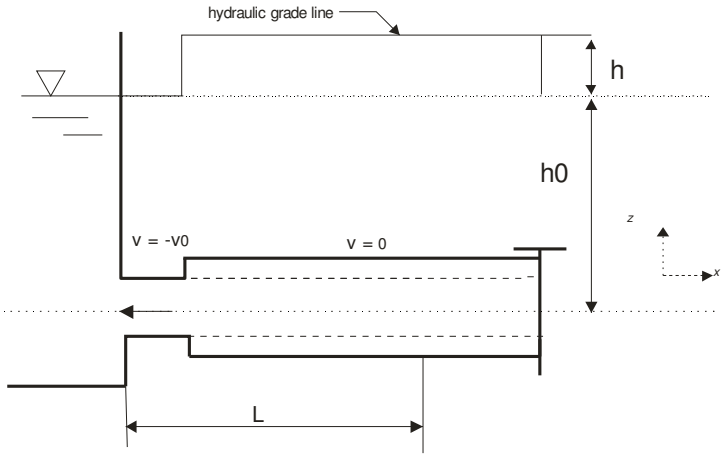

Figure 3.4 - Propagation of pressure wave at t=L/a+ ε

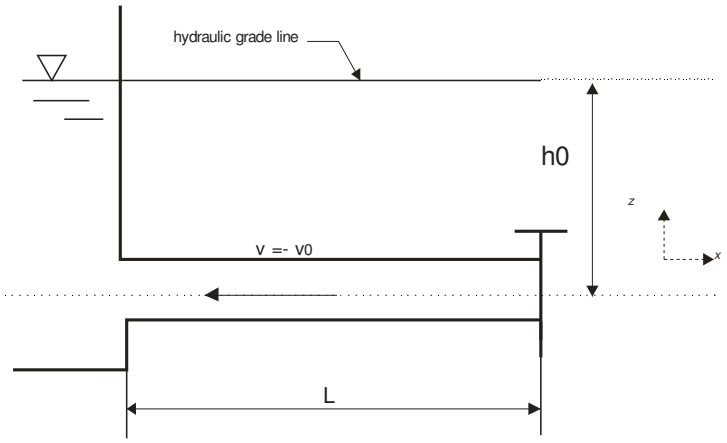

Figure 3.5 - Propagation of pressure wave at t=2L/a

Since the valve is still closed, no fluid is available to maintain these conditions. A *–h* pressure head develops such that the fluid is brought to rest. This low pressure wave travels again backward and brings all of the fluid to rest, causing its expansion and the contraction of the pipe. At the moment the wave is again at the upstream end, the fluid is completely at rest and at the uniform pressure head *–h* with respect to the initial one.

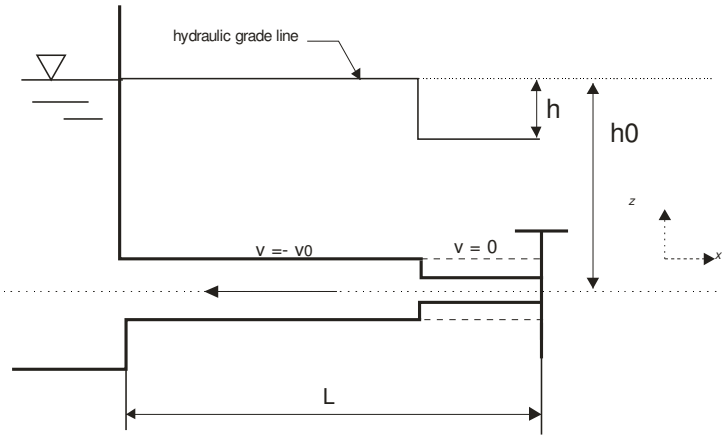

Figure 3.6. - Propagation of pressure wave at t=2L/a+ ε

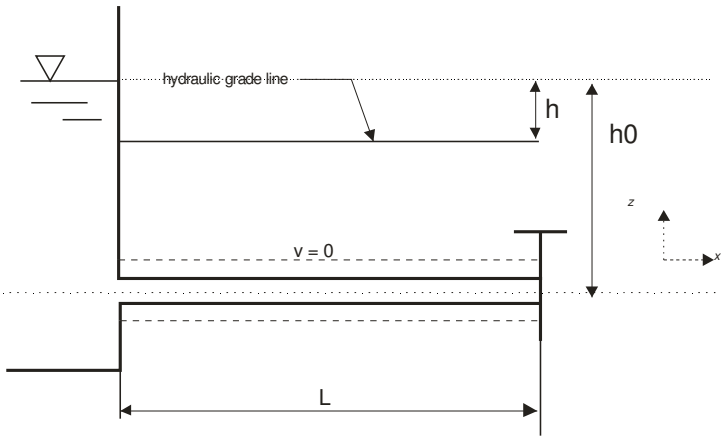

Figure 3.7 - Propagation of pressure wave at t=3L/a

Again an unbalanced condition is present at the reservoir. The fluid flows forward returning to normal conditions, as the wave progresses downstream at velocity *a*. At the instant the wave reaches the valve, the fluid conditions will be the same as at the initial time.

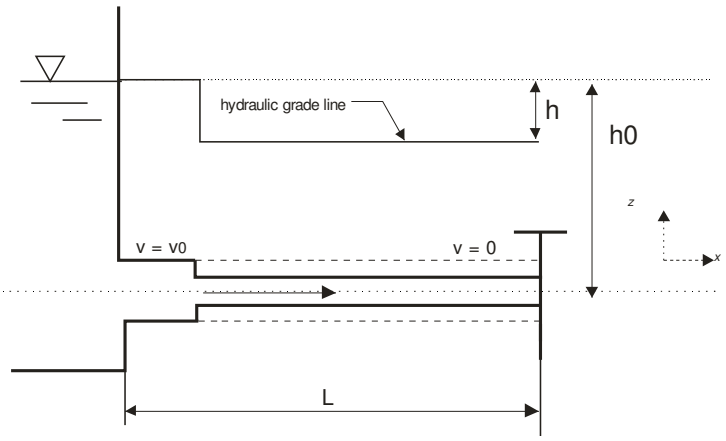

Figure 3.8 - Propagation of pressure wave at t=3L/a+ ε

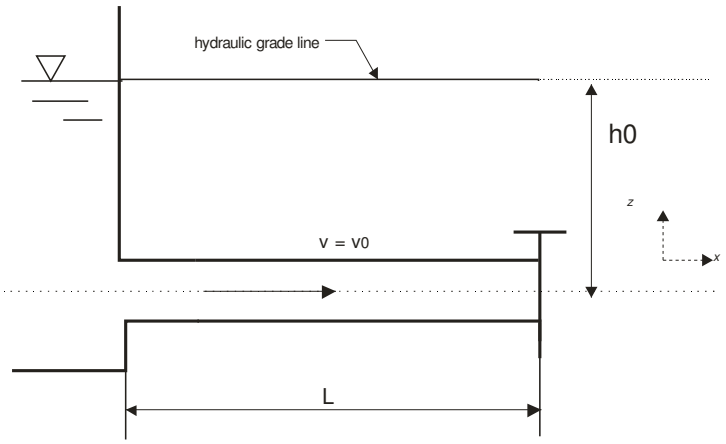

Figure 3.9 - Propagation of pressure wave at t=4L/a

This process will be repeated every *4L/a* if the pipe is perfectly frictionless and no elastic structural interaction is considered. The half interval *(2L/a)* after which conditions are repeated, is termed the *theoretical period of the pipeline*.

In real systems the pressure waves are dissipated due to friction losses as the wave propagates in the pipeline, and the fluid becomes stationary after a short time.

The following characteristics may reduce or eliminate water hammer:

- Low fluid velocities(flow velocity at or below 1.5 m/s for water)
- Slowing closing valves
- High pipeline pressure rating
- Water towers
- Air vessels
- Surge tanks

To prevent this phenomena air vents or vacuum relief valves are installed. Shorter lengths of straight pipe with elbows are preferred to reduce the influence of pressure waves.

Water hammer equations

All methods of analysis of unsteady flow in conduits starts with the equation of motion, continuity energy, plus equations of state and other physical property relationships.

Assuming that the fluid is under a pressure that increases along the pipe length L and that the diameter increases in the same direction of increasing x the following expression for the continuity equation is valid:

$$\frac{\partial P}{\partial t} + v\frac{\partial P}{\partial x} + \rho a^2 \frac{\partial v}{\partial x} = 0 \tag{3.1}$$

The equation of motion, in terms of centreline pressure $P(x, t)$ and average velocity $v(x, t)$, states that the resultant x component of force in the control volume is equal to the time rate of increase of x momentum within the control volume plus the net efflux of momentum from the control volume:

$$\frac{\partial P}{\partial x} + \frac{fv|v|}{2D_H} + \rho g\frac{\partial z}{\partial x} + \rho v\frac{\partial v}{\partial x} + \rho\frac{\partial v}{\partial t} = 0 \tag{3.2}$$

In most treatments the hydraulic grade h, and the discharge Q are preferred dependent variables, while x and t are the independent variables. Using these as variables, and assuming cavitation, leakage and blockage absent, the convective transport terms $u\frac{\partial h}{\partial x}$, $v\frac{\partial v}{\partial x}$, $u\frac{\partial z}{\partial x}$ are very small compared to other terms and therefore neglected. These restrictions cause only 0.1% of errors in the normal engineering situation. The simplified unsteady pipe flow equations are obtained:

$$\frac{\partial h}{\partial t} + \frac{a^2}{gA}\frac{\partial Q}{\partial t} = 0 \tag{3.3}$$

$$\frac{\partial h}{\partial x} + \frac{1}{gA}\frac{\partial Q}{\partial t} + \frac{fQ|Q|}{2gDA^2} = 0 \tag{3.4}$$

The Equations (3.3) and (3.4) are valid as long as the flow is 1D, the duct properties (diameter, wave speed, temperature) are constant and the friction force can be approximated by the Darcy-Weisbach formula for steady state flow. In addition it is always assumed that the friction factor f is either constant or weakly dependent on the Reynolds number.

In the hypothesis of a rigid column analysis, the pipeline is rigid. No useful information could be obtained from the continuity equation in this case. Integrating the momentum equation over a finite pipe line, it is possible to obtain the well-known Allievi-Joukowsky equation:

$$\Delta h = \pm \frac{a}{g} \Delta v \tag{3.5}$$

The pressure peak due to the sudden valve closure is a function of the dimensions of the pipe (diameter and length), speed of the fluid, its density and mostly of the closure time of the valve. The equation above also shows that over an increase in velocity at the gate, the head there must be reduced. So the minus sign has to be used for waves travelling upstream and plus for waves travelling downstream.

The range of validity of this expression is given by a valve closure time less than *2L/a*. A valve closure can be approximated by a series of very small steps of closure spread over a period of time. Each step causes a Δv decrement and a corresponding wave. If the last wave, created during the closure, is emitted before the first wave is reflected back, the sum of all the initial positive small waves will be equal to the corresponding wave produced by an instantaneous closure. On the other hand, if any wave has been reflected before the last wave is emitted, the resulting wave must be smaller than the wave emitted for a closure in less than the time of *2L/a.* Thus, the magnitude of a wave generated by a rapid closure of a valve at the downstream end of a simple pipeline is equal to that of the wave produced by an instantaneous closure. If the closure takes more than *2L/a,* the magnitude of the wave is smaller. For very long pipelines the value of the pipeline period (*2L/a*) can be very large. In this situation, what initially could be intended as a really slow rate of valve movement could result in a sudden closure with the consequent generation of large pressure oscillations. In the case of a network, it can be difficult to establish a value for the reflection time.

Transmitted and reflected pressure waves lead to one main oscillation flow in a pipe-line with a natural frequency of the pipe. The time period after which the natural frequency of water column gets stabilized depends on the elasticity of the pipe material.

Unfortunately water hammer is not only a pressure wave travelling in a liquid at the speed of sound. The conditions in pipeline systems can be far from the idealized situation described by the

classical water hammer theory. Possible sources that may affect the waveform are friction, cavitation and a number of fluid-structure interactions effects (FSI).

Speed of sound

The magnitude of pressure waves depends strongly on the speed of sound. The value of the acoustic velocity itself depends on the bulk modulus or compressibility of the fluid.

For rigid pipe walls, the velocity of water hammer waves in a compressible fluid can be calculated by:

$$a = \sqrt{\frac{K}{\rho}} \tag{3.6}$$

The bulk modulus is affected by pressure, temperature and gas content of the liquid. The free gas, being highly compressible, increases the compressibility of the fluid. When small quantities of gas are available in the liquid, the elasticity tends to that of the gas whilst the density remains close to that for the liquid. The effect predicted from Equation (3.6) is to reduce the pressure wave velocity to well below that of either the liquid or the gas. Assuming homogeneous flow, the pressure wave velocity in a gas-liquid mixture at atmospheric pressure, can be evaluated substituting in the Equation (3.6) the following expressions for mixture bulk modulus:

$$K = \frac{K_l}{1 + \frac{V_g}{V_{mix}}\left(\frac{K_l}{K_g} - 1\right)} \tag{3.7}$$

and density:

$$\rho = \rho_g \frac{V_g}{V_{mix}} + \rho_l \frac{V_l}{V_{mix}} \tag{3.8}$$

So that the speed of sound assumes the following form:

$$a = \sqrt{\frac{\rho_g a_g^2}{\rho_l \alpha (1-\alpha)}} \tag{3.9}$$

One percent of gas by volume reduces the pressure wave velocity in water to 120 m/s compared to 1400 m/s without any gas. If it is relatively simple to calculate the wave speed given a particular percentage of bubble in the liquid, it is not so simple to determine how the bubble content varies with pressure and time. Solids in liquids have a similar but less drastic influence, unless they are compressible.

Not only the bulk modulus of the fluid affects the value of the speed of sound, but also the elastic properties of the duct, as well as the external constrains. Elastic properties include the duct size, wall thickness and wall material; the externals involve type of supports and freedom of movement in the longitudinal direction. To consider the influence of the elasticity of the pipe walls upon the propagating pressure wave, the bulk modulus needs amendment to take the deformation effects into account. Together with the Equation (3.6), derived for the rigid column theory, the water hammer wave velocity is modified in order to account for the bulk modulus reduction due to contraction and expansion of the pipe walls. The following general expression is presented by Halliwell for the wave velocity:

$$a = \sqrt{\frac{K}{\rho(1+\frac{K}{E}\frac{D}{s}\psi)}} \tag{3.10}$$

in which ψ is a non dimensional parameter that depends upon the Poisson's ratio and the pipe restraint. For a thin-walled pipeline wave speed formulas are developed for different kind of support.

For a pipe anchored at its upstream end only:

$$a = \sqrt{\frac{1}{\rho(1/K + D/sE(\frac{5}{4}-\mu)}} \tag{3.11}$$

For a pipe anchored throughout:

$$a = \sqrt{\frac{1}{\rho(1/K + D/sE(\frac{5}{4}-\mu)}} \tag{3.12}$$

For a pipe fixed with an expansion joints throughout:

$$a = \sqrt{\frac{1}{\rho(1/K + D/sE)}} \tag{3.13}$$

The final expression taking into account gas compressibility and wall elasticity for the speed of sound is:

$$a = \sqrt{\frac{1}{(1-\alpha)\rho_{mix}(1/K + D/sE + \alpha_{ref}/p_{ref})}} \tag{3.14}$$

Where p_{ref} is the pressure and α_{ref} the void fraction at reference conditions.

Fluid-Structure Interaction (FSI)

The classical theory of water hammer predicts a squared-wave pressure history in a reservoir-pipeline-valve system subject to sudden valve closure. This square wave is distorted with the introduction of high-frequency pressure oscillations due to secondary effects. This can make the wave front less steeper, increase the system main frequency and invalidate the use of Joukowsky's formula.

If non-zero dynamic stresses and strain in the pipe wall are taken into account the *extended theory of water hammer* has to be considered.

The axial-radial vibration of liquid-filled pipes, excited by water hammer waves are described by the so-called *four-equation model.* It permits the coupled propagation for pressure waves in the liquid and axial stress waves in the pipe wall. The *FSI* coupling mechanism is often referred to as *Poisson's coupling*, because it is induced by radial/axial pipe contractions which are proportional to Poisson's ratio. Due to radial expansion of the pipe, induced by pressure rise in the fluid, axial contractions of the pipe are induced. These contractions send out stress waves and an associated pressure change in the fluid, called *precursor waves*. The precursor waves are stress-wave-induced disturbances in the liquid that travel ahead of the classical water hammer wave. The effects created are initially very small. However their cumulative effect can be significant.

The *FSI* simple model can be represented by the four equations:

$$\frac{\partial v}{\partial t} + \frac{\partial P}{\partial x}\frac{1}{\rho_{fluid}} = 0 \tag{3.15}$$

$$\frac{\partial v}{\partial x} + (\frac{1}{K} + \frac{2R}{Es})\frac{\partial P}{\partial t} - \frac{2\mu}{E}\frac{\partial \sigma_x}{\partial x} = 0 \tag{3.16}$$

$$\frac{\partial \dot{u}_x}{\partial x} - \frac{1}{\rho_{str}}\frac{\partial \sigma_x}{\partial x} = 0 \tag{3.17}$$

$$\frac{\partial \dot{u}_x}{\partial x} - \frac{1}{E}\frac{\partial \sigma_x}{\partial t} - \frac{\mu R}{Es}\frac{\partial P}{\partial t} = 0 \tag{3.18}$$

The model is valid for the low-frequency acoustic behaviour of straight thin-walled, linearly elastic, liquid-filled, prismatic pipes of circular cross-section.

Writing the structural equation for axial motion, it can be immediately realized that this equation is coupled via σ_x, P and μ, representing the boundary conditions that account for the contact between liquid and pipe wall on the interface, with the mass conservation equation. This is what will be referred to as Poisson's coupling. If the ratio s/R of wall-thickness to pipe-radius is then small with respect to unity, circumferential stresses are uniform in the wall cross-section and radial stresses are neglected. If this is not true axial/radial vibration of thick-walled pipes have to be considered and a correction of the FSI model is necessary.

Local FSI can also occur at valves, orifices, expansions, contractions, elbows, bends and branches. The dynamic interaction of a local component with fluid unsteadiness is called *junction coupling*. Steep pressure wave fronts passing unstrained pipe bends will make the bends move. The bend movements provide elastic storage capability for the contained liquid, which will affect the passing pressure waves. The “breathing” of the pipes provides a secondary elastic storage capability which also affects the pressure waves.

Another important phenomenon that has to be considered is the so-called *friction coupling*. It represents the mutual friction between liquid and pipe and, as the Poisson’s coupling, it acts along the entire duct length. In the previous treatment the friction has been neglected, so the initial head everywhere was assumed equal to the reservoir head h_0. With friction, the steady state situation is different. When the disturbance is introduced in the system, a pressure wave starts travelling in the pipeline. As the wave travels upstream, it produces a velocity reduction in layers

of fluid which are at progressively higher initial pressures, owing to friction presence. Then, considering a travelling wave, it is possible to see on the downstream side of the wave a pressure increase transmitted throughout a fluid already at high pressure. The pressure at the valve therefore rises higher and higher as the wave continues its progress in the pipe. This phenomenon is called *line pack* and takes a time equal to *L/a* to be transmitted to the valve. The continuous rise in pressure causes the fluid to compress further. The velocity just downstream of the wave is no longer zero as flow has to continue to supply fluid to fill the additional volume made available by this compression. The velocity difference hence diminishes and so also the wave magnitude is lower. This process is called *attenuation* and it is the process that attenuates the waves, finally extinguishing them. The wave shape is also modified by the line pack.

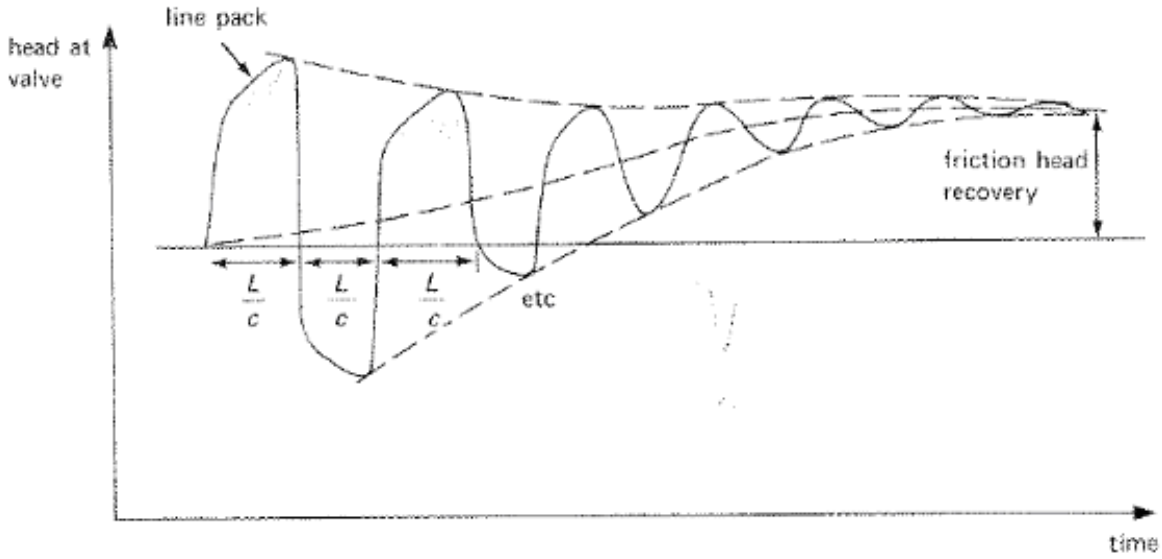

Figure 3.10- Line pack and attenuation [1]

Also, the material response is important for the water hammer phenomena behaviour. The visco-elastic behaviour of plastic pipes influences water hammer events, attenuating pressure fluctuations and increasing the dispersion of water hammer waves.

Column Separation

Concerning liquid transients in a pipeline system, there are two different types of flow regimes to analyse. The first is referred to as *the water hammer regime* or no cavitation case, where the pressure is above the vapour pressure of the liquid. The second is the *cavitation regime,* where the pressure is below the vapour pressure of the liquid. The magnitude of the absolute negative pressure in the system is governed by the flow conditions and the cavitation properties of liquid and pipe walls. Even if the pipe is really simple, additional complications arise if cavitation occurs. This phenomenon is of particular concern because of the strong impulsive load on the structure due to the violent cavity collapse, with consequent severe structural damage.

Two types of cavitation in pipelines can be distinguished depending on the void fraction α (ratio of the volume of vapour to the liquid/vapour mixture volume).

The first is the *discrete vapour cavity* or *liquid column separation.* This phenomenon refers to the breaking of a column in fully filled pipelines. It implies a large value of α and it is assumed to have a local character.

The column separation may occur in fluid transients having high peaks, or in systems in which transients are produced rapidly where the pressure may be reduced to the vapour pressure of the liquid at a specific location. The reduction in pressure causes a negative wave pulse to travel down the pipe reducing the velocity. The difference in velocity between portions of pipe flow tends to put the liquid column into tension, which commercial fluid can not stand. When the vapour pressure is reached a vapour cavity forms into the pipe. The vapour cavity, driven by the inertia of the parting fluid columns, starts growing. The size of this cavity increases until the difference between its internal pressure and the decreasing external pressure is sufficient to offset the surface tension. Once this critical size is reached, the vapour-filled cavity becomes unstable and expands explosively. Depending upon the system geometry and the velocity gradient, the cavity may become so large to fill the entire cross section of the pipe thus divide the liquid in two columns as in the specific case of column separation. This usually occurs in vertical pipes and pipes having steep slopes or sharp edges. The cavity acts like a vacuum retarding the columns, causing a significant increase in the wave reflection time. Such a lengthening for the pipe period ($2L/a$) is characteristic of the presence of separation. The cavity will diminish in size only when the columns change in flow direction. The pressure inside a cavity is equal to the sum of the

partial pressures of the liquid vapours and the released gases. If the temperature of the liquid vapours is constant then the partial pressure of the liquid is constant. However the partial pressure of the gas can increase or decrease if the molar fraction in the cavity increases or decreases. If a cavity forms and collapses several times during a transient, the cavity increases in size with successive cavity formations. The following graph shows the typical pressure signature of a fluid transient in a pipeline modified by the presence of separation.

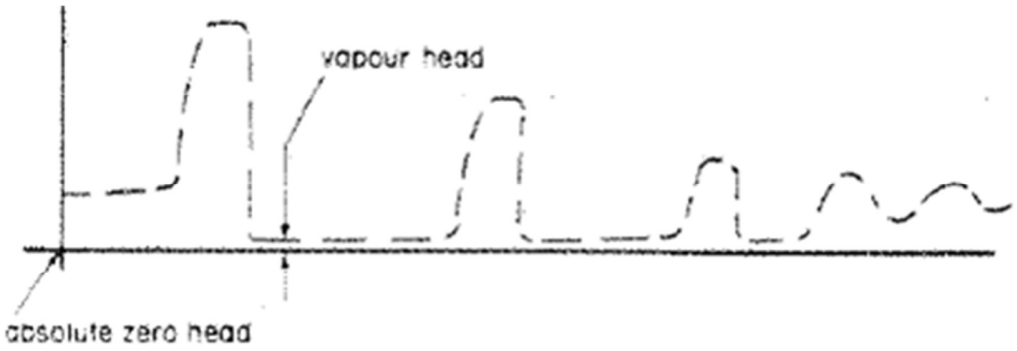

Figure 3.11- Pressure diagram for a pipeline where separation is occurring[13]

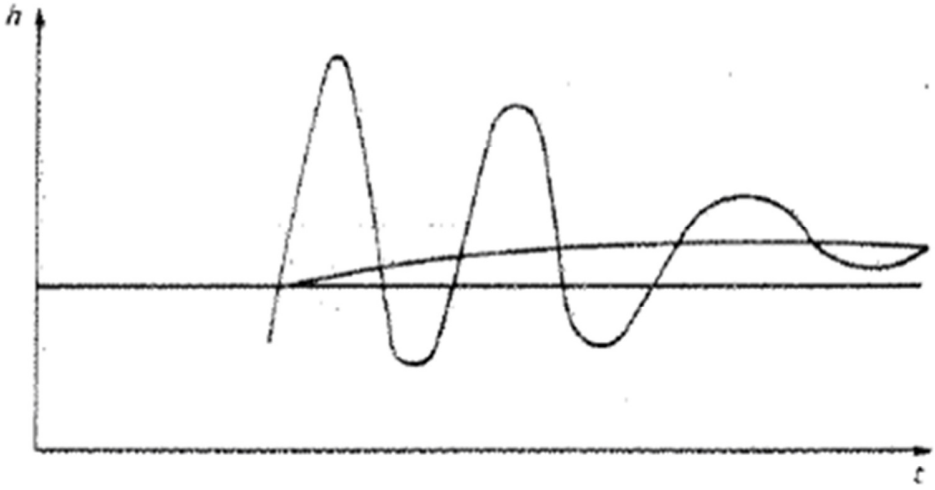

Figure 3.12- Pressure diagram for a pipeline where separation is not occurring[13]

The latter cavity flow regime is the *distributed vaporous cavitation* or two-phase (*bubbly) flow*. It implies a small value of α. It is more common in case of horizontal pipes or pipes having mild slopes. The vaporous cavitation consists of a region of two-phase flow of both vapour and liquid appearing over an extended length of the pipe with the pressure at the liquid vapour pressure.

If the liquid in the pipelines contains dissolved air or gases, a reduction below the saturation pressure causes gas bubble formation at the many nuclei generally present in technical liquids. These small bubbles greatly decrease the wave speed. If the temperature increases but the pressure is kept constant then the cavitation hammer decreases due to the decreased speed of sound in liquid and saturation pressure increase.

The collision of two columns or of one column with a closed end, or simply the cavities collapsing may cause a large and nearly instantaneous rise in pressure. A severe hydraulic load for the whole system is created. The duration of the pressure pulse is about one tenth of a 2L/a period and, if the difference in velocity between the columns at the moment of collapse of the cavity is Δv, a head increase of $a\Delta v/2g$ may be expected. The head directly caused by the cavity collapse is less than the water hammer head generated at the beginning, but a narrow short-duration pulse occurs. The resulting maximum head in the system could be greater than the maximum head predicted by Joukowsky equation, if the cavity collapse occurs exactly at the arrival of a pressure wave front. This head increase may be sufficient for the pipe to rupture. The maximum pressure head due to the collapse of a cavity in a simple valve-pipe-reservoir system is given by:

$$h_{\max} = \frac{a}{g}\left|v_f\right| + 2h_{r-v} \tag{3.19}$$

where v_f is the velocity of the liquid column at the valve just before cavity collapse and h_{r-v} is the difference in elevation between the downstream valve and the upstream reservoir pressure head.

The location and intensity of column separation is influenced by several system parameters including the cause of the transient regime (rapid valve-closure, pump failure, turbine load-rejection), layout of the pumping system (pipeline dimensions, longitudinal profile and position of the valves) and hydraulic characteristics (steady flow-velocity, static pressure-head, skin

friction, cavitation properties of the liquid and pipe walls). Therefore it is very hard to judge the severity of the pressure peak following cavity collapse that may or may not exceed the Joukowsky's pressure rise and cavities may form at the valve or/and along the pipe.

The situation can even be worse: the occurrence of water column separation can trigger a series of cavity formations and collapses resulting in a series of impulsive loads on the structure. The first cavity is often a single coherent void this will shatter into a cloud of smaller bubbles as a result of the violence of the first collapse. The cavities will grow and diminish according to the dynamic pressure of the system.

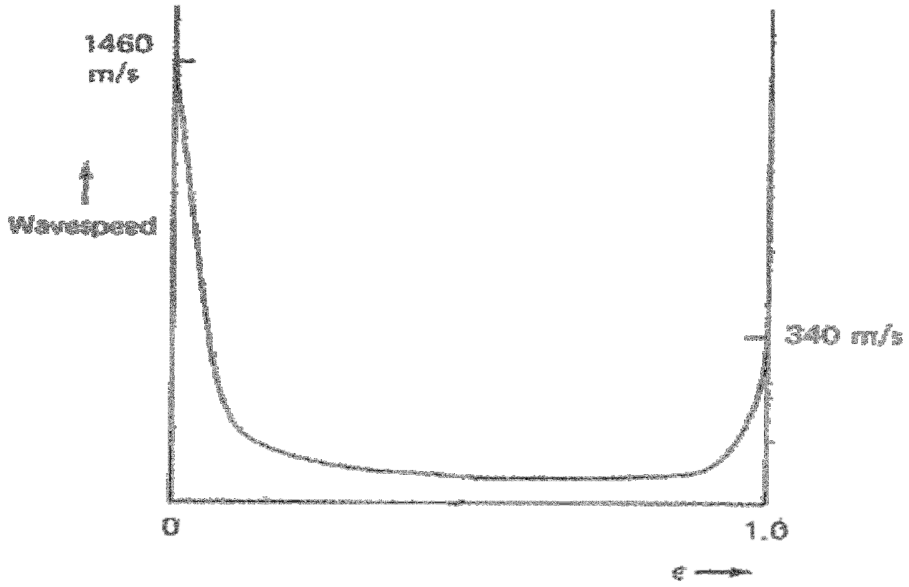

Figure 3.13 - Wave speed against fractional volume of gas for a water-air mixture[14]

Because of the presence of the bubbles, the liquid in a cavitating flow is a mixture of the released gases and the liquid. Experimental investigations have shown that there is more dissipation of the pressure waves in a gas-liquid mixture than in a pure liquid. The additional dissipation is due to the heat transfer to the liquid when the bubbles are expanded and compressed. To compute the energy dissipation in cavitating flows, the total shear stress is determined by adding to wall shear stress, the shear stress due to non-adiabatic behaviour of a spherical bubble:

$$\tau_{bubble} = C\alpha_0 \rho_l g D|\Delta h| \frac{v}{L|v|} \tag{3.20}$$

where C is an unknown constant and α_0 the void fraction at the reservoir pressure.

Accompanying the generation of vapour there is also a release of gas from solution in the liquid. At atmospheric pressure in a liquid there will commonly be a content of free bubbles. When the pressure changes the bubble content will change. Due to pressure drops caused by the water hammer phenomenon, there will be an increase in volume of bubbles present. This change in volume can be really large if the drop in pressure is great. A very small amount of gas comes out when the pressure is below atmospheric pressure, but progressively more and more comes out as the pressure drops further. If the diffusion of gas in the fluid towards bubbles is a relatively slow process, only small quantities of gas evolve during most transients and the concentration of dissolved gas changes only slightly. However, due to the strong relationship between free gas void fraction, pressure and wave propagation speed, even a small quantity of free gas can have a profound influence on the behaviour of low pressure transient waves. For gas to come out of solution sufficiently rapidly, on the order of pressure transient, it is necessary for the pressure to drop sufficiently below a certain value, the so called *gas head*.

The presence of free gas does not significantly affect the formation of the separation bubble but it is considered to have a cushioning effect upon its closure. This is due to the fact that the solution for gas bubbles is slower than their evolution, so that the gas bubbles are left floating in the liquid after the main vapour-filled cavities collapsed. Thus they are available to reduce the magnitude of the pressure waves that would have been generated, decreasing the effective bulk modulus of the fluid.

Summarizing, a system in which cavitating flow and column separation occur can be divided in three regions: (1) water hammer (2) cavitation (3) column separation.

In the water hammer region, the void fraction is so small that it can be neglected, hence the velocity of the pressure waves does not depend upon pressure. In the cavitating region, gas bubbles are dispersed throughout the liquid and the fluid behaves like a gas-liquid mixture. In such flow the speed of sound depends upon the void fraction, which depends on the pressure. The classical water hammer equations are not valid in cavitating regions. The third region may be

present simultaneously in piping systems: cavitation occurs in one part of the system and column separates at some critical location. These phases can occur in sequence as well. For example the system can be considered initially as a water hammer region, then the void fraction increases due to the reduction in pressure and so the flow becomes a cavitating flow. With a further reduction in pressure, the fluid column can separate at one point. Then, when the transient-state pressure increases due to wave reflection, the separate columns rejoin, the cavities collapse and the whole system becomes a water hammer region again.

3.2.2. Numerical solutions for 1D water hammer equations.

There are two basic approaches for the solution of unsteady internal flow in hydraulic system: a solution in the time domain or *water hammer methods* and a solution in the frequency domain.

The former is the traditional way of proceeding and it has the advantage of incorporating nonlinear convective inertial term in the equations of fluid flow with higher difficulties in managing it for complex geometries or complex fluids, like cavitating flows.

The latter is useful for a complex geometry, like for pumps transients analysis, and if the fluid is cavitating. The non-linear terms can not be included and the method is accurate only for small amplitude perturbations of the mean flow. In this case is possible to know the stability limits but do not evaluate the amplitude of large unstable motions.

Application of time domain methods to 1D fluid flow normally consists in three components:

- Conditions for the conservations of mass and momentum in the fluids
- Thermodynamic constraints for governing the changes of state of the fluid
- Response of the containing structure to the pressure changes in the fluid

The analysis is made simpler when it is possible to assume both fluid and structure to behave barotropically. The importance of this assumption lies in the fact that it allows to have a non-ambiguous definition of the sound speed for waves travelling in the system

The equations governing 1D water hammer flows can seldom be solved analytically. This pair of equations (1), (2) is system of quasi-linear hyperbolic, partial differential equations and a close form solution is not available. However by neglecting or linearazing the non-linear terms, various graphical and analytical methods have been developed in the time domain. These are

approximate methods and can not be used to analyze large systems or systems with complex boundary conditions.

The main ones are:

- Method of characteristic
- Graphical methods
- Arithmetic method
- Algebraic method
- Implicit method
- Linear analysis

The *Arithmetic methods* neglect friction and the Joukowsky's equation is written in the form:

$$h \pm \frac{a}{g} v = C \tag{3.21}$$

Denominated A the conditions at the upstream end of the pipe (reservoir) and B the ones at the downstream end (valve), the plus is for a pressure wave travelling upstream (from B to A. The Equation (3.21) takes the form:

$$h_A + \frac{a}{g} v_A = h_B + \frac{a}{g} v_B \tag{3.22}$$

Know the condition at B in terms of h_B, v_B a piece of information in A, L/a second later, permits to know h_A, v_A. for a wave travelling in the opposite direction:

$$h_A - \frac{a}{g} v_A = h_B - \frac{a}{g} v_B \tag{3.23}$$

From the application of this pair of equations many times, plus the required boundary conditions the solution of the transient is obtained.

The *graphical water hammer* neglects friction in its theoretical development but utilizes means to take it into account as a correction factor. The arithmetic Equation (3.21) may be adapted to a graphical solution plotted as a straight line on an *hv*-diagram (*h* ordinate, *v* abscissa).

The *implicit method* is a finite difference procedure. It is mostly used in the free surface flow calculation, however it can be used for other applications. The procedure is particular applicable in cases when the storage and capacitive effects are more important than the inertial terms. The requirement to maintain a certain relationship between the time increment Δt and the length Δx is relaxed. This offers the opportunity for a more flexible scheme in dealing with complex systems. When applied to water hammer problems it is necessary to adhere to the Courant condition in the time step-distance interval relationship in order to maintain a good level of accuracy.

The *linear analyzing method* consists of a linearization of the friction term, and dropping other nonlinear terms in the equation of motion. An analytical solution to the equations may be found for a sine wave oscillation. Two main categories are defined: steady-oscillatory fluctuations set up by some forcing function and free vibrations of the piping system. The name *impedance method* has been given to the steady-oscillatory studies. By means of harmonic analysis, the complex period forcing function may be decomposed into a family of sine wave motions. Each of these may be handled by the equations, then the solutions added to yield the complete solution.

The *method of characteristics* has become quite well known and it is largely used for the solution of 1D hydraulic transient problems. This method involves finding moving coordinate systems in which the two partial differential equations (PDE) (3.1) (3.2) are converted into ordinary differential equations (ODEs). These equations are expresses in a finite difference form. This result is achieved with a simple procedure.

A linear combination of the two PDE is calculated:

$$L = L_1 + \lambda L_2 \tag{3.24}$$

$$\mathrm{L1} := \frac{\partial h}{\partial x} + \frac{1}{gA}\frac{\partial Q}{\partial t} + \frac{fQ|Q|}{2gDA^2}$$

$$\mathrm{L}_2 = \frac{\partial h}{\partial t} + \frac{a^2}{gA}\frac{\partial Q}{\partial t}$$

where λ is an unknown multiplier. Assuming $Q=Q(x,t)$ and $h=h(x,t)$, and defining:

$$\frac{1}{\lambda} = \frac{dx}{dt} = \lambda a^2 \tag{3.25}$$

It is possible to obtain the following definition for λ:

$$\lambda = \pm\frac{1}{a} \tag{3.26}$$

Finally the equation (3.24) can be transformed to obtain the characteristic method equation:

$$\frac{dQ}{dt} + \frac{gA}{a}\frac{dh}{dt} + \frac{f}{2DA}Q|Q| = 0\text{, if} \tag{3.27}$$

$$\frac{dx}{dt} = a \tag{3.28}$$

$$\frac{dQ}{dt} - \frac{gA}{a}\frac{dh}{dt} + \frac{f}{2DA}Q|Q| = 0\text{, if} \tag{3.29}$$

$$\frac{dx}{dt} = -a \tag{3.30}$$

In the *x-t* plane, Equation (3.21) and (3.23) represent two straight lines having a slope ±*1/a*. These are the so called *characteristic lines.* Physically they represent the path traversed by a disturbance. At the time t_0 the wave starts moving from B and then after a time $t+\Delta t$ it is in P and it has moved along the distance $\Delta x = a\,\Delta t$.

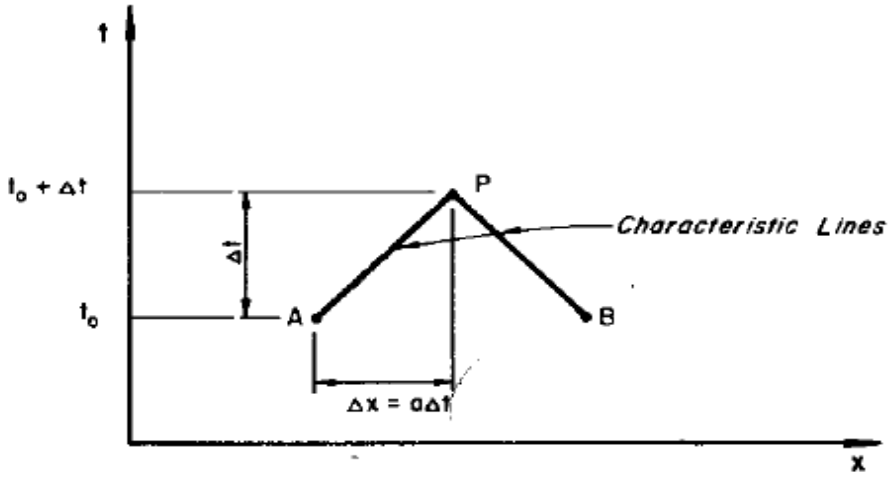

Figure 3.14 -. Characteristic lines [1]

Mathematically these lines divide the *x-t* plane into two regions, which may be dominated by two kinds of solutions. The solutions may be discontinuous along these lines. Considering a simple pipeline-reservoir-valve system as in Figure (3.1) the Equations (3.28) and (3.30) are valid along the entire length *L* of the pipe and special boundary conditions are needed at the ends (*x=0* and *x=L*). When the valve is closed the flow throughout the valve is stopped and results in a pressure rise in the upstream direction. Because of this pressure rise, a wave travels in the upstream direction. If the path of the wave is plotted in the *x-t* plane, it will be represented by the line BC in Figure (3.15). The conditions in *Region I* depend only upon the initial conditions because the upstream boundary conditions did not change, whereas in *Region II* they depend upon the conditions imposed by the down-stream boundary. Thus, the characteristic lines separate the two types of solution.

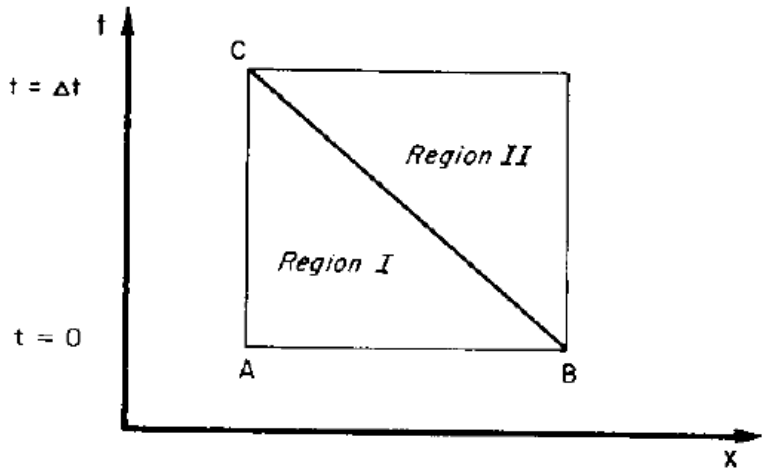

Figure 3.15 - Characteristic lines for excitation at the downstream end [1]

If disturbances are imposed on both sides of the pipe, the region influenced by the initial condition is represented in Figure (3.16).

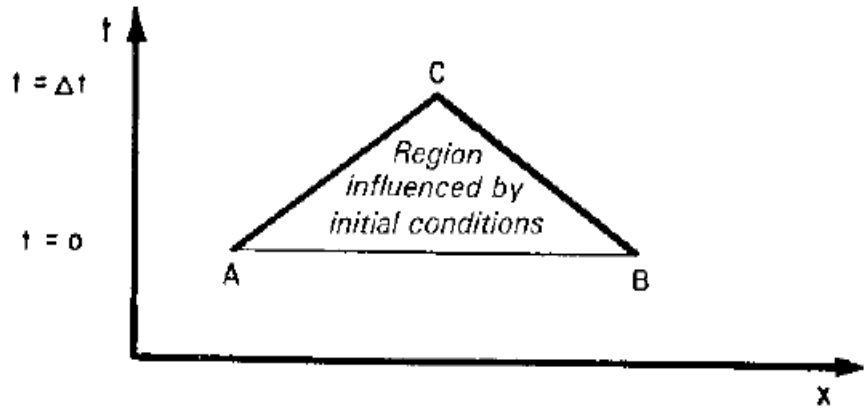

Figure 3.16 - Characteristic lines for excitation at the upstream and downstream end [1]

In other words, by imposing the Equation (3.28) and (3.30) it is possible to eliminate on independent variable *x* and convert the PDE (3.1) and (3.2) into ODEs in the independent variable *t*. However these equation are valid only in the *x*-*t* plane: the Equation (3.27) is valid along the straight, if *a* is constant, line given by Equation (3.28) and the he typical numerical solution by the characteristic method is obtained graphically.

Equation (3.29) is valid along the straight line described by Equation (3.30).

Lets assume that Q and h are known at points A and B and the values at point C from Figure (3.16) are the ones that have to be calculated. This can be done by solving the Equations (3.27) and (3.29) as finite-difference equations:

$$C^+ : h_p = h_A + \frac{a}{gA}(Q_p - Q_A) + \frac{f\Delta x}{2gDA^2} Q_A |Q_A| \tag{3.31}$$

$$C^- : h_p = h_B + \frac{a}{gA}(Q_p - Q_B) + \frac{f\Delta x}{2gDA^2} Q_B |Q_B| \tag{3.32}$$

These two compatibly equations are basic algebraic relations that describe the transient propagation of pressure head and flow in a pipeline. The solution consists in finding *h* and *Q* for each point of the grid along $t = \Delta t$, then proceeding for $t = 2\Delta t$ until the desired time duration is reached. At any interior grid section point, the two compatibility equations are solved

simultaneously for the unknown Q and h. Examination of the grid shows that the end points of the system being influenced by the interior points after the first time step. Therefore, in order to complete the solution to any desired time, it is necessary to introduce the appropriate boundary conditions at any points in the mesh which lies at the end of the pipe, a junction of the pipe with pipe of different sizes or any other component. These conditions are in terms of special relationships that define, at the boundary, the discharge, the head or a relationship between them.

The characteristic methods have many advantages:

- Stability criteria are firmly established
- Boundary conditions are easily programmed
- Minor terms may be retained if desired
- Very complex system may be handled
- Best accuracy of any other finite difference methods

3.3. EcosimPro modelling and validation work

EcosimPro is an objected-oriented Physical Simulation Modelling tool for the solution of different dynamic system. It can be used to study both steady state and transients.

The major question is about the validation, the quality of the output, the status, the operational use of such modelling for designing and checking the behaviour of a system during a fluid transient. The DASSL solution method based on ODEs is used instead of the characteristics method traditionally used for this type of problem. The speed of sound is calculated by taking into consideration the elasticity of the pipe and the fluid compressibility.

The ESPSS libraries are used to implement some specific test cases relevant to propulsion systems and compare them to experimental data for validation purposes. The specific test case chosen is the test setup described in Reference [21]

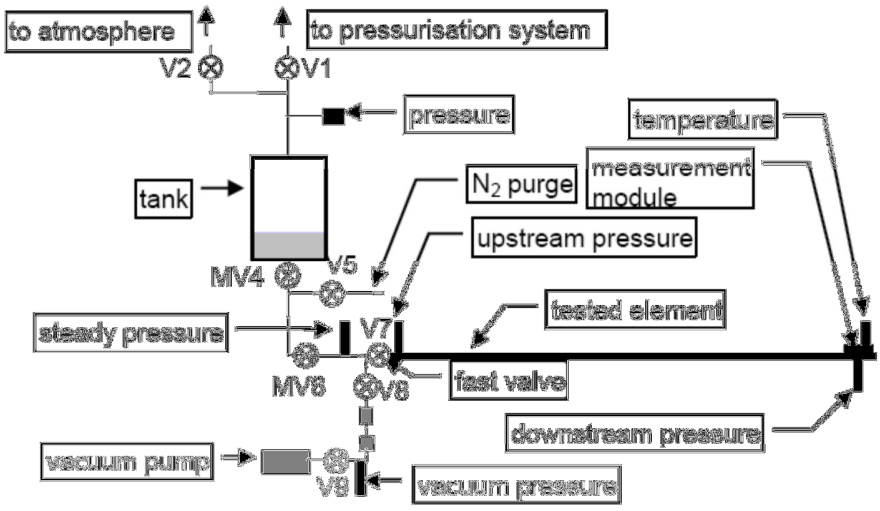

Figure 3.17 - Test setup reference [21]

The test setup is defined by a line filled up to the valve V7 that isolates the empty line up to a dead end. Two main pressure measurements are available: P_{up} near V7 and P_{dw}

Based on the test set up, by using exclusively the generic object of the ESPSS library, with the particular dimension of the hardware, a simplified model equivalent to the real system is obtained in EcosimPro.

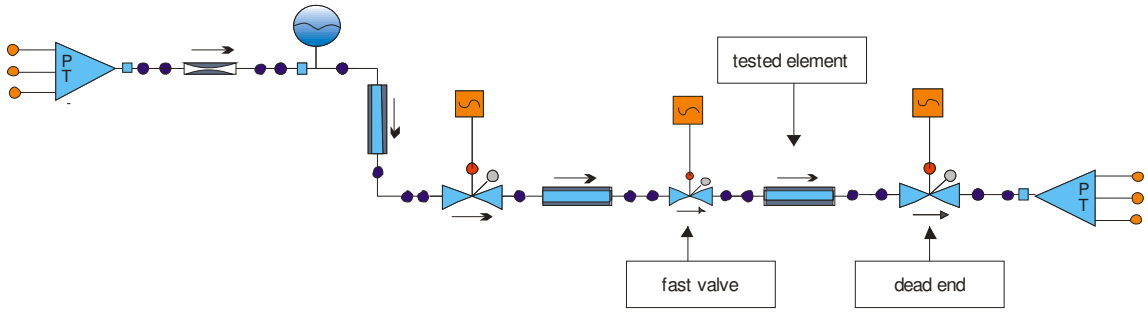

Figure 3.18 - Test schematic

EcosimPro allows for the user to display the propagation of the pressure waves along the pipeline and plot any variable of the system model. With the right boundary conditions and geometrical

dimensions, a good agreement between the experimental results and the simulation results could be obtained. The following phenomena can be shown in simulation results:

- The pressure rises in the pipe due to the sudden stop of the fluid. The wave is reflected in the open end as a negative flow. This negative flow is stopped again at the close end of the pipe creating the wave pressure path shown in Figure (3.19).

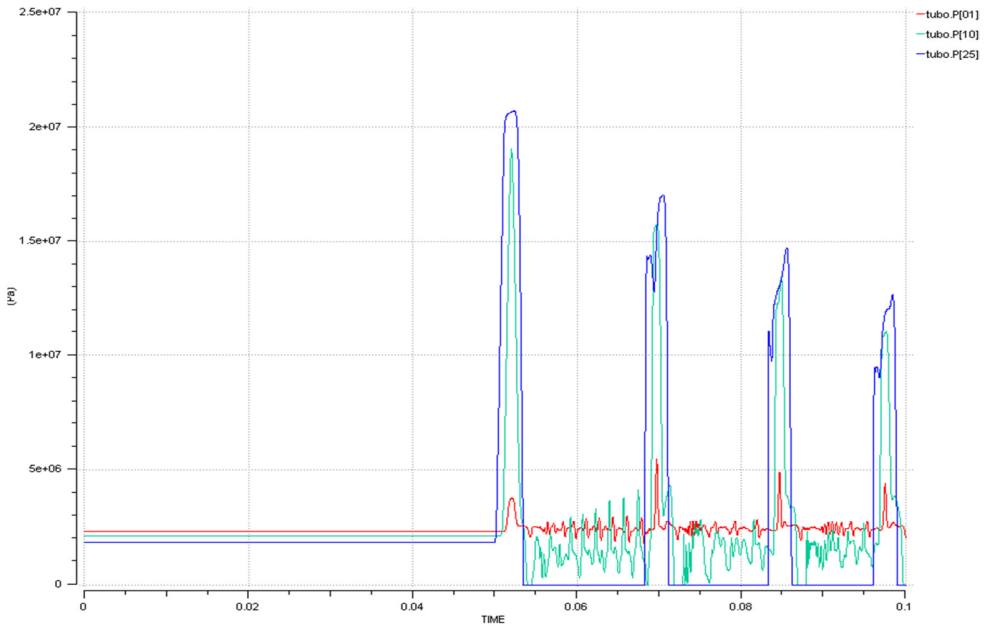

Figure 3.19 – Simulation result

- The vapour pressure is reached in the pipe and a consequent column separation and vapour bubble formation is observed in the pressure peaks. The classical water hammer theory wave shape is modified and same fluctuation can be visualized in the spikes in Figure (3.20).

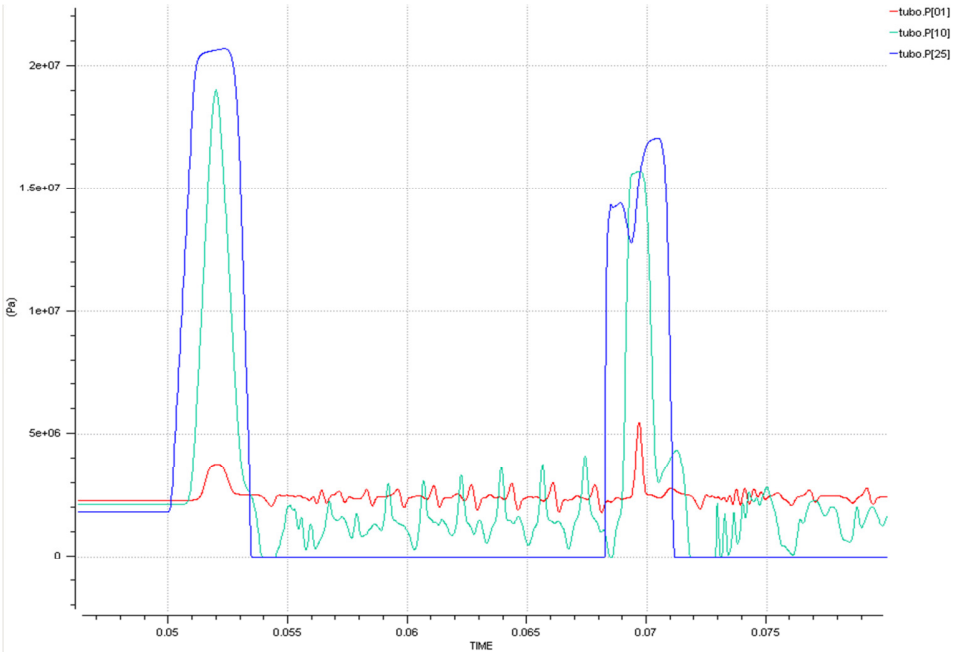

Figure 3.20 – Simulation results detail

The filling of the straight empty tube from a pressurized tank at pressure P_{TANK}; induces a first water hammer peak pressure at the end of the filling in agreement with Joukowsky's equation. Very similar values of peak pressures for the first peak pressure are obtained in the EcosimPro schematic.

The first peak is followed by a second water hammer peak having lower amplitude due to the damping induced by the friction on the tubing walls. The time interval between the two first peaks in the simple case analysed is predicted by the following relation:

$$\Delta t = \frac{\Delta p}{P_{TANK}} \frac{2L}{a} \tag{3.33}$$

The duration between the two first peaks is also nearly identical and the damping for the second pressure peak is also compliant with experimental data.

TEST BENCH P2

4.1. Introduction

Test facilities are an indispensable element for the development and acceptance for space systems and components. Liquid rocket engines for launch and space application as well as their subsystems need to be verified and qualified during hot-runs. Test verification during development/qualification as well as during acceptance testing for production are essential steps. A simulation tool that could allow for testing subsystems in the same manner as during complete engine tests will reduce development time and costs. Test facilities with environment control are unique and are specially designed for their needs. Uses of test data for computer simulations, as code calibration, grant a reduction of the total tests needed with a positive outcome of cost reduction.

In the following chapter the test bench P2 for storable hypergolic bipropellants is briefly described. The equivalent EcosimPro model is then presented.

4.2. Test bench functional description

4.2.1 Lampoldshausen Test Centre

In the frame of the consolidation of the different space propulsion activities of ASTRIUM Propulsion in the 90`s, all testing activities were concentrated at the Lampoldshausen location.

The Lampoldshausen Test Centre is located at the German Aerospace Centre (DLR) and is the propulsion test centre supporting programs of the European Space Agency. It is specialized in the design, development, manufacture, and testing of thrusters and complete propulsion systems for orbital satellites, interplanetary space probes, upper stage systems and launch vehicle roll control systems. Hot-fire testing of thrusters, rocket engines and complete propulsion systems is performed here. A growing number of test facilities for storable and cryogenic propulsion systems, on component and engine level, have been located in this area since 1954. An important contribution to its growth was given by the Ariane Launcher (Ariane 5) new development studies.

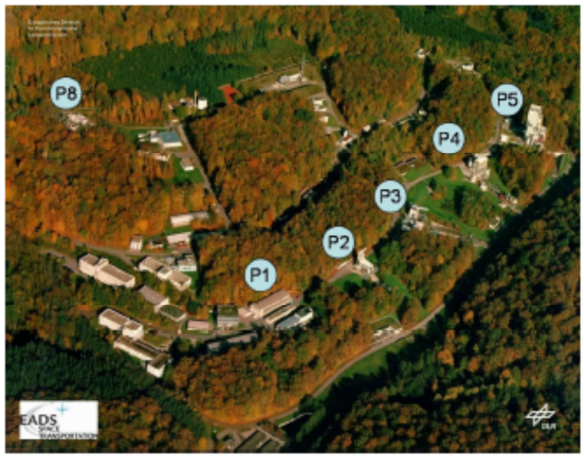

Figure 4.1 - European Test Centre for Space Propulsion

4.2.2. P2: general overview

P2 test bench is a sea-level and vacuum test facility for liquid propellant rocket engines having a thrust up to 100 kN using Earth storable hypergolic bipropellants. Test stand P2 is designed to test rocket engines and also complete stages in a vertical configuration.

It is composed of a 30 m high concrete tower sunk into the ground for half of its height.

The engines can be lowered into the test cell through the top opening and their exhaust gases vented to the exterior.

Two test cells were constructed in the test bench: one cell for engine development, the other for the stage testing, both under sea-level conditions. Both test cells consist of an upper building, a steel construction (shelter), concrete ground work that accommodates the thrust deflector and carries the intermediate floor, and the intermediate floor, that enables easy servicing of the decontamination system and supports the adapter for the supersonic diffuser. Due to the toxicity of the hypergolic propellants the concrete ground plate is designed as a bathtub directly connected with the central neutralization facility.

The test rig is a steel structure capable to carry loads of up to 60 tons of thrust. It provides mounting pads for the four tanks, the pipe network and the test specimen mounting.

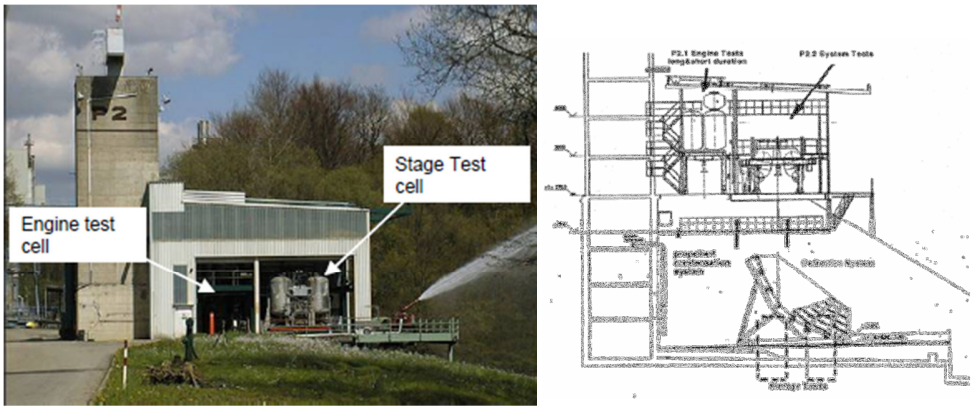

Figure 4.2- P2 complete and side view

The test facility provides the capability to:

- Perform hot runs for up 1100s with the development/qualification models under sea-level conditions
- Vacuum tests
- Test the operation of the engine with an active actuator and swirling the engine in one plane within 4.3°
- Test the function of flight type pressurization equipment of the stage
- Carry out the cold tests for facility and test specimen for the preparation of hot test
- Conduct cold flow tests.

The tests programmed in P2 test bench are mainly the following:

- Sea level tests, HF investigations - AESTUS upper stage engine for Ariane 5
- EPS stage tests including hot firing campaigns
- AESTUS long duration tests
- AESTUS engine production - cold flow acceptance tests
- AESTUS II turbopump variant (RS 72) development tests
- Ariane 5 upper stage (EPS) pressure control assembly tests
- EPS-PFE delta-qualification and production acceptance tests (cold flow tests)

- Automated Transfer Vehicle (ATV) -PQM-2, PQM-3 complete propulsion system tests
- ATV Component tests
- Sea level tests for 400 N ESA programmes, e.g. Cluster, MSG
- 10 N thruster sealing tests for the Cluster programme
- AVUM testing (VEGA upper stage) under vacuum conditions

The P2 is foreseen to be in the frame of the upcoming storable propellant engine development programs like FLPP Storable.

The description of the main subsystems composing the facility is given in the following sections.

4.2.3. Pressurization system

The pressurization system consists of a tank pressurization system, a pressure supply for pneumatic operated equipment, dome pressure regulator, valves and jet pumps for the condensation system, and a supply of the pressurized air for shop located at test stand and for breathing air.

The tank pressurization system is subdivided into three major elements: the pressurization for the run tanks, pressurization of the storage tanks and pressurization/venting of the propellant drums during filling of the test stand tanks.

The pressurization of the run tank is achieved by the pressuring gas supplied by a source common to both the oxidizer and the fuel branch of the system. Each branch has its own pressure regulator, non-return valve and associate valves for operation and control. The tank pressurization can be operated with nitrogen or helium. The gaseous nitrogen is provided by the local buffer vessel of 1 m^3 at 200 bar pressure. The system is capable of pressurizing run tanks, 350 l and 4700 l, depending on the valve position chosen. The tanks are protected by overpressure by safety valves which assure a relief of tank pressure in case a certain limit is exceeded.

The test facility is equipped with a system supplying pressurized air. This system provides breathing air for the protection suits during filling or defiling of the propellant tanks.

For the pressurization of the storage tanks, the pressuring gas is supplied by a source common to both the oxidizer and fuel side but each branch has its own shut-off valve and pressure regulator. The system is capable of pressurizing the 300 l propellant storage tanks located at the lower side of the test stand P2 during the propellant transfer from the storage tank to the run tank. The transfer is actuated by means of a pump located at each storage tank.

The pressurization system is also used as a pressure source for the electrically-pneumatically operated valve. The pressure control branch is composed of an appropriate manually operated shut-off valve and a manually operated primary pressure regulator.

4.2.4 Propellant supply system

The system is composed of two main items: propellant tank and the connected feed lines, a pipe network with associated equipment.

The propellant tanks are capable for operating with MMH and NTO or MON, and are filled from the bottom. The propellant supply system itself presents two different alternative run tank configurations: 350 l, operation of at least 60 s, and 4700 l tank, for up to 1100 s for hot run, depending on the test case. For both tank configurations the same hardware of feed lines is provided. Tank pressure and propellant temperature transducers are present. In Table (4.1) the geometrical characteristics of the tanks are presented.

Table 4.1 – Tank dimensions

TYPE	VOLUME (l)	SIZE (mm)	PROPELLANT
Runtank	350	Φ 600 x 1600	NTO, MMH
Runtank	4700	Φ 1500 x 3100	NTO, MMH

The feed lines have a total length (propellant outlet to interface test specimen) of approximately 4 m. The line is equipped with tank isolation valves, flowmeters, temperature transducers, pressure transducers, cavitating venturi or variable flow control valve, manual valve, open

evacuation circuit, automatic shut-off valve, with an open/close time equal or less 150 ms, and heater, to heat the propellant up to 40° C.

Bubble free propellant is assured by evacuation of the feedline prior to filling with propellants.

4.2.5 Purge system

In general this system allows for purging the specimen with gaseous nitrogen, gaseous helium and also with water supplied from a separate water tank. The purge system is supplied by a pressure source common to that of the pressurization system. There are two separate branches for purging the fuel side and for the oxidizer side.

The complete lines with the main elements are shown in the Figure (4.3).

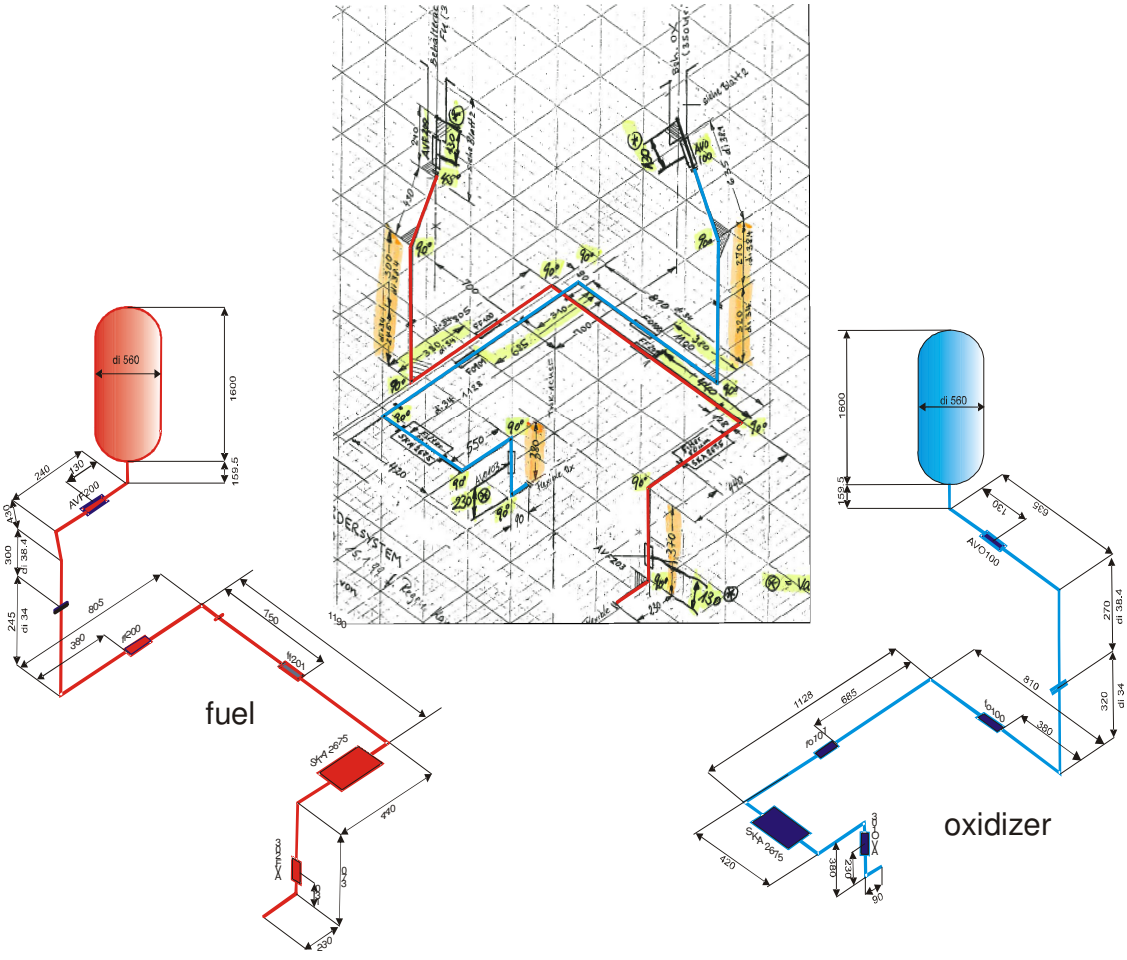

Figure 4.3 - Complete P2 feed line system

4.3. EcosimPro model

4.3.1. General overview

In this section the components of the P2 model in EcosimPro are described. The relevant physics used for the specific components is described together with the input parameters.

The EcosimPro model is built from very individual hardware components. Every single component has its own numerical code and is connected by ports to other components. Ports define the inlet value of a component like temperature and pressure. Special components are needed for defining boundary conditions as a function of time. If everything is linked together the final model is established.

NTO and MMH feed lines are constituted by the same items. The complete list of implemented elements simulated in EcosimPro is given in Table (4.2):

Table- 4.2 - Line components

COMPONENT	NAME	QUANTITY
Runtank (350l)	Tank_CylDomes MMH Tank_CylDomes NTO	1 per each line
Flow meter	FF_AN_241 FF_AN_242 FO_AN_241 FO_AN_242	2 per each line
Filter	SKP2675_OX SKP2675_FU	1 per each line
Shut-off valve	AVF200 AVF203 AVO100 AVO103	2 per each line

The complete P2 model is presented in Figure (4.4). All implemented parameters for modelling the different components are explained in the following paragraph.

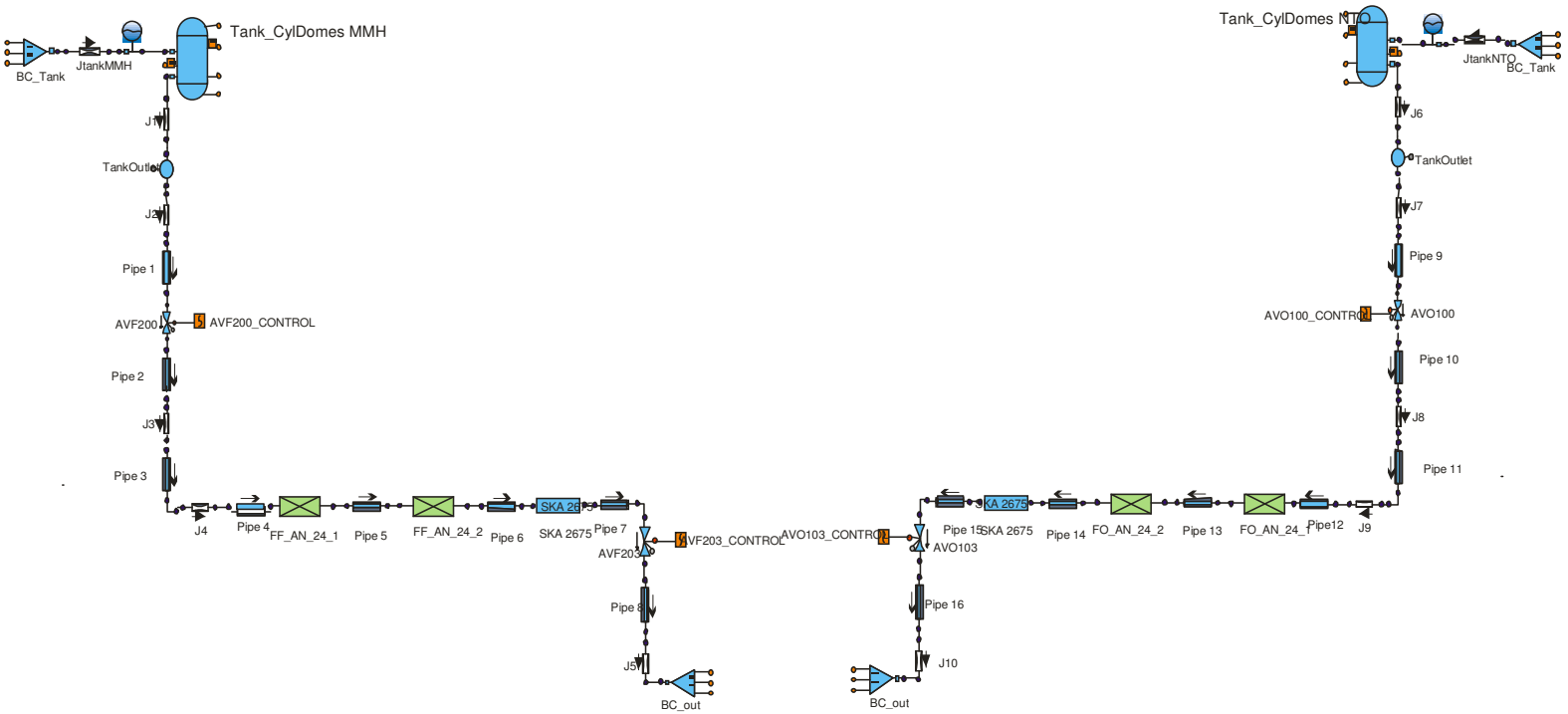

Figure 4.4 – Complete P2 schematic modelled in EcosimPro

4.3.2. P2 components

Runtank

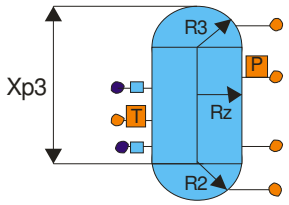

Figure 4.5 - Running tank schematic 1

A runtank model, as depicted in Figure (4.5), has been chosen from the EPSS EcosimPro library as a 1DCylindricDome-tank. This component incorporates the relevant equations for conservation of energy, mass, and state equation. Two fluids can be contained: a liquid which can evaporate and boil, and a pressurizing gas as a non-condensable gas. The phase of the existing fluid in the tank depends on the boundary condition and an initial condition imposed on the system, and is calculated automatically from the code. In the specific case of P2 test bench MMH and NTO are chosen as main fluids and Nitrogen as pressuring gas.

The CylDomeTank considers a constant or a dynamic heat transfer between the fluid and the tank walls. The dynamic model is based on Prandtl, Grashof, Rayleigh and Nusselt numbers and an additional external heat source is feasible for modelling the insulation layer according to its conductance properties. However, no great stress is put upon the heat transfer for the analyzed case: temperature of the gas, liquid and wall is set homogeneous and equal to room temperature (290 K).

The heat exchange model for the vaporization exchange in mass between liquid and gas volume is made without taking into account any boiling phenomena.

The tank component is subdivided into *n* discrete volumes of the same size according to a staggered grid in the liquid and gas side. According to the present analysis no thermal stratification has been considered for the tanks and the number of fluid volumes is chosen equal to 1.

The complete set of input parameters, from Reference [22],. is presented in Table (4.3).

Table 4.3- Tank schematic input parameters

DESCRIPTION	VALUE	PROPELLANT
Lower dome radius (m)	0,378	NTO/ MMH
Upper dome radius (m)	0,378	NTO/ MMH
Cylindrical part radius	1,476	NTO/ MMH
Elevation of the tank bottom relative to body axis (m)	1,0745	MMH
Elevation of the tank bottom relative to body axis (m)	1,476	NTO
Walls thickness (m)	0,02	NTO/ MMH
Wall material	Steel 321	NTO/ MMH
Initial liquid temperature (K)	290	NTO/ MMH
Initial gas temperature (K)	290	NTO/ MMH

The cylindrical portion at the outlet is modelled as an equivalent cylindrical capacity EcosimPro component with same volume as the real one (red part in Figure (4.6)) in order to account for the accumulation of mass in this section and the change in direction of the fluid. This component is an adiabatic volume with a given number of fluid ports. The basic equations of conservation of mass and energy account for density and temperature calculation. No momentum equation is implemented so that no pressure drop is considered. No fluid wall interaction is implemented.

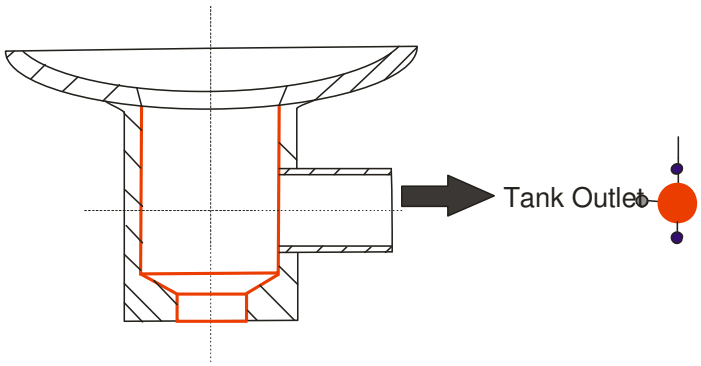

Figure 4.6 - Tank outlet schematic

The input data are presented in the Table (4.4).

Table 4.4- input parameter volume component

DESCRIPTION	VALUE	PROPELLANT
Fluid volume (m^3)	0.0016	NTO/ MMH
Volume height (m)	0.2245	NTO/ MMH
Elevation at the bottom relative to body axis (m)	1.476	NTO
Elevation of the of the volume bottom relative to body axis (m)	1.0745	MMH
Ports angle (deg)	{0, 90}	NTO/ MMH

The potential energy content of the fluid is simulated by means of the introduction of an other EcosimPro components *Junction*. This element is the basic resistive element component and it represents a concentrated loss with constant throat area and sonic velocity limitation. By means of those, the vertical position of the fluid ports is specified and the correspondent energy content calculated:

$$\Delta P_j = \rho g (z_{top} - z_{jun,j}) \tag{4.1}$$

With the junction at the tank outlet it is possible to simulate the exit area of the tank in terms of pressure losses and limitation of the mass flow rate.

The input parameters for the junctions are: the z-position, the cross section for which the corresponding pressure drop is calculated and the loss coefficient. For the choice of the latter see the next section.

Feed Line

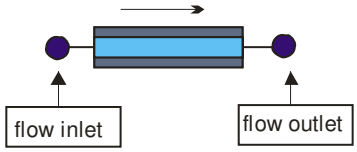

Figure 4.7 - Pipe element schematic

The lines are implemented with equations of mass that account for fluid density calculation, energy for the temperature, and state equations for pressure. Also, the momentum equation accounts for distributed pressure loss calculation. The component used is the basic *Pipe* component, a cylindrical area-varying pipe with a non-uniform 1D mesh. It is programmed with an internal pressure, temperature and content of non-condensable gas. These variables are stoked junction-wise, on the first and the last junction of the component and the equations governing the flow are solved numerically to retrieve the profile of the relevant flow variables, density and pressure losses. The inlet and the outlet flow are calculated due to pressure differences from inlet to internal, and internal to outlet.

It's also included model for the heat transfer with either a constant or variable heat transfer coefficient. However, in this case, no important contribution is expected from the heat exchange between the wall of the pipes and fluid.

For the simulation of the feed lines, each diameter, length and change in height, direction or cross section of the pipes have to be listed and implemented in the code. Dedicated input tables account for the variation in cross section in terms of non-dimensional cross section (diameter/nominal diameter) versus non-dimensional axial position (axial length/ total length).

The hydraulic diameter of the first control volume is chosen for friction loss calculations and concentrated bend loss calculations. This choice made in the code implementation has to be considered in further line-loss specifications.

A uniform grid size distribution is used in all pipes. The numerical *centred* scheme is selected: state variables (pressure, temperature, velocity) are discretized in the cell centre and the flow variables (mass flow, enthalpy flow) are discretized at the cell interface.

The variation in the height of the line and the corresponding change in potential energy, as well as the additional losses due to the presence of bends on the lines are implemented with a J*unction* component. An important point about flow line simulation is to retain the actual pressure losses in the line. There are two main sources of loss: friction, as a distributed loss on the pipelines, and presence of elbows and bends, as a local concentrated loss. For the former, a model accounting for pressure losses already exists in EcosimPro and is presented in the following section. For the latter, the existing function in the *Pipe* schematic is not fulfilling the line features. For a corresponding simulation, the presence of bends is modelled with a *Junction* located in the specific positions.

The input data are presented in Table (4.5) and a complete description of the individual parameters is given in Section 4.3.3.

Table 4.5 – Bends schematic input parameters

DESCRIPTION	**VALUE**
Junction elevation relative to a body axis system J3 (m)	0.38
Junction elevation relative to a body axis system J4 (m)	0.37
Junction elevation relative to a body axis system J8 (m)	-0.017009
Junction elevation relative to a body axis system J9 (m)	0.0076915
Junction area when fully open J3 J4 J8 J9 (m^2)	π*(pipe radius)^2
Loss coefficient J3/ J8	0.41
Loss coefficient J4/ J9	0.47

Valves

Two security ball-valves are present for every line (NTO and MMH side).

A ball valve is a valve with a spherical disc, which controls the flow through it. The sphere has a hole through the middle so that when it is in line with both ends of the valve, flow will occur. When the valve is closed, the hole is perpendicular to the ends of the valve, and flow is blocked.

These shut-off valves are mainly described by an area-varying dependent pressure loss equation implemented in the EcosimPro system. An internal gas state is not considered. A heat transfer model is not implemented in the code of the component and not needed due to the small dimension of the valve compared to the overall system.

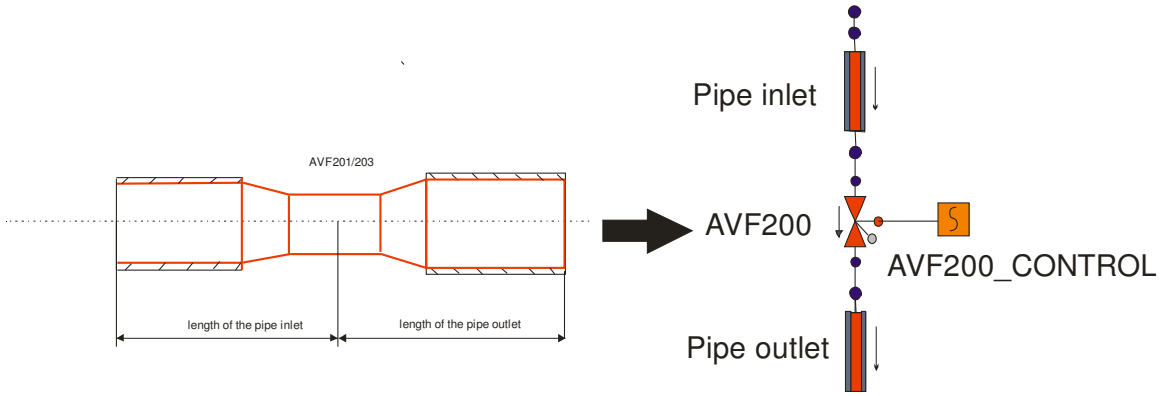

Figure 4.8 - P2 ball-valves schematic

A discharge coefficient sourced for the pressure loss in the system. The determination of the discharge coefficient is described in the following section. For mass flow calculation through the valve, the equation of subsonic and supersonic orifice flow is used. The schematic input values are listened in the Table (4.6).

Table 4.6 - Valve schematic input parameters

DESCRIPTION	**VALUE**
Area when fully opened AVF/ AVO (m^2)	π*(throat radius)^2
Loss coefficient AVF/ AVO	0
Elevation at the bottom relative to body axis AVF200 (m)	0.915
Elevation at the bottom relative to body axis AVF203 (m)	0.130
Elevation at the bottom relative to body axis AVO100 (m)	0.970
Elevation at the bottom relative to body axis AVF103 (m)	0.230

The valve displacement time is regulated by a control block that opens and closes the device following a given time table. For the test case analysed in Chapter 6, no displacement of the P2 safety valve is considered.

Flow-meters

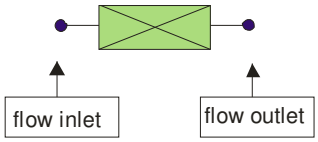

Fig.4.9 - Schematic of the flow meter

Two flow meters are available for every line (NTO and MMH). The flow meters used in P2 test bench, are of turbine type and no basic EcosimPro component can be used for modelling those. The creation of a new item is then necessary. The component is mainly simulated by a pressure drop, function of the specific characteristics of the device and the mass flow rate crossing it. The basic pressure drop equation is used as explained in full in Section 4.3.3.

The input parameters are listened in Table (4.7).

Table 4.7 - Flow meters schematic input parameters

DESCRIPTION	**VALUE**	
Junction elevation relative to a body axis system (m)	0.38	FO_AN_241/ FO_AN_242
Junction elevation relative to a body axis system (m)	0.37	FF_AN_241/ FF_AN_242
Reference pressure loss (Pa)	98066.52 * 0.49	FO_AN_241/ FO_AN_242
Reference pressure loss (Pa)	98066.52 * 0.49	FF_AN_241/ FF_AN_242
Reference mass flow rate (kg/s)	5.96	FO_AN_241/ FO_AN_242
Reference mass flow rate (kg/s)	5.96	FF_AN_241/ FF_AN_242

Filters

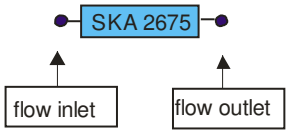

Fig.4.10 - Schematic of the filter

The filters present on the line are also mainly modelled by a pressure drop equation accounting for the specific component behaviour. A new EcosimPro component has been created to match the actual discharge coefficient of the filter. See section 4.3.3 for a more detailed description.

The input parameters are listened in Table (4.8).

Table 4.8 - Filter schematic input parameters

DESCRIPTION	VALUE	NAME
Junction elevation relative to a body axis system (m)	0.38	SKP2675_OX
Junction elevation relative to a body axis system (m)	0.37	SKP_2675_FU
Interpolation coefficient k_0	-0.017009	SKP2675_OX
Interpolation coefficient k_1	0.0076915	SKP2675_OX
Interpolation coefficient k_2	0.0164048	SKP2675_OX
Interpolation coefficient k_0	-0.019974	SKP_2675_FU
Interpolation coefficient k_1	0.0090417	SKP_2675_FU
Interpolation coefficient k_2	0.0166169	SKP_2675_FU

4.3.3. Simulation input parameters

Friction losses

The pressure losses along a straight tube of constant cross section are calculated from the Darcy-Weisbach equation:

$$\Delta P_{FR} = \zeta_{FR} \frac{\rho v^2}{2} \tag{4.2}$$

The loss coefficient ζ_{FR} is calculated according to the equation:

$$\zeta_{FR} = f \frac{L}{D_H} \tag{4.3}$$

The use of the hydraulic diameter D_H as the characteristic length in the resistance Equation (4.3) is acceptable only when the thickness of the boundary layer is very small compared to the pipe cross section. For turbulent flow D_H is the optimum parameter to use. The hydraulic resistance of laminar flow can not be evaluated using D_H as a characteristic length and appropriate correction have to be made.

The friction factor *f* is a function of the local Reynolds number and the relative roughness of the pipes, and it is implemented in the code as the following relation valid for laminar, turbulent and transient flow:

$$f = 8\left[\left[\frac{8}{\mathrm{Re}}\right]^{12} + \frac{1}{(A+B)^{3/2}}\right]^{1/12} \tag{4.4}$$

where:

$$A = \left[2.457 \ln \frac{1}{(7/\mathrm{Re})^{0.9} + 0.27\varepsilon / D_H}\right]$$

$$B = \left[\frac{37530}{\mathrm{Re}}\right]^{16}$$

The calculations are automatically carried out by the code using the rugosity and geometrical input parameters. A value of the roughness for steel feed line pipes is chosen, for the first attempt, equal to 0.000575 m, as from Reference [23]

Pressure losses of pipe bends

Bending of a flow in curved tubes and channels results in the appearance of centrifugal forces directed from the centre of curvature to the outer wall of the tube. This causes an increase of the pressure at the outer wall and a decrease at the inner wall. The flow velocity will correspondingly be lower at the outer wall and larger at the inner wall. Thus a diffuser effect occurs near the outer wall, leading to a flow separation from both walls. The behaviour of the

flow when flowing from a curvature into a straight section is accompanied by these effects in the reverse order.

The appearance of centrifugal forces and the presence of boundary layers at the walls explain the occurrence of a transverse flow with vortex-formation, superimposed to the main flow parallel to the channel axis.

The main portion of pressure losses in curved tubes is due to the formation of eddies at the inner wall, together with secondary flows. The magnitude of the resistance coefficient and the flow structure vary within the following main factors: Reynolds number, rugosity, bending angle, relative radius of curvature (r/D) of the pipe.

In the majority of cases the total loss coefficient of the elbows and bends is due to two contributions: a local resistance of the bend and friction effects.

The total loss coefficient of pipe bends is implemented in the code as the result of the following coefficient for the effect of an bending angle:

$$\zeta_{ANGLE} = 0.957\frac{\alpha}{90} + 0.266\sqrt{\frac{\alpha}{90}} + 0.407\sin(\alpha) - 0.833\sin(\alpha/2) \tag{4.5}$$

And for the radius effect:

$$\zeta_{RADIUS} = 0.21\sqrt{\frac{R}{D}}\frac{\alpha}{90}\ for(R/D > 1)$$
$$\zeta_{RADIUS} = 0.21\left(\frac{R}{D}\right)^{2,5}\frac{\alpha}{90}\ for(R/D < 1) \tag{4.6}$$

And for roughness effect:

$$\zeta_{RUG} = MIN\left(2{,}1 + 10^6\left(\frac{\varepsilon}{\mathrm{D}}\right)^2\right) for(R/D > 1.5)$$
$$\zeta_{RUG} = MIN\left(2{,}1 + 103\left(\frac{\varepsilon}{\mathrm{D}}\right)^2\right) for(R/D < 1.5) \tag{4.7}$$

Finally the total pressure loss calculated for a pipe bend is:

$$\zeta_{BEND} = \zeta_{ANGLE}\zeta_{RUG}\zeta_{RADIUS} \tag{4.8}$$

In the EcosimPro *Pipe* model these equations are implemented and led to pipe bend loss calculations when the number of bends, the radius of curvature and the angle of curvature are

specified. A problem arises for the choice made by the program for the *D* value: the diameter used as the reference value is the hydraulic diameter of the first control volume of the pipe numerical grid. This leads to errors if the pipes have a variable cross section. In the specific case of the investigated P2 pipes this occurs and a correction is made to compensate that effect: the previous pipe component is divided into two separate components where the bend is present and a *Junction* component is added to account for the local pressure losses. The value of the loss coefficient in the pipe is then calculated according to Equation (4.8). In Table (4.9) the specific value for the junctions are summarized.

Table 4.9 - Input values for Junctions

$\alpha(deg)$	R_{BEND} (m)	D (m)	R/D	ζ_{ANGLE}	ζ_{RADIUS}	ζ_{RUG}	Min (2, ζ_{RUG})	ζ_{BEND}	NAME
90	0.04	0.0384	1.04	1	0.2	2.49	2	0.41	J3/ J8
90	0.04	0.034	1.17	1	0.19	2.69	2	0.47	J4/ J9

For the *Junction* not mentioned no special assumptions are made and the loss coefficient is automatically calculated by the code from the orifice area and the adjacent connected flow area assuming an abrupt area change.

Flow meter pressure losses

The turbine flow meter is mounted directly in the flow line and consists of a cylindrically bored housing, a flow straightener and turbine assembly and a magnetic pickup as shown in the Figure (4.10). Flow passing through the turbine causes it to revolve at a speed directly proportional to fluid velocity. The signal frequency will then be similarly proportional to the volumetric flow rate, and then give the flow rate measurement.

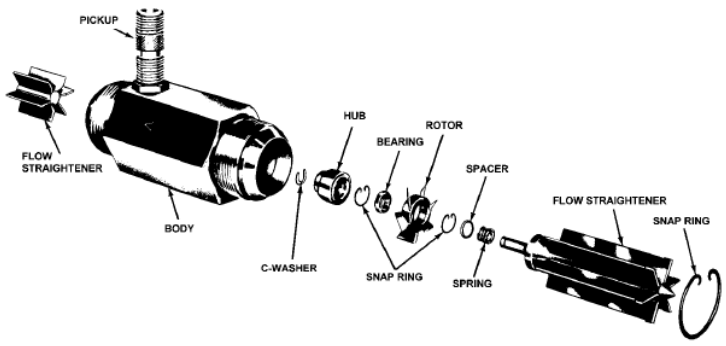

Figure 4.11 - Turbine flow meter

As can be inferred from the functional description above, the turbine flow meters pressure losses are mainly linked to two different components:

- Pressure loss due to the complete volume of the cylindrical housing, essentially of a hydrodynamic type, and thus proportional to the dynamic pressure of the incoming flow and to the inlet cross-section
- Pressure loss due to the turbine element in the flow, split into hydrodynamic component and a component linked to the lift on the blade. The former could be summed to the first one and considered as a single pressure drop. The latter is very small and could be neglected for the case analysed.

From calibration data, a reference value of the pressure drop for a reference mass flow rate is known. Using the calibration as input data, a dynamic pressure drop relation, as a function of the mass flow rate, was calculated.

$$\Delta P = \frac{\dot{m}^2}{\dot{m}^2_{ref}} \Delta P_{ref} \tag{4.9}$$

The input value $\dot{m}^2_{ref}$, ΔP_{ref} are obtained from manufacture data. Using this relation (4.9) he code of the basic EcosimPro resistive element is changed. In the following lines only the code fundamental lines are discussed:

dP_loss = (dP_NOM*(m**2))/(m_NOM**2)

Figure (4.12) shows the behaviour of the EcosimPro component modified in terms of pressure loss vs. mass flow rate

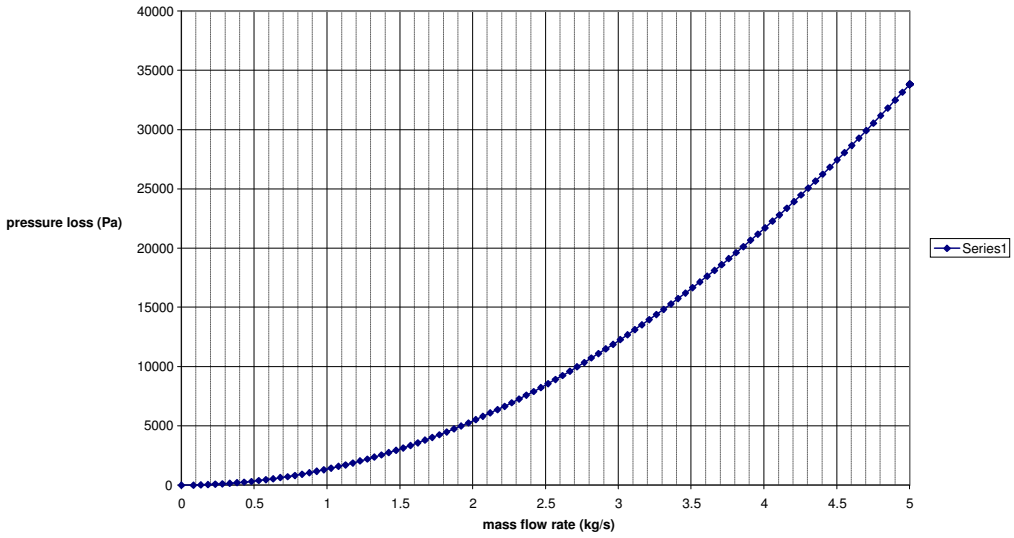

Figure 4.12 – Flow meters pressure drop

Filter pressure losses

Two filters are present on the lines have different characteristics and they contribute to the pressure losses of the feed line. The pressure loss in this component is obtained from the interpolation of a quadratic curve for the specific type of filter:

$$\Delta P = k_0 + k_1 \dot{m} + k_2 \dot{m}^2 \qquad (4.10)$$

The value of the coefficients k_0, k_1, k_2 is obtained from manufacture data.

In the following lines only the code fundamental lines are reported:

dP_loss = 1e5*(k0+k1*m+k2*m**2)

In Figures (4.12) and (4.13) are plotted the behaviours achieved in the EcosimPro component modified in terms of pressure loss vs. mass flow rate. The provided curve resulted in negative pressure losses for small flow rates so that a related correction is necessary before the implementation in the code.

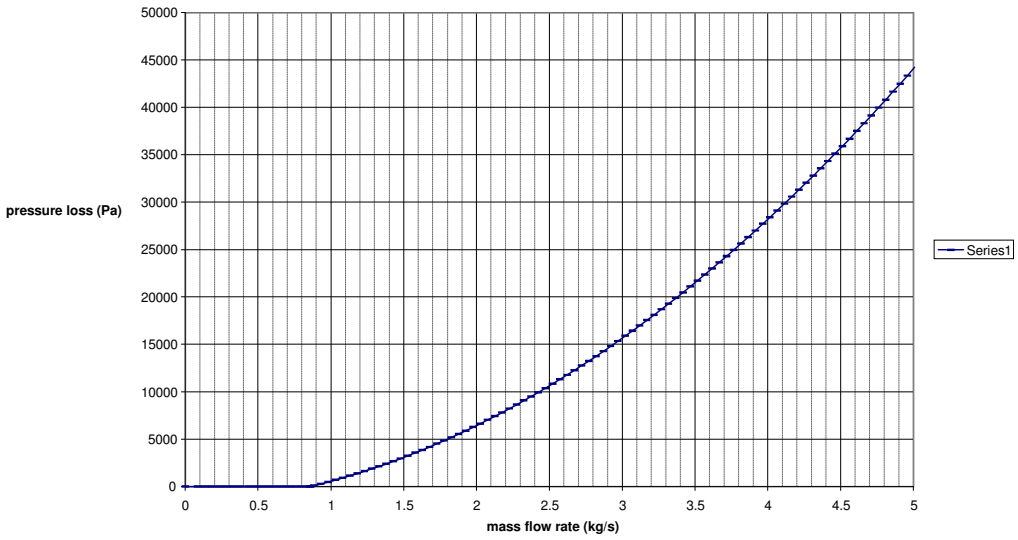

Figure 4.12 – Fuel line filter pressure loss vs. mass flow rate

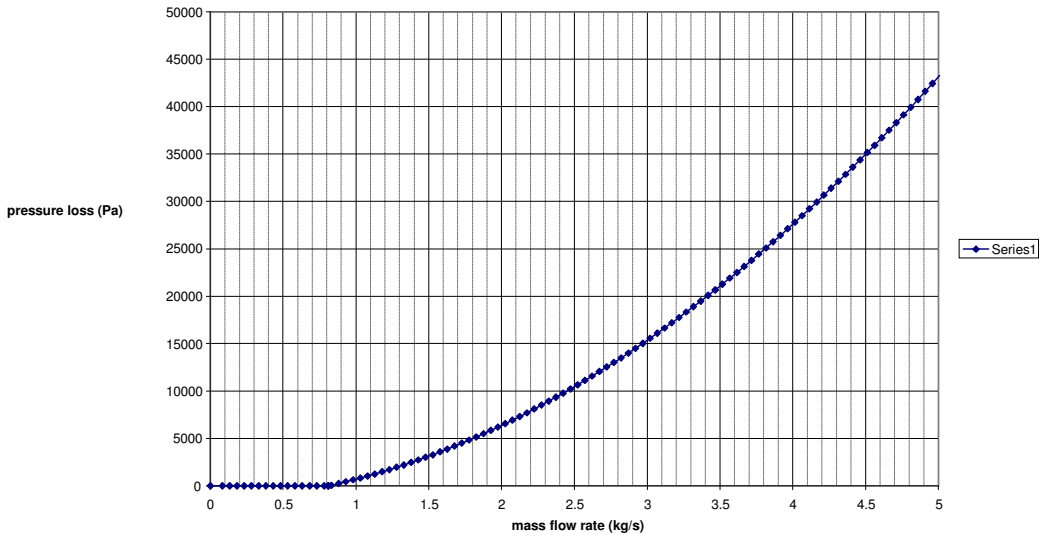

Figure 4.13 – Flow meters pressure loss vs. mass flow rate

4.3.4. Lines characteristics verifications

According to the input choices made, the steady state behaviour of the two feed lines was analysed for a primary validation of the model. The input parameter parameters are given in Table (4.10).

Table 4.10 – Schematic input parameters. -

Tank pressure (Pa)	20e5
Tank temperature (K)	290
Environment temperature (K)	290
Lines initial pressure (Pa)	20e5
Lines initial temperature (K)	290
Pressurant gas	nitrogen

The pressure of the tanks is kept constant as well as the temperature which is set equal to the ambient temperature. The boundary conditions, in terms of back pressure, are changed from the storage propellant tanks pressure of 20 bar to 0 bar. The steady state is then investigated and variation in terms of mass flow rate is reported in Figure (4.14) as function of the backpressure.

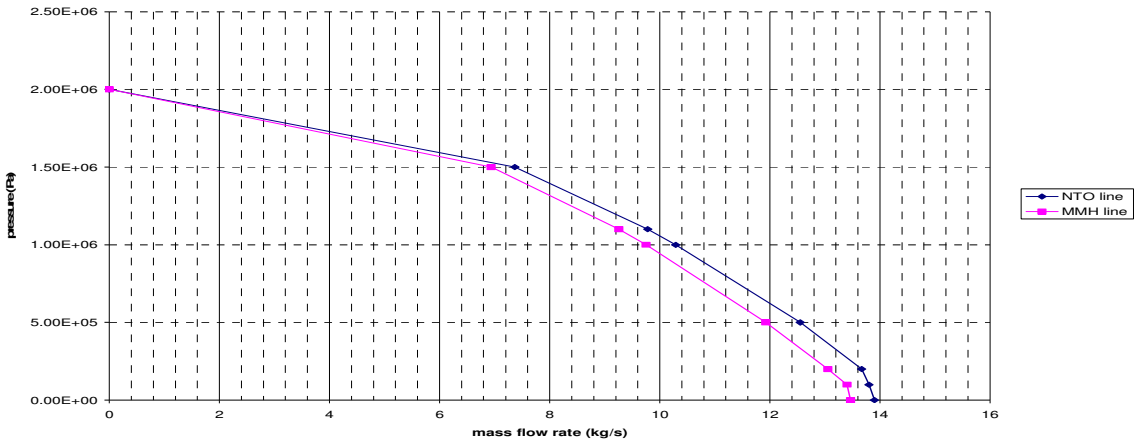

Figure 4.14 - Mass flow rate vs. back pressure

5. TESTED ENGINE

5.1 Introduction

The Ariane 5 was a completely new launcher compared to the past Ariane 1 to 4 vehicles.
It was developed under the direction of as cooperation between ESA and under the technical lead from CNES. The work started in 1988 and the first design was sized for the Hermes manned spacecraft, which was later cancelled. As a result, development of an upper stage version capable of launching two geosynchronous satellites at a time was funded. The pressure fed upper stage engine AESTUS is one of the two configurations currently available for this purpose.
In the following chapter the Ariane 5 and more specifically its upper stage are described. Then the correspondent EcosimPro model is presented.

5.2. General overview

5.2.1. Ariane 5

The heavy launch vehicle Ariane 5 has completed is development with two successful qualifications flights in 1997 and 1998.
The launch vehicle Ariane 5 is basically a three stage vehicle (EAP-EPC-EPS/ESCA). Two solid boosters provide 90 % of Ariane 5's thrust at lift-off. A cryogenic core stage, ignited on the ground, provides the remaining thrust for the first part of the flight after the booster separation until the upper stage separation.

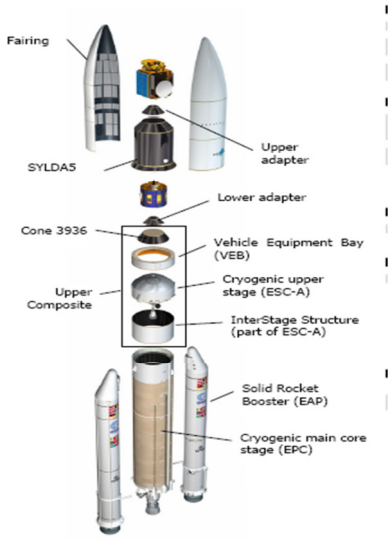

Figure 5.1 - Ariane 5ESC

Ariane 5's cryogenic main stage is called EPC (Étage Principal Cryotechnique). It consists of a large tank 30m height with two compartments, one for liquid oxygen and the other for liquid hydrogen, and a Vulcain engine at the base with a thrust of 115 tons. Attached to the sides there are two solid boosters EAB (Étage d'Accélération à Poudre), each delivering a thrust of about 630 tons.

Depending on the payload, different configurations are available, based upon the utilization of different upper stages. The ESCA (Étage Supérieur Cryotechnique version A) uses cryogenic propellants, liquid hydrogen and liquid oxygen, while the EPS (Étage à Propergols Stockables) has a storable propellant engine, fuelled with MMH and NTO.

The original Ariane 5 launcher was the Ariane 5G, currently terminated. The following generation, Ariane 5E, is based on the powered first cryogenic stage engine Vulcain 2. This engine provides an increase in thrust through an overall mixture ratio and liquid oxygen mass increase. It is able to place heavy payload in GTO, to injection into sun synchronous or polar orbit as well as for launching the space tugboat ATV towards the ISS.

Two satellites can be mounted using a SLYDA (System de Lancement Double Ariane). Three satellites are possible using the SPELTRA (Structure Porteuse Externe Lancement Triple Ariane). Up to eight secondary payloads, small satellites or experimental packages, can be carried with an ASAP (Ariane Structure for Auxiliary Payloads) platform.

The typical sequence of events for a GTO mission is given in Figure (5.2).

The cryogenic main core is ignited and burns for 7 s before the solid boosters start operating initiating the lift-off. Separation of the boosters occurs at burn out of the EAP's close to 140 s after main engine ignition. Fairing separation follows at 190 s.. The main stage shut-down occurs when the intermediate target orbit is reached and separation happens 6 s after. The detached main stage starts the re-entry procedure and splashdown in the Atlantic Ocean for standard mission. The upper stage ignition occurs after few seconds after the separation. The upper stage cut-off happens when the final orbit is reached

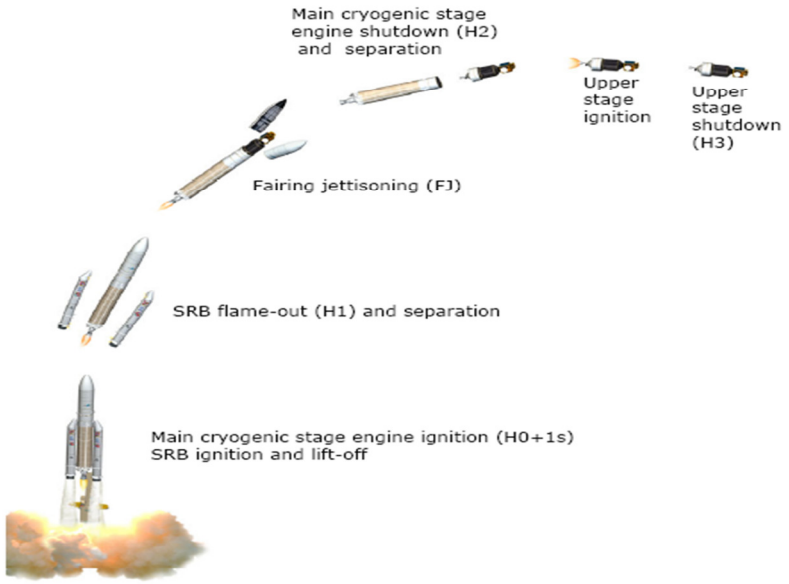

Figure 5.2 - Ariane 5 mission profile.

5.2.2. The upper stage engine: AESTUS

ASTRIUM Space Transportation is responsible for the entire Ariane 5 Upper Stage EPS, with the AESTUS engine. The engine was developed at the Ottobrunn Space Propulsion Center during the period from 1988 to 1994. The first operating flight of AESTUS was on Ariane 5 flight 502, launched in 1997.

The AESTUS engine is the key propulsion component of the upper stage and provides a thrust of 30 kN and the required specific impulse for payload insertion in GTO, LEO and SSO. Using its re-ignition capability, AESTUS can be used also on ES-ATV version of the Ariane 5 for the placement of the Automated Transfer Vehicle (ATV) into LEO.

During the period from 2003 to 2006, the engine underwent a re-ignition qualification program in readiness for the first launch of the ATV, and the in-orbit re-ignition was demonstrated during the first flight of ATV aboard Ariane 5 flight 528, on March 9th 2008.

In ATV mode the first ignition occurs immediately after the separation of the upper stage/ATV composite from the main cryogenic stage. At the end of the first burn, a ballistic phase commences and lasts for 45 min. A second ignition provides a short duration burn for injecting the ATV into the target LEO, after separation from the upper stage. A third final ignition is used for de-orbiting the upper stage into a safety re-entry trajectory for burn-up in the upper atmosphere.

The AESTUS engine consists of the following elements:

- Cardan located at the top of the injector

- Coaxial injector
- Combustion chamber regeneratively cooled by fuel
- Nozzle extension radiatively cooled
- Propellant valves for fuel and oxidizer, pneumatically operated
- Propellant and pressurant lines
- Actuators struts to gimbal the engine in the pitch and the yaw direction. The electromagnetic activation elements are part of the stage.

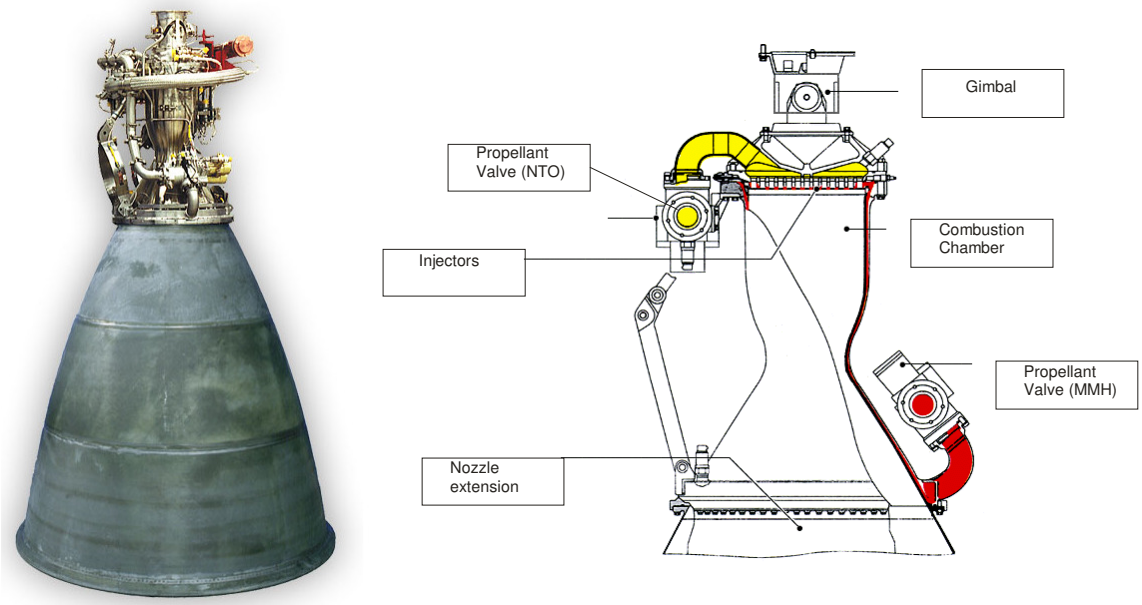

Figure 5.3 - AESTUS

The propellants used are: NTO and MMH, with an oxidizer-fuel ratio (O/F) of 1.9. The initial operating mixture ratio was 2.05 - also in the first flights - which was later reduced in the frame of an EPS stage performance improvement program which included MMH tank elongation.

Both of these propellants are liquid at room pressure and temperature and can be safely stored. Ignition of the engine results from the hypergolic chemical reaction that occurs spontaneously when the propellants meet in the combustion chamber. The thrust chamber is composed of a single combustion chamber gimballed to allow 7.5° of thrust vector control and a bell-shaped nozzle with an expansion ratio of 85.

AESTUS is a pressure-fed system. The stage feedsystem consists of two fuel tanks and two oxidizer tanks. The fuel tanks and oxidizer are cylindrical with spherical poles. Different lengths of the tanks are given due to the different volumes of fluid required. The shape is a result of a balance between walls thickness and safety in storing the propellant at the suitable propellant pressure, in order to minimize the structural mass of the stage.

The fuel and oxidizer tanks are pressurized with helium from a pair of high pressure spherical tanks. The helium is stored at 400 bar and then the pressure is set, by a dedicated pressure regulator, to 23 bar. The propellant is delivered to the engine at 17.8 bar. The combustion chamber itself operates at 11 bars.

The AESTUS thrust chamber design is based on the regenerative cooling concept. Prior the combustion the MMH is pressurized into a distribution manifold, causing then the fuel to flow trough narrow, closely arranged channels built in the combustion chamber, thus ensuring the cooling. The MMH enters the injectors' head where a manifold produces a uniform flow rate for the 132 parallel injector elements.

The injectors are of coaxial type where the NTO is injected in the centre while the MMH via radially shaped slots around. The design of the injector elements causes swirl mixing and atomization of the propellants, assuring a combustion efficiency of 98% to be realized during the combustion process in the combustion chamber at the throat.

Upon leaving the injectors elements and entering the combustion chamber, the hypergolic propellant spontaneously ignite and are burned and accelerate up to sonic conditions at the throat.

Varying the number of the coaxial elements, the basic AESTUS design can be used to higher or lower thrust levels compared to the basic one of 30 kN.

The combustion temperature in the chamber reaches about 3000 K. Controlling this temperature and separate it from the storable fuel at about 290 K only by a stainless steel wall was one of the major challenges during the engine development.

After leaving the combustion chamber the final acceleration of the hot gases to supersonic velocities is achieved by the expansion in the nozzle extension.

While the combustion chamber and the throat nozzle are regeneratively cooled the nozzle extension dissipates heat by radiation.

Before the engine is started, the system is purged with helium to clearly separate the primed propellants. The oxidizer valve is opened, followed after a short delay, by the fuel valve. The full thrust is delivered after 0.4 s the start signal.

The shutdown is initiated with MMH valve closure, followed shortly by the closure of the oxidizer valve. The engine is then purged with helium to control the shut down process.
and to prepare the engine for the restart. The restart capacity has been proved for an improved range of orbit options. The standard total burn time is 1100 s, and vacuum exhaust velocity is 3420 m/s. Table (5.1) summarises the performance characteristics of AESTUS engine.

Table 5.1 AESTUS performance characteristics

Vacuum thrust	30 kN
Vacuum specific impulse	324 s
Total propellant mass flow rate	9.308 kg/s
Propellant mixture ratio (NTO/ MMH)	1.90
Chamber pressure	11 bar
Characteristic velocity	1.684 m/s
Engine feed pressure	17.8 bar
Nozzle area ratio	85
Engine mass	111 kg
Nominal single firing (GTO)	1100 s

5.3. AESTUS EcosimPro model

5.3.1. General overview

In this section the components of the AESTUS EcosimPro model are described and the important physics used for the components is explained together with the input parameters. The NTO and MMH complete feed lines are modelled and all important physical phenomena are taken into account.

The EcosimPro model is built from single hardware components. Every single component has its own code and is connected by ports to the other components. The ports define the inlet value of a component as temperature and pressure. Special components are then needed for setting boundary conditions as function of time. When everything is linked together, the model is established.

The function and the layout of these components are described in detail in Section 5.4. The complete list of items simulated is given in Table (5.2).

Fuel side	Oxidizer side
Calibration orifice	Flexible hose
Flexible hose	Engine valve
Engine valve	Dome
Inlet manifold	Injector
Cooling channels	
Dome	
Injector	

Table- 5.2- AESTUS schematic components

The complete AESTUS model is presented in the Figure (5.4) and all the choices made for modelling the different components are explained in the following paragraphs.

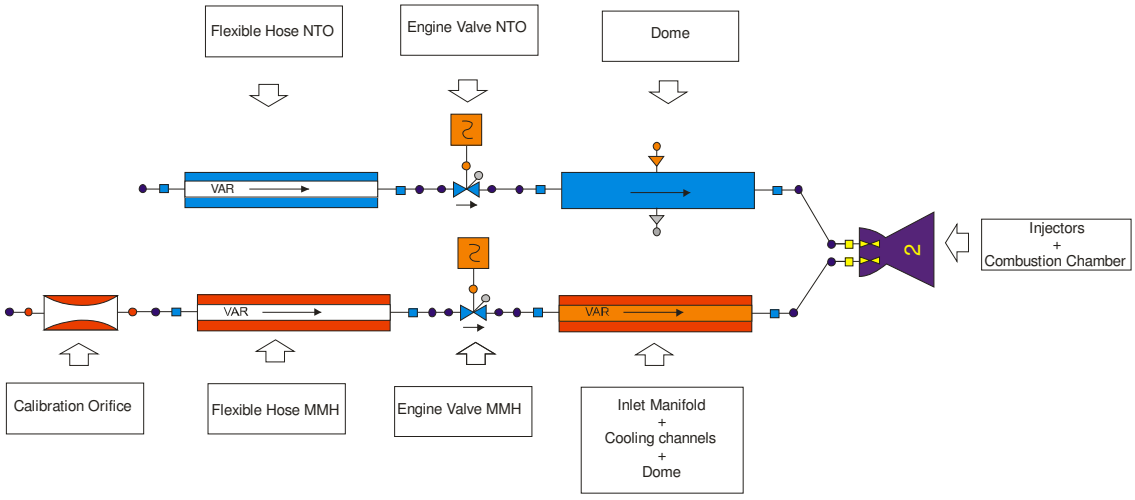

Figure 5.4 - AESTUS schematic

5.3.2. AESTUS components on fuel side

Fuel line set

The fuel line setup enables the fuel flow from the MMH combiner to the fuel valve assembly. To fulfil the gimbal capability of the engine, the fuel side is equipped with a flexible hose, a convoluted stainless tube. The ends forming the interface to feed system (MMH combiner outlet) and the valve assembly are rigid tubes. The sealing of these interfaces is provided by an O-ring.

The fuel line set also includes the fuel calibration orifice, by which the required nominal O/F ratio can be adjusted to maximize parallel consumption of both propellants. The orifice

diameter is determined during the engine calibration depending upon the C_D value of the individual components.

Based upon the experience with previous models the inner or calibration diameter of the orifice is predicted in the range of 17 to 24 mm. The final diameter will be adjusted according to ΔP measurement.

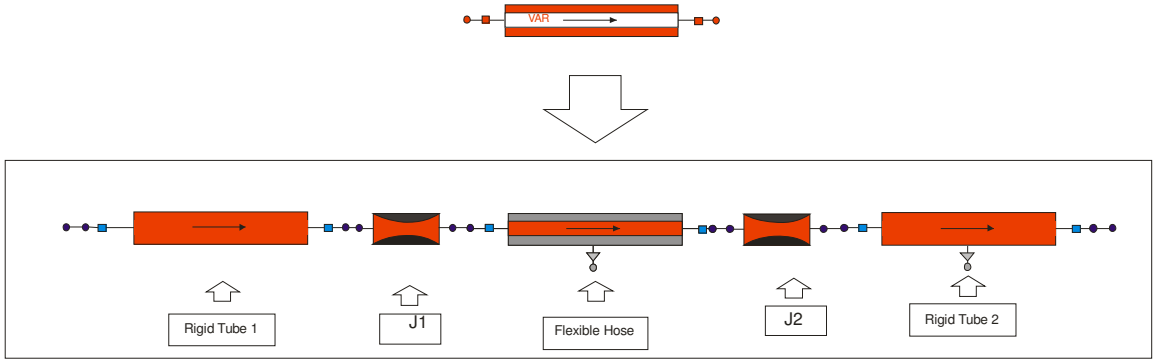

Figure 5.5 - Fuel line schematic

The fuel line assembly is simulated by alternation of *Pipe* and *Junction* elements.

The calibration orifice is mainly represented by a pressure drop equation with sonic speed limitation implemented in the *Junction* component. The value of the loss coefficient is calculated to get the desired value for the pressure drop as presented in Section 5.3.

The flexible hose is simulated by means of a *Pipe* component with characteristic equivalent values for thickness and Young's modulus, to account for the specific mechanical behaviour.

The rigid tubes at the ends are obtained by means of *Tube* components. *Tube* and *Pipe* are essentially the same component, however in the former no fluid-wall interaction is considered. A greater influence of this kind of phenomenon is perceptible in flexible tube and can be considered to be a negligible influence in rigid stainless steel pipes.

Equation of mass, energy, state and momentum are implemented for density, temperature, pressure and pressure loss calculations. The components are programmed with an internal volume and inner pressure and temperature. The inlet and outlet mass flow rate is calculated due to the pressure differences from inlet to outlet of the *Pipe.*

The *Junction* accounts for the pressure losses present on the item. The value of the loss coefficient are dedicated to the specific components in order to achieve the right pressure loss on the line as form Reference[24]. In section 5.4 the detailed calculations are described.

The set-up of input parameters is presented in the Table (5.3).

Table 5.3 – Fuel line set schematic input parameters

Area when fully opened J1/ J2 (m^2)	0.001257
Loss coefficient J1/ J2	1.17
Length flexible hose (m)	0.5438
Internal flexible hose diameter (m)	0.040
Equivalent flexible hose thickness (m)	0.005
Young modulus	3.14e9
Length rigid tube 1 (m)	0.200
Internal rigid tube 1 (m)	0.040
Length rigid tube 2 (m)	1
Internal rigid tube 2 (m)	0.040

Engine Valve (MMH)

The fuel valve assembly is composed of five components:

- main valve
- main pilot valve
- purge pilot valve
- purge valve
- check valve.

The same valve assembly is also present in the oxidizer side.

The check valve is located between the purge valve and the propellant outlet port, sealing off the propellant from entering the purge valve.

The main valve provides or cut-off the propellant, while the purge valve feeds the helium at the valve shut off, to push possible residual propellants out of the main valve. This valve is closed by means of a loaded spring and then pneumatically opened by the force exerted by the pressurized helium on a piston. The helium pressurization is obtained by a latch 3-way valve piloted by a solenoid. To open the valve the solenoid coils are pulsed with voltage and the electromagnetic force moves an armature. Then the control pressure of the helium is enough to drive the pistons which finally move the poppets of the main and purge valve. The pilot valve is bi-stable so that the opening and closing is only

initiated by short command durations - latching is done over magnetic forces.

For the present analysis, the valve considered is the main valve of the assembly because of its direct influence on fluid behaviour in terms of pressure losses and mass flow rate control. The

others are taken into account as time delay on the propellant release. The engine valves simulated in the model are mainly described by an area-varying dependent pressure loss equation implemented in the EcosimPro component.

A loss coefficient is used for the pressure loss calculation. The determination of the loss coefficient is described in Section 5.4.

The volumes associated with this device are implemented as extra volumes in the components upstream and downstream the valve.

Due to the small dimensions of the valve, the code of the component does not need the implementation of a heat transfer model, which is neglected.

The input parameters can be seen in Table 5.4.

Table 5.4 - Engine valve (MMH) schematic input parameters

DESCRIPTION	**VALUE**
Area when fully opened FV (m^2)	0.00314159
Loss coefficient FV	0.428

The valve displacement time is regulated by a *Control Block* that opens and closes the device following a given table in time. The time table is directly obtained from valve testing results and allows for the representation of the whole valve characteristic.

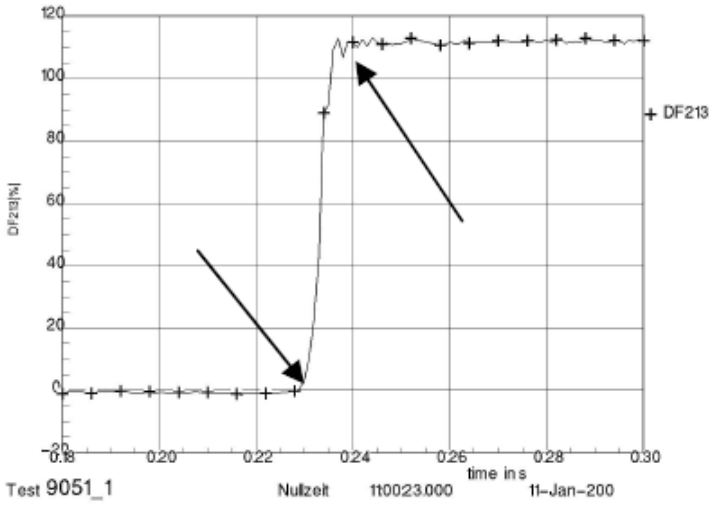

Figure 5.6- Valve opening characteristics [24]

Cooling Channels

The coolant inlet manifold is located at the divergent part of the combustion chamber. It provides the fixation lashing for the lower part of the gimbal struts. The fuel is led into the inlet manifold and distributed to the 184 cooling channels.

The cooling channels are milled into the combustion chamber liner and covered by electro-chemically deposited nickel layers. To adjust the flow velocity of the coolant to the local demands of the heat transfer, the area of the cooling channels is suitably varied. For this reason the cooling channels are milled with different widths and depths into the liner.

The fuel finally flows through the cavity ring and into the manifold, the distribution space of the injectors.

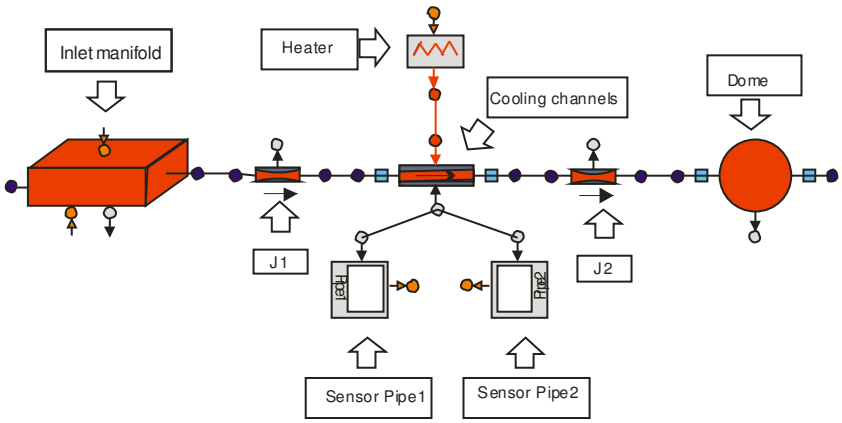

Figure 5.7 - Inlet manifold and cooling channels fuel dome schematic

The inlet manifold for the fuel is suitably shaped as an equivalent rectangular *Pipe*. The cross section and the length are chosen in order to have a simpler geometry that could observe the actual physical phenomena. The total volume of the item is obtained from the actual component volume plus an extra volume added to account for the volume of the engine valve and the inlet bend tube.

The cooling channels milled in the liner are modelled as an unique *Pipe* components with a constant cross section, instead of 184 channels of variable cross section. The channel length and cross section area are calculated to obtain the actual volume.

The heat transfer in the cooling is also obtained adding a *Heater* component that reproduce the actual heat flux from the combustion chamber walls to the channels. This component represents an electrical heater connected to the control system, and it produces a heat flow equal to the value of the command signal.

Finally, the distribution volume before the fuel injectors it is obtained as a spherical *Volume* of the same size, due to its small dimension.

Flow density, temperature, pressure and local and distributed pressure drops are calculated via mass, energy, state and momentum equation, implemented in EcosimPro items. The components are programmed with an internal volume and inner initial pressure and temperature. The mass flow rate is calculated due to the pressure differences from inlet to outlet of the *Pipe* and to concentrated pressure drop in the *Junctions.*

The *Junction* loss coefficients are the parameters used in the engine model to account for the actual pressure losses. The values of the loss coefficient are dedicated to the specific components. The pressure loss values are acquired form Reference[24]. In section 5 4 the detailed calculation are described.

The set-up of input parameters is presented in the Table (5.5)

Table 5.5 – Cooling channels schematic input parameters

Characteristic cross section width inlet manifold (m)	0.03
Characteristic cross section height inlet manifold (m)	0.03
Length inlet manifold (m)	1.170
Area when fully opened J1/ J2 (m^2)	0.0006
Loss coefficient J1/ J2	5.01
Length cooling channels (m)	0.8
Internal diameter cooling channel (m)	0.028
Volume manifold (m^3)	0.0001

Fuel Injector

The injectors are fundamental elements for the correct functioning of the combustion chamber. The actual geometry is showed in Figure (5.8), together with the EcosimPro schematic.

The fuel mass flow rate per element is calibrated by four radial bores in the sleeve. The fuel enters the injectors radially and flows in an annular cylindrical cavity and then it is injected in the combustion chamber trough the slots. This shape provides a better atomization of the fuel stream with good influence on combustion stability.

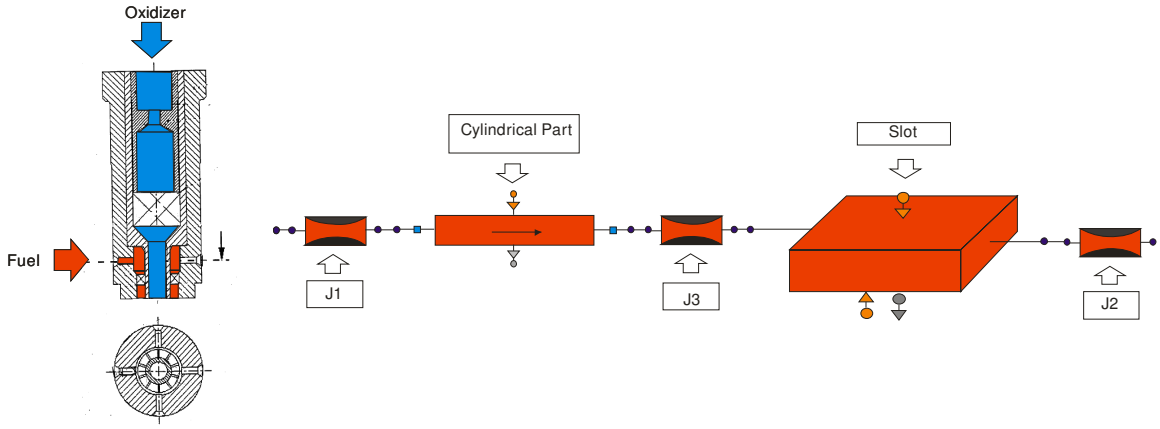

Figure 5.8 - AESTUS injector element schematic

The volumes of the injectors are reproduced as a dedicated cylindrical area-varying *Pipe* for the annular part and as *Rectangular Pipe* for the slots. The whole volume is obtained with 132 parallel elements shaped as described.

Equation of mass, energy, state and momentum are implemented for flow conditions calculation. The *Junction* components account for the pressure losses present. The values of the loss coefficient are dedicated to the specific components in order to achieve the actual pressure losses on the line as form Reference[24].The total pressure loss on the component is distributed in a non-homogeneous way on the different elements of the item. The major pressure drop is set for the slots. In Section 5.4 the detailed calculations are described.

The set-up of input parameters is presented in the Table (5.6)

Table 5.6 - Fuel injector schematic input data

Area when fully opened J1 (m^2)	0.000756
Loss coefficient J1	1.9
Length cylindrical part (m)	0.005175
Internal diameter cylindrical part (m)	0.0027
Number of parallel tubes	132
Area when fully opened J3 (m^2)	0.00336
Loss coefficient J3	4
Characteristic cross section width slot (m)	0.0006
Characteristic cross section height slot (m)	0.003
Length slot (m)	0.001125
Area when fully opened J2 (m^2)	0.000264
Loss coefficient J2	1.392

5.3.3. AESTUS components: oxidizer side

Oxidizer Line Set

The oxidizer flow from the NTO feed system is connected with the inlet of the valve assembly via the oxidizer line set. To fulfil the gimbal capability of the engine, the line is equipped with a flexible hose, a stainless tube covered by a stainless steel weave. The ends assuring the interface to feed system (NTO combiner) and the valve assembly are rigid tubes. The sealing of these interfaces is provided by an O-ring.

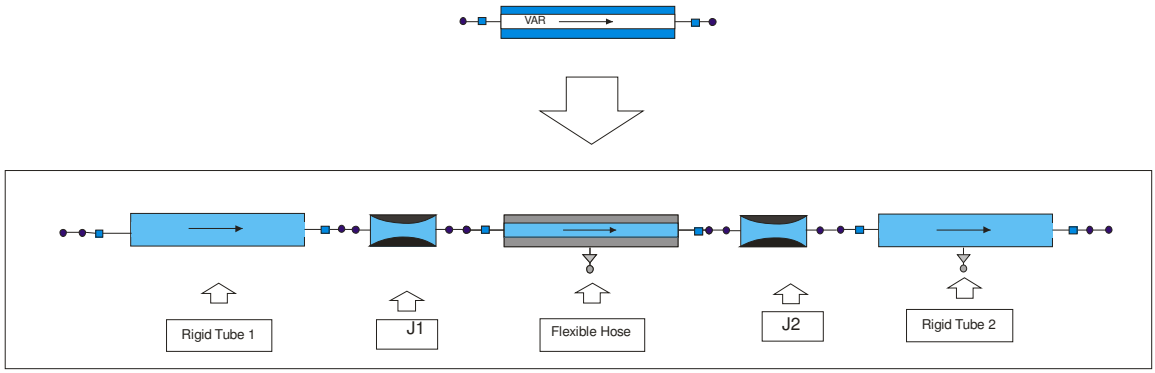

Figure 5.9- Oxidizer line set schematic

The oxidizer line assembly is simulated by alternation of *Pipe* and *Junction* elements. The flexible hose is simulated by means of a *Pipe* component with defined equivalent value for thickness and Young's modulus, to account for its mechanical behaviour. The rigid tubes at the ends are obtained by means of *Tube* components.

Equation of mass, energy, state equation and momentum are implemented for density, temperature, pressure and pressure drop calculations. The components are programmed with an internal volume and inner pressure, temperature. The inlet and outlet mass flow arte is calculated due to the pressure differences from inlet to outlet of the *Pipe.*

The *Junction* components account for the pressure losses present on the item. The values of the loss coefficient are set for specific components in order to achieve the actual pressure loss on the line as from Reference [24]. In Section 5.4 the detailed calculation are described.

The set-up of input parameters is presented in the Table (5.7)

Table 5.7 – Oxidizer line set schematic input parameters

Area when fully opened J1/ J2 (m^2)	0.001257
Loss coefficient J1/ J2	1.17
Length flexible hose (m)	0.5907
Internal flexible hose diameter (m)	0.040
Equivalent flexible hose thickness (m)	0.005
Young modulus	3.14e9
Length rigid tube 1 (m)	0.200
Internal rigid tube 1 (m)	0.040
Length rigid tube 2 (m)	0.200
Internal rigid tube 2 (m)	0.040

Engine Valve (NTO)

The oxidizer valve assembly is identical in the fuel side. Thus the description is already covered in Section 5.3.2.

The engine valve is mainly described by an area-varying dependent pressure loss equation implemented in the EcosimPro component. A loss coefficient is used for the pressure loss calculation. The computation of the loss coefficients is described in Section 5.4.

The volumes associated with this device are implemented as extra volumes in the components upstream and downstream the valve. Due to the small dimension of the valve heat transfer is neglected.

The input parameters can be seen in Table (5.8).

Table 5.8 – Engine valve (NTO) schematic input parameters

DESCRIPTION	**VALUE**
Area when fully opened (m^2)	0.00314159
Loss coefficient	0.593

The valve displacement time is regulated by a *Control Block* that opens and closes the device following a given table in time. The time table is directly obtained from valve testing results and allows the representation of the whole valve characteristic.

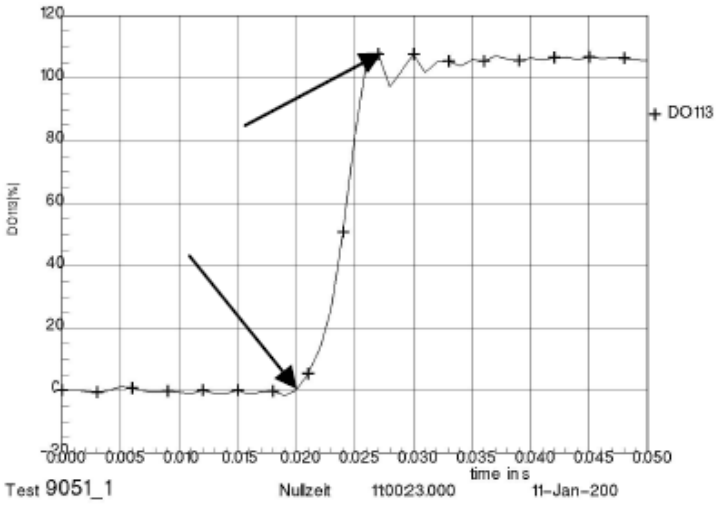

Figure 5.10 - Valve opening characteristics

Dome

Before being injected in the combustion chamber the oxidizer flows in a dome. The oxidizer dome covers the element and ensures an equal distribution of NTO over it. In this way homogeneous distributions in terms of pressure and velocity are achieved.

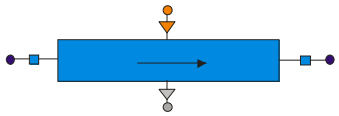

Figure 5.11 - Dome schematic

The complicate geometry of the items is simplified in a cylindrical *Pipe*, with a diameter equal to the one of the combustion chamber and a length calculate in order to obtain the whole volume of the actual component. An extra volume is added to take into account the volume of the bended tube at dome inlet.

The input parameters can be seen in Table (5.9).

Tab 5.9 – Dome schematic input parameters

DESCRIPTION	**VALUE**
Length of the dome (m)	0.037
Internal diameter of the dome (m)	0.021

Oxidizer Injectors

The injectors are fundamental for the correct functioning of the combustion chamber. The actual geometry is showed in Figure (5.12) together with the EcosimPro schematic.

The oxidizer enters the injection element from a coaxial cavity in the injector body and flows in the central cylindrical opening.

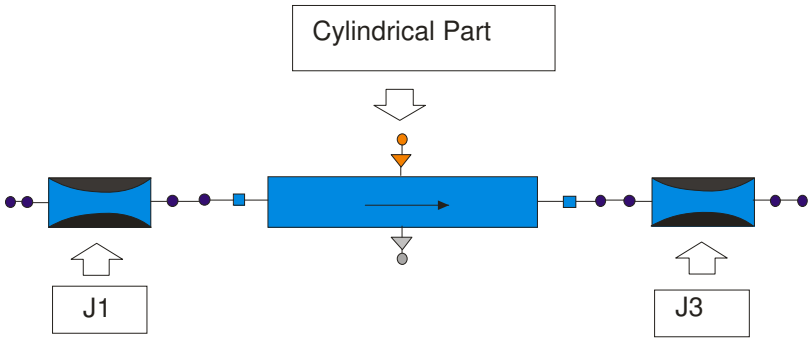

Figure 5.12 - Oxidizer injectors schematic

The volumes of the injectors are reproduced as a dedicated *Pipe*. Equation of mass, energy, state and momentum are implemented for the flow conditions calculations. The *Junction* accounts for the pressure losses. The values of the loss coefficient are dedicated to the specific components in order to achieve the right pressure loss on the line as from Reference [24]. In Section 5.4 the detailed calculations are described.

The set-up of input parameters is presented in Table (5.10)

Table 5.10 - Oxidizer injector schematic input data

Length of the cylindrical part (m)	0.02
Internal diameter cylindrical part (m)	0.0207
Area when fully opened J1/ J2 (m^2)	0.00034
Loss coefficient J1/ J2	2.724

Combustion chamber

The combustion chamber comprises a cylindrical part and a nozzle, the convergent section forming the throat inlet and the divergent portion ending at the expansion ratio of 10. It provides the combustion of propellants at a high efficiency (98%) and the acceleration of

gases up to Mach equal to 1 in the throat. A oxidizer pre-flow enters the combustion chamber, and only after some milliseconds the MMH starts flowing.

The combustion chamber is modelled as a special boundary condition for the system, regulating the back pressure and temperature, as well as the mass flow rate of fuel and oxidizer depending on the O/F ratio.

No real volumes for the combustion chamber are modelled in the system.

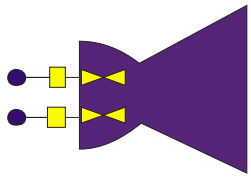

Figure 5.13 - Combustion chamber schematic

5.3.4. Simulation input parameters

Flexible mechanical characteristics

To account for the elastic behaviour of the flexible hose the mechanical properties of the pipe need some attention. A dedicated test campaign has been carried out to characterize the mechanical properties of the flexible hose for the propellant feed lines of the stage. The objective of the analysis was to ascertain whatever the engine flexible hoses can withstand the pressure stresses of any potential water hammer phenomena.

The Young's modulus and the wall thickness implemented as input data in the code are taken from Reference [25].

Pressure Losses

Each manufactured engine has a specific hydraulic characteristic, all given generic values are valid for a so called "mean engine", as a mean value of all hot tested AESTUS engine. The mean pressure drop in every single element is defined for a reference value conditions in terms of mass flow rate and density of the fluid.

In the following table the value for AESTUS components and the correspondent values of reference mass flow rate and density are given.

Table 5.11 – Reference pressure drop AESTUS components

COMPONENT	ρ_{REF} (kg/m^3)	$\dot{m}_{REF}$ (kg/s)	ΔP_{REF} (bar)
Calibration orifice	874	3.21	0.1
Fuel flexible	874	3.21	0.1
Engine valve (MMH)	874	3,21	0.312
Cooling channels	780	2.876	1.442
Fuel injectors	780	2.876	3.509
Oxidizer flexible	1447	5.986	0.2952
Engine valve (NTO)	1447	5.986	0.4428
Oxidizer injectors	1447	5.986	5.932

From the given pressure drop over mass flow rate and fluid conditions, the loss coefficient can be calculated in the following way:

$$\zeta = \frac{2 \cdot \Delta P_{REF} \cdot \rho_{REF} \cdot A}{\dot{m}_{REF}^{\ 2}} \tag{5.1}$$

This value is then halved in the junction upstream and downstream the *Pipe* components in order to reach the desired pressure drop.

The injectors pressure loss need special attention. While no combustion is going on in the combustion chamber, the backpressure that these items experience is the atmospheric pressure (1bar) under the considered P2 test facility conditions (vacuum conditions given for flight application). In this case the injectors start cavitating during the oxidizer pre-flow, so that the pressure drop is assumed to be 15% higher than the nominal value. When the combustion starts, the back pressure increases and reaches the nominal value (11bar), so that the pressure drop of the injectors is equal to the reference value in Table (5.11).

This behaviour has to be reproduced in order to have the right transient response of the model. For this purpose a dedicated part of the code is modified in order to have the loss coefficients as a step function of time. Until the pressure in the combustion chamber is equal to the ambient pressure, the injectors have an increased loss coefficient. When the combustion chamber pressure goes to the combustion value of 4 bar (to avoid cavitation for Pc=10 bar matric points), the loss coefficient drops to the reference value.

Combustion boundary conditions

The combustion process is described by means of the fundamental rocket relation

$$P_C = \frac{\dot{m}c^*}{A_t} \tag{5.2}$$

The pressure in the combustion chamber is a function of the fuel mass flow rate, specific velocity and throat area. In the actual engine indeed an oxidizer pre-flow is experienced before the fuel valve is also opened. This behaviour is also reproduced in the component of the EcosimPro component. Until no fuel mass flow rate is entering the chamber the back pressure for the system would be the ambient pressure and the temperature the ambient temperature. When the fuel mass flow rate is high enough to let the combustion process starts, the back pressure changes following Equation (5.2).

Heat flux

The heat flux to the wall combustion chamber has been artificially reproduced by the *Heater* component. The input value of the heat flux reproduced by these items is given by an incoming control signal. In this specific case the value of this signal is implemented as a linear law of the mean mass flow rate between the inlet and the outlet of the channel as from the following relation:

$$Q_{IN0} = k\frac{(\dot{m}_1 + \dot{m}_{100})}{2} \tag{5.3}$$

The mean value of the mass flow rate in the channel is chosen in order to avoid instability problems in the code calculation. The entire channel is divided in 100 control volumes, in order to achieve a better approximation of an almost linear temperature profile.

K is a dedicated parameter calculated from a reference value of the heat load on the combustion chamber. The reference data are reported in the following table and taken from Reference[24]:

Table 5.12 – Heat loads reference values

DESCRIPTION	**VALUE**
Reference mass flow rate (kg/s)	3.21
Combustion chamber heat load (kW)	838

A dedicated time law, let the heat input signal achieve the actual temperature time profile.

$$\dot{Q}_{IN} = 3(Q_{IN0} - Q_{IN}) \tag{5.4}$$

6. MODEL VALIDATION

6.1 Introduction

Since studies of the new Ariane 5 have been initiated EADS-ST was selected to the development of the Vulcain I thrust chamber HM60 and the upper stage engine Aestus. For both developments specific facilities were needed.

Aestus development started with a subscale engine, performed at the test facility P1. The full scale investigation of the injectors and combustion chambers were performed at sea level conditions at the P2 facility.

In the following chapter the complete PCA (pressure control assembly) validation test is presented. Test and simulation results are compared and used for validating the P2 and AESTUS EcosimPro model.

6.2 Test Description

For the validation purposes of this chapter 0673-005 Flight Validation Test was selected: PCA test objectives, engine as passenger.

Prior to the test analysed, Aestus engine ARTA07 was taken to complete the dynamic stability qualification program for the AESTUS engine with three tests performed in September 2004 at sea level condition in the test bench P2 in Lampoldshausen.

Afterwards, without intermediate dismounting, the engine was used to conduct the combined tests engine-pressure regulator described in the following chapter. For these test campaign, between September and October 2004 27 tests with hot-firing where performed, with a hot total firing time of 520 s.

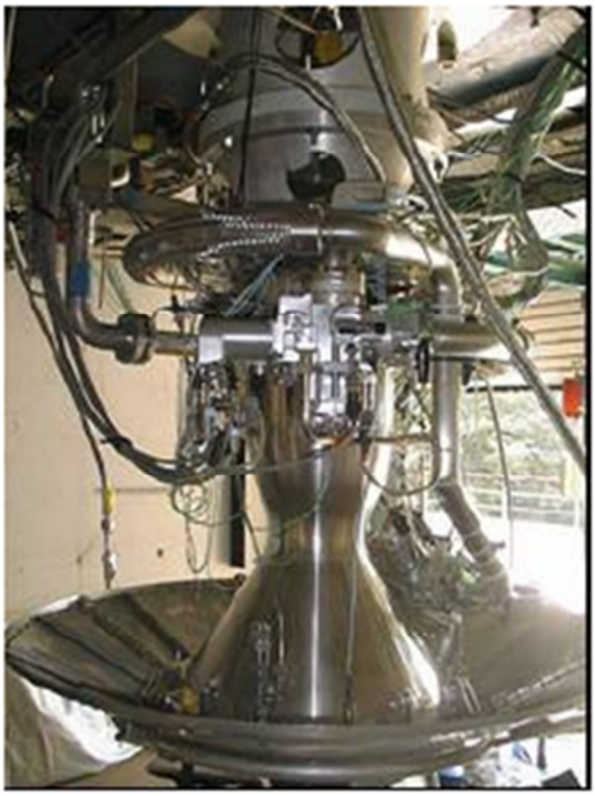

Figure 6.1 - Aestus engine ARTA07 installed on P2

All results obtained are about performance parameters, like combustion efficiency and characteristic velocity, hydraulic characteristics of the engine for the cooling channels and the injectors head, C_D values and the combustion chamber noise level.

Main tests objectives of this campaign were:

- verification of the engine calibration with an appropriate orifice on MMH side
- investigation of the flight anomaly of F516 with unexpected peaks of the dynamic pressure signal in the combustion chamber.
- investigation and determination of the chugging regime during the shutdown mode
- performance of steady state tests to validate the hardware production
- execution of long duration tests resulting in total 220 s hot firing.

Specifically the passenger test for the combined AESTUS–PCA/pressure regulator selected was useful for validating the pressure regulator performance at minimum lock-up pressure and for investigating the limits of the pressure regulator with the influence on the shut down behaviour.

The hardware configuration is described by the following components:

- ARTA07 combustion chamber with improved instrumentation: static and dynamic pressure sensors and acceleration transducers in the cavity ring,
- ARTA07 fuel manifold with dynamic and static pressure sensors, liquid and surface temperature measurement,
- ARTA07 injector head and related fluid temperatures, dynamic and static pressure measurements,
- Oxidizer dome with additional instrumentations: dynamic and static pressure sensors and temperature measurements,
- PVA's fuel and oxidizer with complete instrumentation, static and dynamic pressure transducers, accelerometer and thermocouples.

Test conditions for the specific case are summarized in the following:

Table 6.1 – Test conditions for 0673-005 test

NTO tank pressure (bar)	18.383
MMH tank pressure (bar)	18.010
NTO tank temperature (K)	290
MMH tank temperature (K)	290
Firing time (s)	10
O/F	1.9
MMH mass flow rate (kg/s)	3.081
NTO mass flow rate (kg/s)	5.880

These data are implemented in the EcosimPro for test bench-engine combined system. The non-condensable mass fraction is set equal to 1 for all components after the engine valves (initially closed) to simulate gas-fluid interaction at the valve opening. A non zero mass

fraction could also be implemented in the components before the valve in order to account for an initial gas content in the fluid.

6.3 Comparison with test results

The general transient behaviour of the EcosimPro model is compared with test result obtained during the test campaign in terms of mass flow rate and pressure in the test bench lines and in the engine itself.

Test measurements considered for characterising the transient behaviour of test bench-engine combined system are

- m_OX: oxidizer mass flow rate, mean value measured by the two flow meter on P2 line
- m_FU: fuel mass flow rate, mean value measured by the two flow meter on P2 line
- PO_106: mean total oxidizer inlet pressure
- PF_206: mean total fuel inlet pressure
- PT_8 : mean total pressure in the fuel manifold
- PT_10: mean total pressure in the oxidizer fuel dome
- PT_12: mean total pressure in combustion chamber

In Figure (6.2) is reported a general scheme of the test facility used, where measurement points are highlighted.

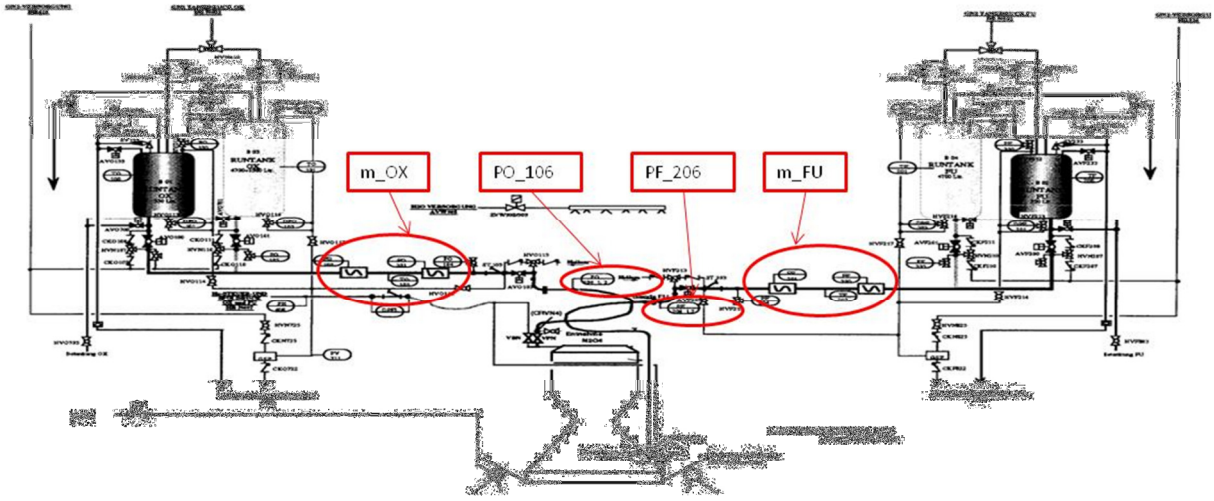

Figure 6.2 – Test measurement points.

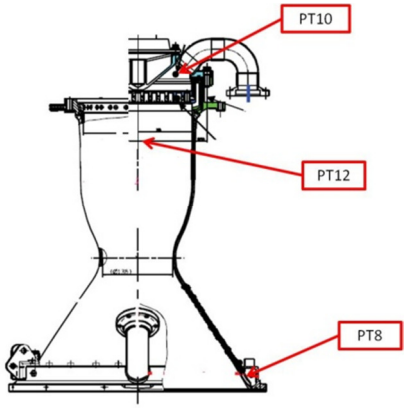

Figure 6.3 - Engine measurement points.

Comparison of numerical results starts with the analysis of the behaviour of the mean mass flow rate.

In Figure (6.4) the oxidizer and fuel mass flow rate from test data are compared with the results obtained in the simulated system in EcosimPro.

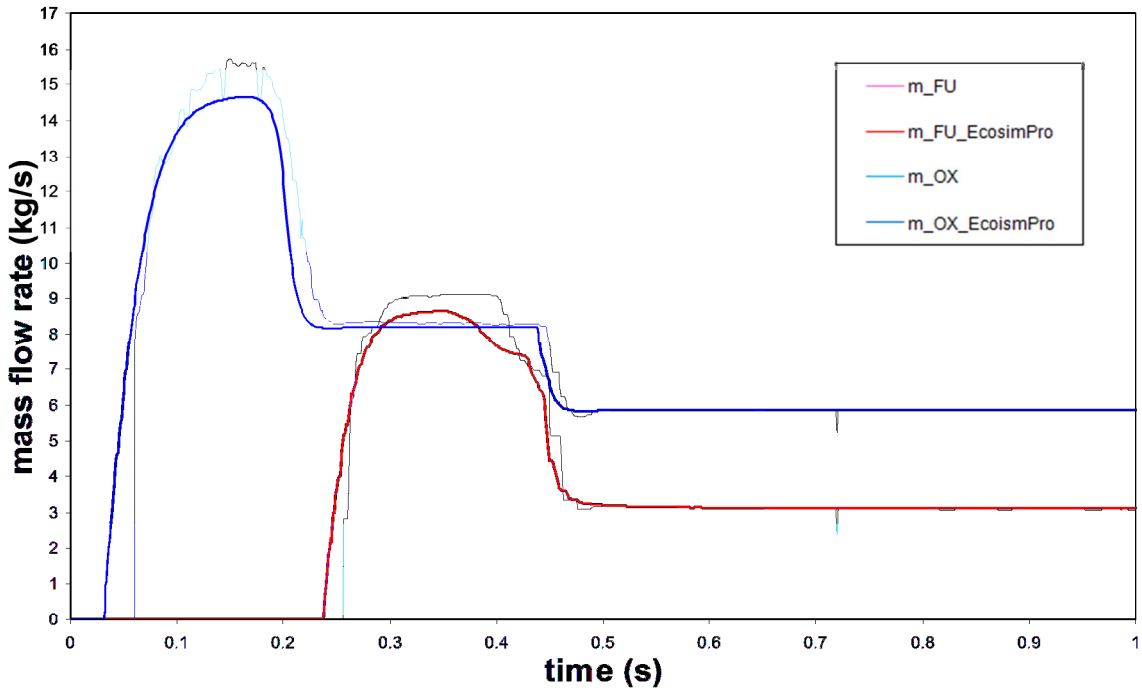

Figure 6.4 – Oxidizer and fuel mass flow rate: comparison with test results

The general behaviour of the simulated system matches test results in both oxidizer and fuel side: the mass flow rate increases in the oxidizer side while the dome is filled and then reaches a lower quasi-steady value. As soon as the fuel is delivered in the engine and the combustion starts, this value decreases and the final steady state condition is reached.

The same behaviour is followed also by the fuel mass flow rate: after the engine valve opens increases reaching a quasi-steady state value while filling the volumes (manifold and cooling channels) before entering the combustion chamber, then rapidly decreases to the final steady state value at the ignition.

From the displayed plot it can be observed that the first peak, due to the filling of the dome in the oxidizer side and to the filling of volumes in the fuel side, shows :

- Difference in timing and slope due to: turbine flow meters inertia, behaviour of the losses especially under unsteady flow conditions and errors in fluid properties implementation.
  The inertia of the turbine creates a delay in the measurement of approximately 0.02s, the same delay showed in comparing simulation results with test data. and
- 7% underestimation of MMH and NTO mass flow rate peaks.
  Due to the different resistance in the P2 lines, mainly due to higher level of resistance in simulated flowmeters, the mass flow rate in the simulated system is lower.

The validation of the numerical model is completed with the analysis of the pressure measurements at the interface between the feed line and the engine, in the fuel manifold and in the oxidizer dome.

At the interface between P2 test bench and ARTA07 engine are positioned two steel flexible lines. In Figure (6.5), (6.6) test and simulation results for this components are compared in terms of mean pressure at the entrance and exit of the pipe considered.

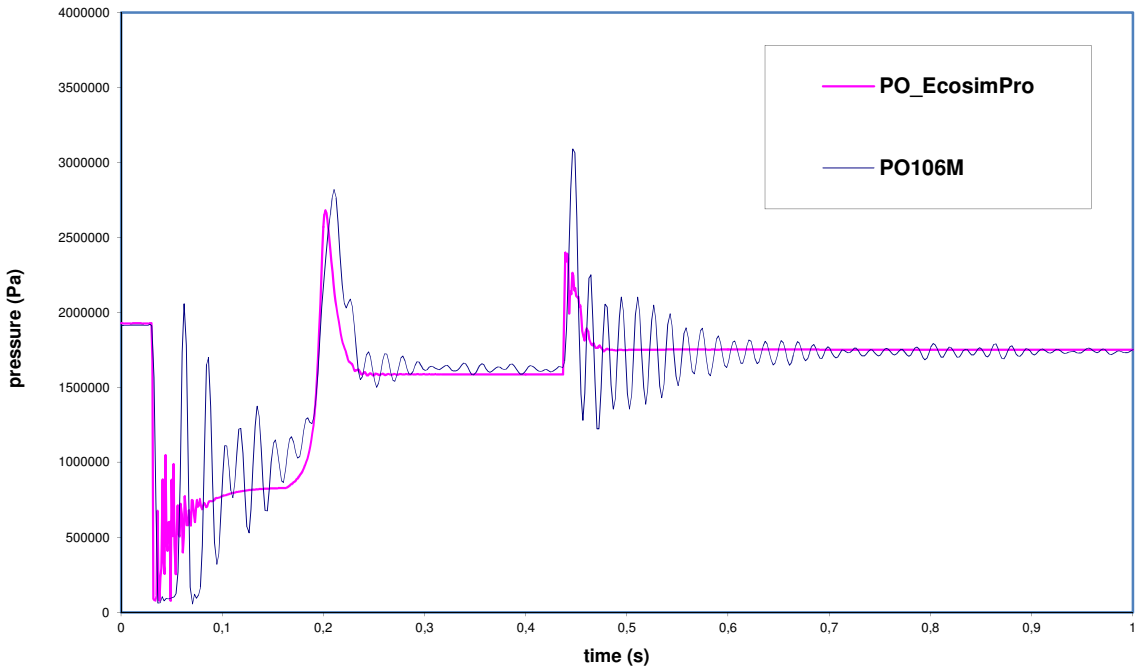

Figure 6.5 – Oxidizer flexible pressure: comparison with test results

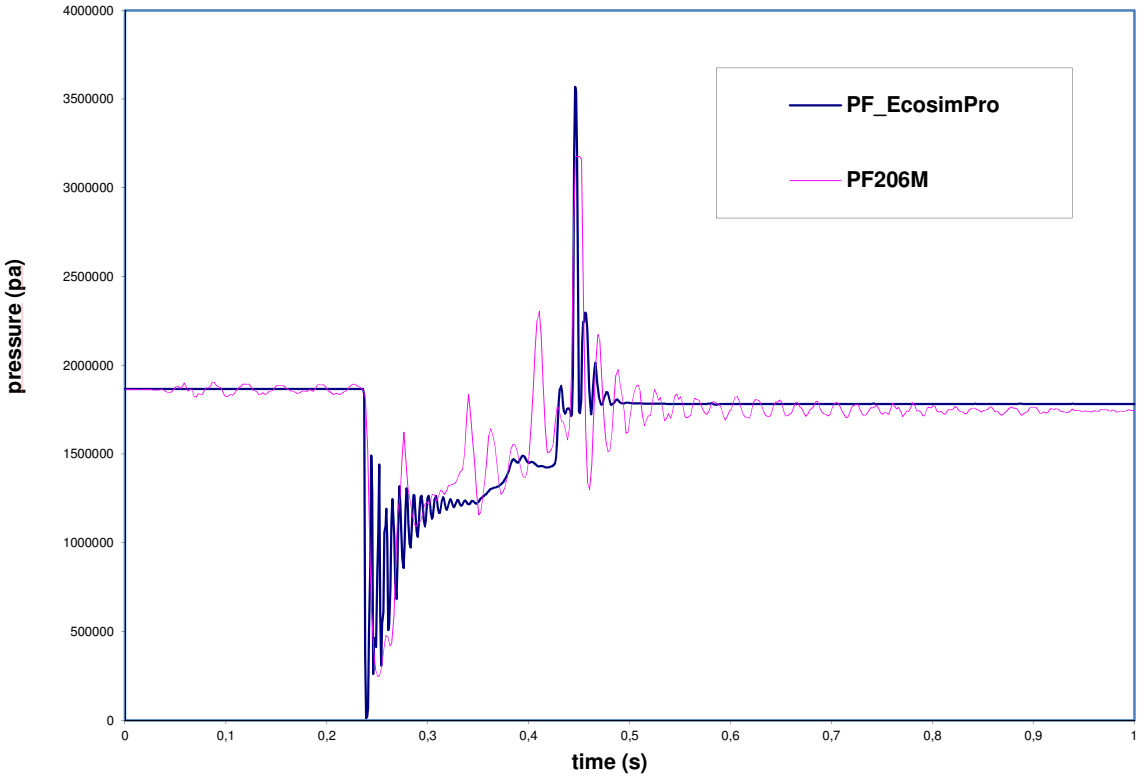

Figure 6.6 – Fuel flexible pressure: comparison with test results

In both oxidizer and fuel side a instantaneous decrease of pressure from the tank value is visualized as soon as the engine valves are opened. A dynamic pressure, in addition to the normal static pressure, is created within the pipe and fluctuations in pressure, are visualized.

A pressure peak in the oxidizer side, due to the filling of the dome, follows the water hammer phenomenon. Then another pressure peak is generated, for fuel and oxidizer, at the ignition.

Comparing test and numerical model results, it is observed a good agreement with the general transient behaviour, the measured pressure peaks and the steady-state behaviour.

The water hammer frequency is approximately doubled compared to measured data. The mismatching is mainly attributable to different characteristics between the fluid simulated and the real fluid in terms of content of dissolved gas (not properly simulated in the numerical model) and in a difference in measurement data shown. Sensors used for pressure measurements during the test campaign are positioned at the final end of capillary tubes, while simulation results are showing pressure fluctuation directly in the pipes. Due to this the water hammer behaviour illustrated by test data is deviated.

In Figure (6.7), (6.8), (6.9) is shown a matching of the general transient behaviour in timing and slope, a good agreement with measured pressure peaks and with steady-state behaviour in fuel manifold, oxidizer dome and combustion chamber.

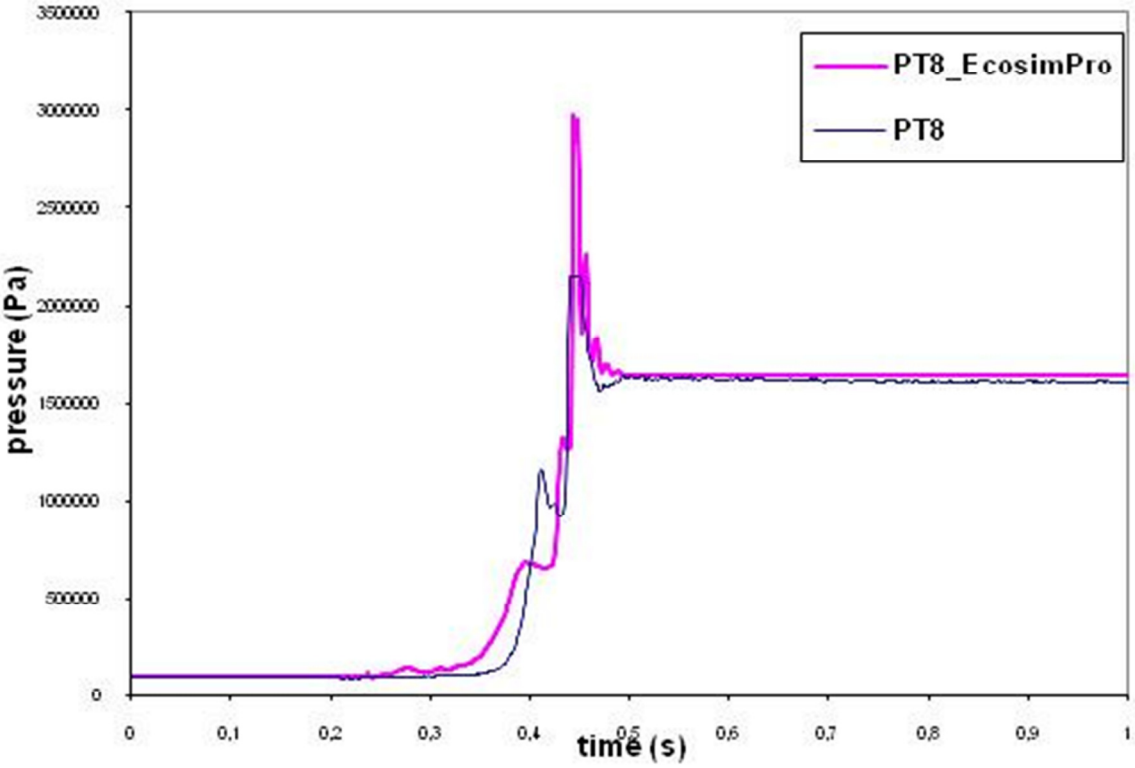

Figure 6.7 – Manifold pressure: comparison with test results.

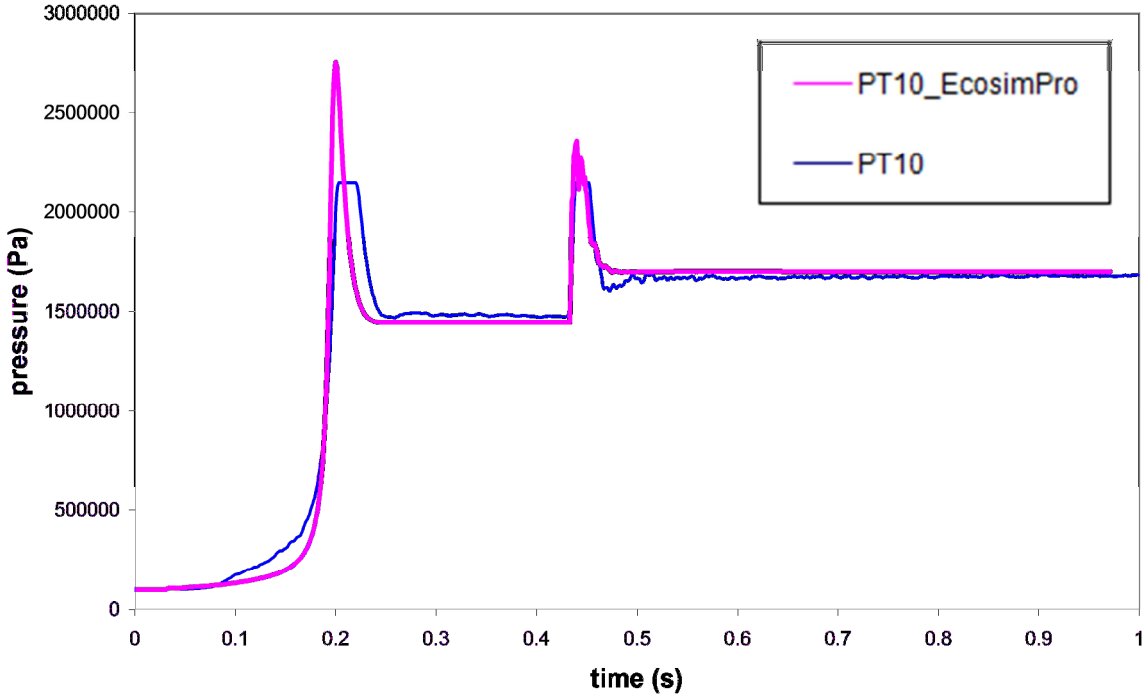

Figure 6.8 – Oxidizer dome pressure: comparison with test results

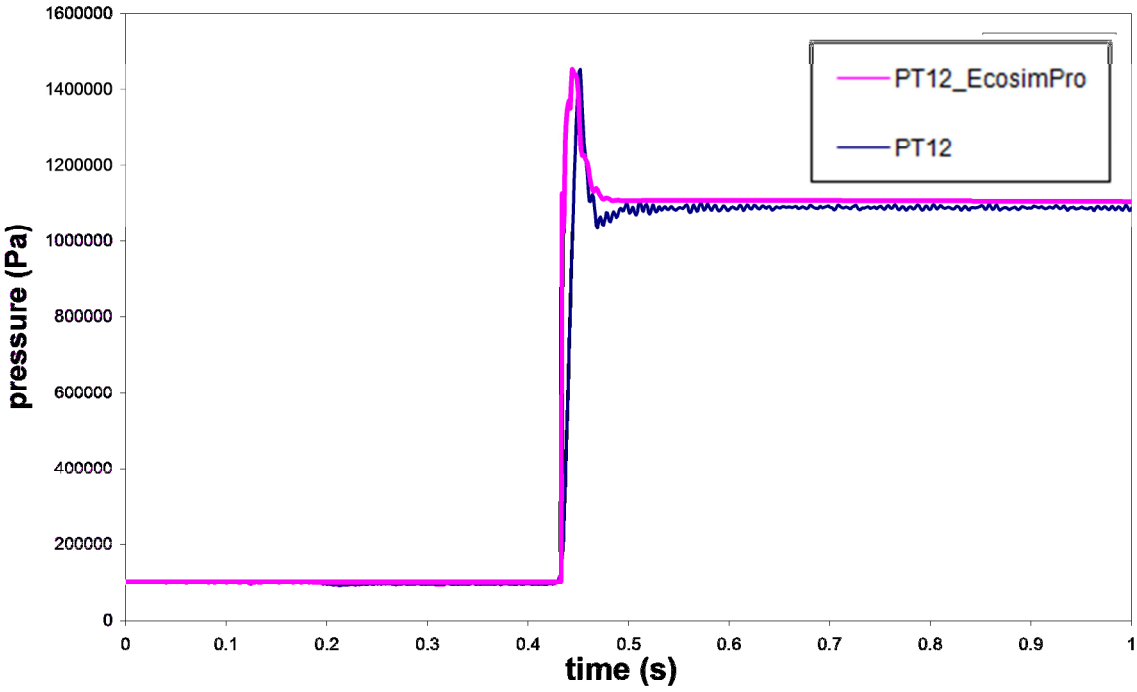

Figure 6.9 – Combustion chamber pressure: comparison with test results

Comparison of test and numerical model results shows a general good agreement of EcosimPro model with the actual system, so that validation process could be considered successfully completed.

6.4 Sensitivity study

After validation, the numerical model is used for a preliminary study and evaluation of critical fluid-system parameters affecting transient behaviour.

Roughness

Starting from the value assumed for steel feed line pipes equal to 0.000575 m, pipe roughness is halved. In Figure (6.10) numerical model results for different values of roughness of the pipes are compared in order to understand how the difference in lines resistance due to the changing in pipe roughness is acting on the behaviour of the general system.

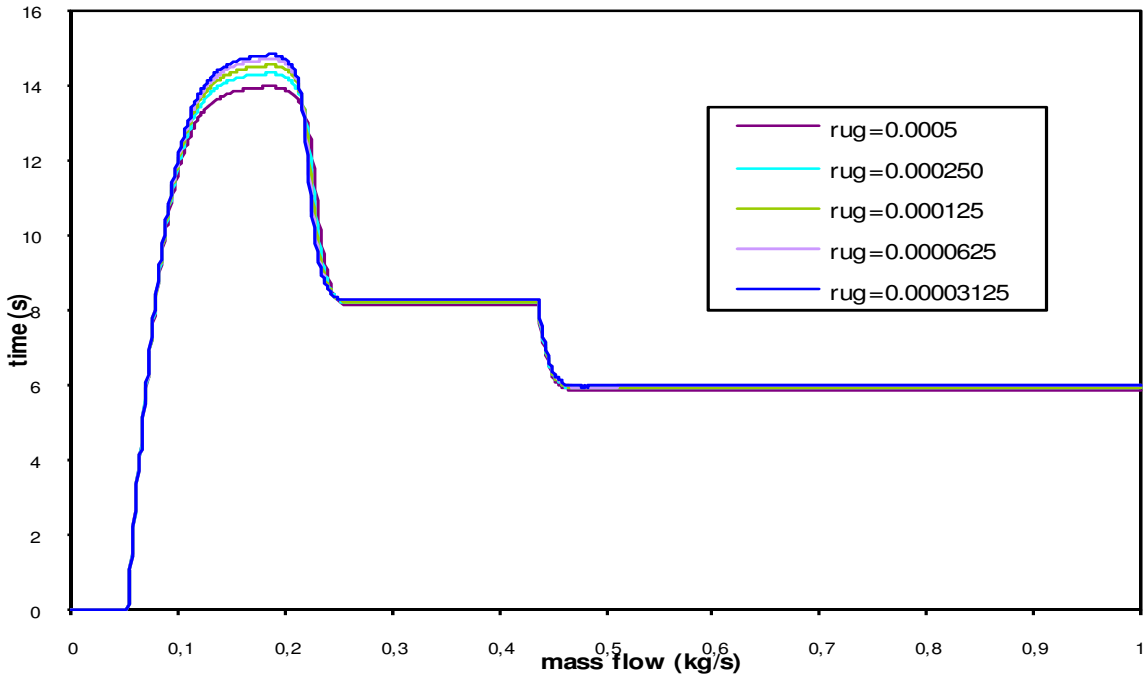

Figure 6.10 – Mass flow rate variation with different internal pipe roughnesses

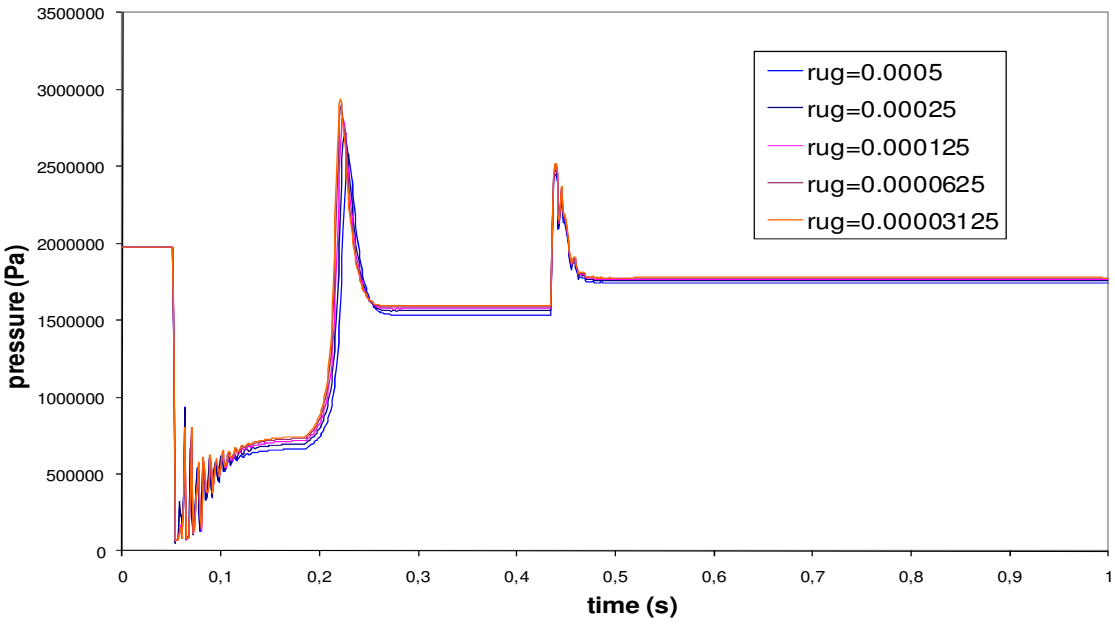

Figure 6.11 – Dome pressure variation with different internal pipe roughness

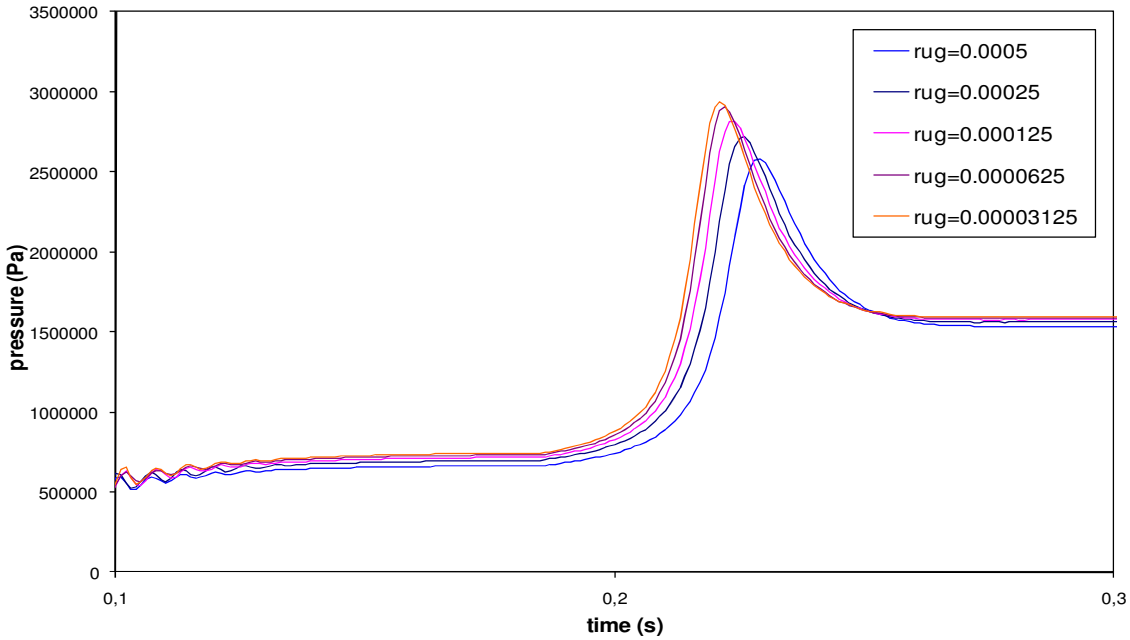

Figure 6.12 – Dome pressure variation with different internal pipe roughness

In terms of mass flow rate peaks are increased by approximately 10% for 1/10 of the initial pipe roughness.

For lower values of pipe roughness pressure peaks are reduced and a time shifting of the peak itself can be observed, due to the modification of the speed of the travelling wave, for the decreased energy loss and pressure drop.

N_2 fluid content

The speed of sound at which the traveling wave is moving is strongly affected by the content of gas of the fluid considered. Nitrogen content of the simulated system is changed and in Figure (6.13), (6.14) numerical model results for zero non-condensable mass fraction and for 6% of free gas content of the saturation value[27].

Free gas represents the entire quantity which the liquid is capable to absorb when subject to system pressure (tanking pressure) assuming that the liquid is saturated. The quantity solved up to the saturation level is governed by Henry's law:

$$x = pk \tag{6.1}$$

depending on absorption characteristics of the liquid in combination with different kind of gas and the partial pressure of the pressurizing gas.

The value obtained from the plotted curve for the specific gas is chosen according to tank pressure for the analyzed test case in order to simulate as much as possible actual fluid characteristics.

Once the liquid is subject to any depressurization below the saturation level, gas goes out of solution, forming regularly distributed, dispersed bubbles which may even change over locally into discrete bubbles. Those bubbles are compressible, acting as springs, enable the liquid to expand upon being subjected to any sudden pressurization. Waves propagation through a piping system with speed of sound impose local depressurization, which cause absorbed gas to out-gas, forming bubbles, thus increasing fluid compressibility.

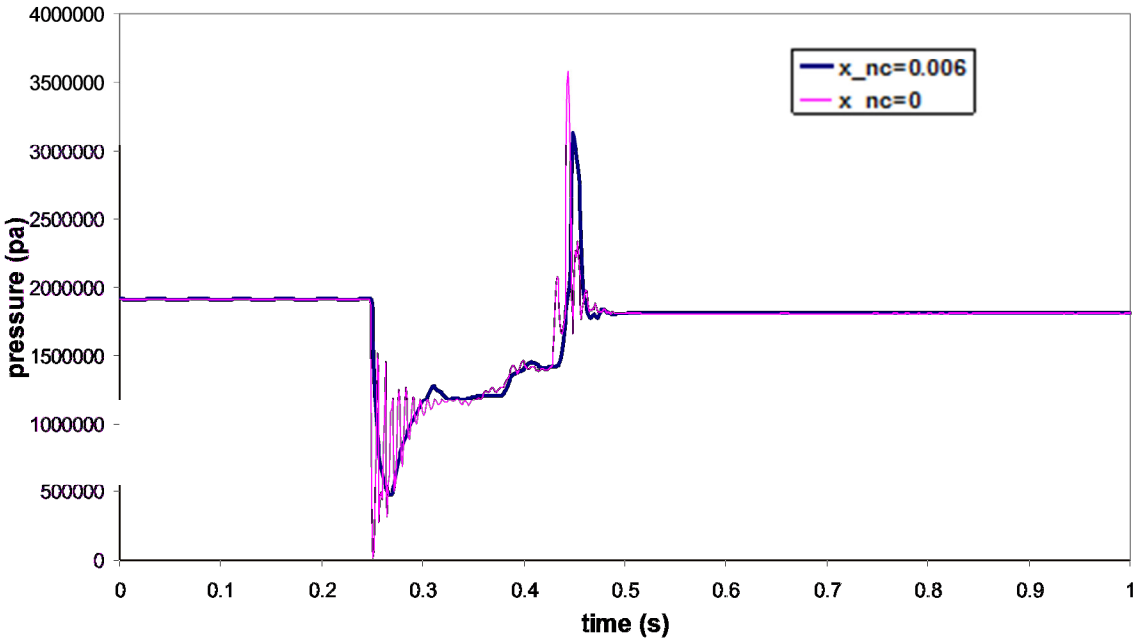

Figure 6.13 – Manifold pressure variation with different internal pipe roughness

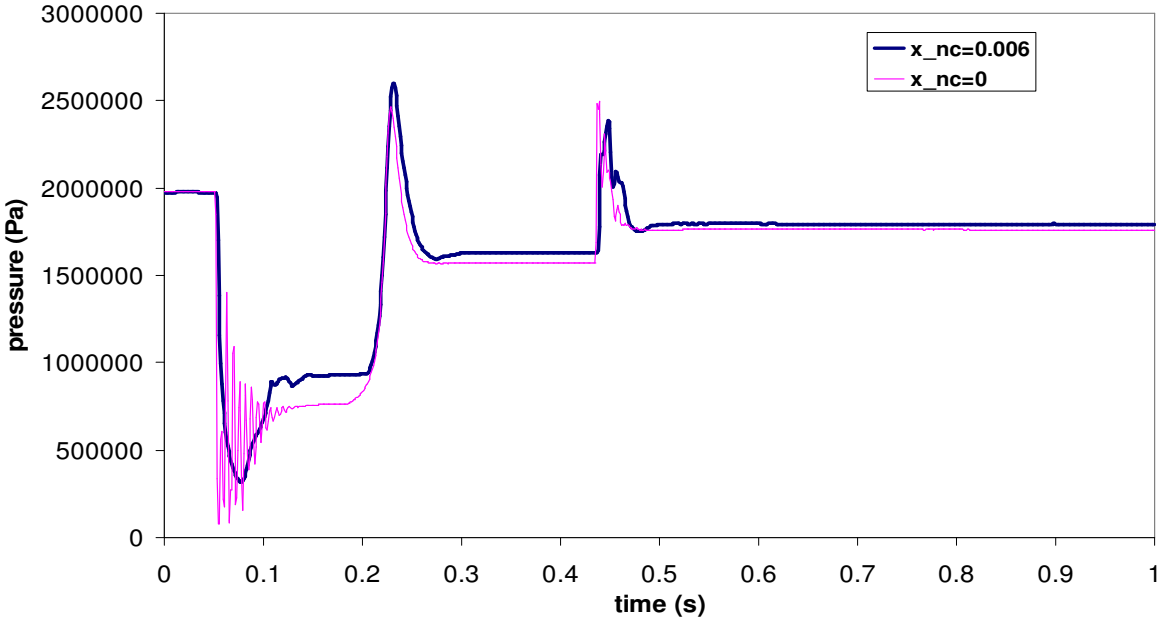

Figure 6.14 – Dome pressure variation with different internal pipe roughness

It can be observed that water hammer frequencies are dumped by 0.6% when N_2 is present in NTO and MMH due to pressurization effects.

At the oxidizer interface it is observed a slight increase of pressure peak for increased N_2 content and a slight deviation for steady-state condition due to changed fluid properties.

Line volume increase

The last parameter evaluated is the presence of an increase in the line volume. This variation is obtained by a geometrical modification of one of the pipe which as the internal diameter progressively increased.

In Figure (6.15) is visualized the geometrical modification of the simulated pipe: half of the volume in the centre of the pipe is increased.

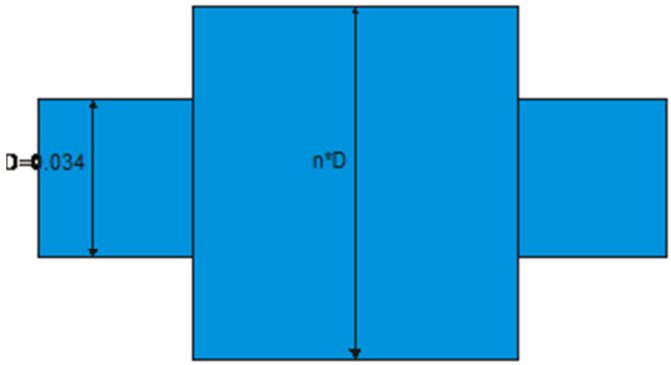

Figure 6.15 – Schematic of investigated pipe section

If the reflective boundary is close enough, the pressure reflected waves start interacting and could increase or decrease the effective magnitude of the water hammer waves as the frequencies itself. The results obtained in system simulations with a different internal diameter are plotted and compared in Figure (6.16).

In the specific case, it is analysed pressure fluctuations behaviour at the exit of a test bench pipe upstream the engine.

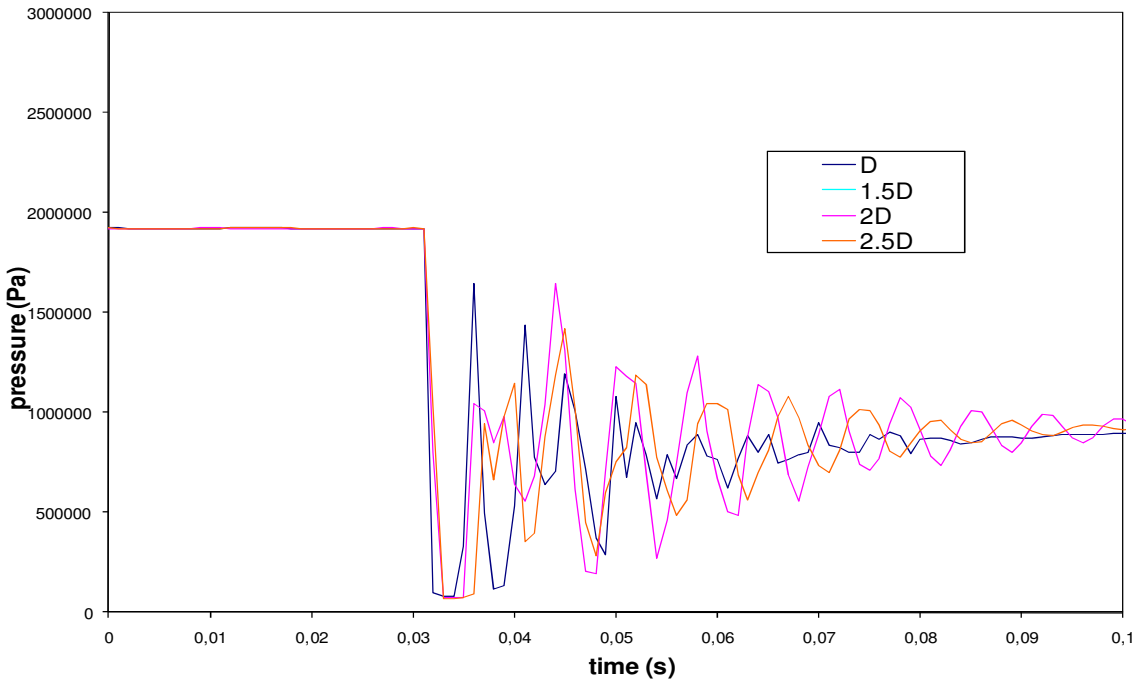

Figure 6.16 – Pressure fluctuation at the end of the investigated pipe

It is observed that when the internal diameter is increased of the half of the initial value no remarkable results are obtained.

Instead it is observed a 40% decrease of pressure peaks when doubling the diameter of the investigated pipe section. An additional frequencies is triggered by reflection phenomena due to the change in cross section and water hammer phenomenon are reduced due to increased damping effects.

7. CONCLUSIONS AND OUTLOOK

Test facilities are an indispensable element for the development and acceptance for space systems and components. Liquid rocket engines for launch and space application as well as their subsystems need to be verified and qualified during hot-runs. Test verification during development/qualification as well as during acceptance testing for production are essential steps.

Use of test data for computer simulations, as code calibration, grant a reduction of the total tests needed with a positive outcome of cost reduction.

EcosimPro is a 1D-numerical tool for modelling and simulation of transient and steady-state flow behaviour.

Within this study a detailed P2 geometry into EcosimPro 4.4 is implemented and performed a coupled flow behaviour of P2 and AESTUS upper stage engine.

Simulated conditions with ECOSIM are not the flight conditions (not relevant feed system and also not relevant environment -atmospheric conditions). The EcosimPro computations are made on P2 feedsystem under atmospheric conditions and results from the simulation are compared to development tests performed under these conditions.

Transient and steady-state comparison with real test measurements showed the following main results:

- Good agreement with steady-state-pressure and propellant mass flow rates behaviour.
- Good agreement with transient start-up in terms of water hammer peaks.
- Frequencies are not matched well due to: 1D-restrictions of code, uncertainties in the intensity and behaviour of the losses especially under unsteady flow conditions and errors in implementation of fluid properties.

Hence the numerical models are modified and adjusted successfully so that simulation results meet the measured values within acceptable ranges.
The selection of the P2 was made to have a first EcosimPro model of the test facility which is foreseen to be used for other development programs. This model is also seen as a platform for definition of eventual modification needs of the P2 feed system in order to get more representative of real flight feed systems

Future tool developments and studies have to focus on:

- Implementation of improved fluid property data bases, especially for NTO (equilibrium condition between NO_2 and N_2O_4 depending on pressure and temperature).
- A deeper understanding and investigation of possible influences of pressurization gas content in the liquid fluid on transient behaviour.
- Further development of a tool for characterizing the influences of a non-flight-like feed system necessary.

SYMBOLS

E_{tot}	total energy	J
ρ	density)	kg/m^3
m	mass flow	kg/s
H	Enthalpy	J
V	volume	m^3
Q	heat flux	W/m^2
P	pressure	Pa
v	velocity	m/s
I	Inertia	m^4
A	area	m^2
G	mass flow per unit area	kg/s m^2
ζ	pressure drop coefficient or loss coefficient	
T	temperature	K
st	thickness	m
E	Young's modulus	Pa/m^2
K	fluid bulk elasticity modulus	N/ m^2
a	speed of sound	m/s
μ	Poisson's ratio	
f	Darcy-Weisbach friction factor	
L	pipe length	M
D	internal pipe diameter	M
D_H	hydraulic mean pipe diameter	M
g	gravitational acceleration	m/s^2
h	hydraulic pressure head	M
τ	frictional force per unit area	N/ m^2
$\dot{u}_x$	axial pipe velocity	m/s
σ_x	axial pipe stress	Pa
α	void fraction	
t	Time	S
v	kinematic viscosity	$m^{2/s}$
ε	rugosity	M
α	pipe bend angle	Deg

R	radius	M
x	mole fraction of dissolved gas	
p	gas partial pressure	Pa
k	gas equilibrium constant	

Indices

mix	mixture liquid /gas
nc	non condensable gas
up	Upstream
dw	Downstream
th	Throat
b	Backward
f	Forward
jun	Junction
dif	Diffusive
fch	phase change
sat	Saturation
0	initial condition
fluid	Fluid
str	Structure
g	Gas
l	Liquid

BIBLIOGRAPHY

[1] Benjamin Wylie, Victor L.Streeter,*"Fluid transient*", Mc Graw Hill

[2] A.S.Tijsseling, "*Water hammer with fluid-structure interaction in thick-walled pipes"* Journal Computers and Structures, 85, 2007: 11-14

[3] A.Dudlik, H.M. Prasser Forsch Ingenieurwes, *"Water hammer and condensation hammer scenarios in power plants using new measurement system",* Forschung im Ingenieurwesen 73, 2009: 67-76

[4] Ming Zhao, Mohamed S.Ghidaoui, *"Efficient quasi-two dimensional model for water hammer problems",* Journal of Hydraulic Engineering Vol.129, 2003: 12-19

[5] A.R. Lohrasbi, R.Attarnejad, "*Water hammer analysis by characteristic method",* American J. of Engineering and Applied Sciences Vol.4, 2008: 287-294

[6] Thomas Repp, "*Fluiddynamic water hammer simulations with consideration of fluid-structure interaction",*Journal of Applied Mechanics Vol.21, 1998

[7] A. Bergant, A.Simpson, A. Tijsseling, *"Water hammer with column separation :a review of research in the twentieth century"* Journal of fluid and structures Vol.22, 2004: 135-171

[8] A. Bergant, A.R.Simpson, "*Cavitation inception in pipeline column separation",* proceedings of the 28th IAHR Congress, Graz, Austria

[9] R.Lecourt, J.Steelant, *"Experimental investigation of water hammer in simplified basic pipes of satellite propulsion system"* AIAA-2002-3699

[10] I. Gibek, Y. Maisonneuve, *"Waterhammer tests with real propellant"* AIAA 2005-4081

[11] "*Handbook of hydraulic fluid technlogies",* Georg E.Totten, 1998

[12] M:Hanif Chaudhry,Ph.D, *"Applied hydraulic transient*", Von Nostrand Reinhold, 1987

[13] J.A.Fox, *"Transient flow in pipes, open channels and sewers"*, Halsted Press, 1989

[14] A.S.Tijsseling, *"Poisson's coupling beat in extended water hammer theory",* Proc. of the 4th Int. Symp. on Fluid-Structure Interactions, Aeroelasticity, Flow-Induced Vibration and Noise, Dallas, USA, ASME - AD, Vol. 53-2, 529-532.

[15] A.G.T.J.Heinsbroek, A.C.H.Kruisbrink, *"Fluid-structure interaction in non-rigid pipeline system- large scale validation experiment"*, Applied Mechanics Reviews Vol.54-2, 2001: 455-582

[16] Anton Bergant, A: Tijssenling, J.P.Vítkovsky, D.I.C: Covas, A.R. Simposn, M.F.Lambert, *"Parameter affecting water-hammer wave attenuation, shape and timing",* Journal of Hydraulic Research *Vol.46, 2008: 373-381*

[17] D.S. Miller, *"Internal flow systems"*, Flowmaster

[18] Ashok Joshi, PG Jayan, *"Modeling and simulation of aircraft hydraulic system", AIAA2002-4611*

[19] Philip J.Knowles, *"Helium absorption into Nitrogen Tetroxide(NTO) and aerozine-50 (A-50)",* Journal of Spacecraft and Rockets Vol.9-9, 1972: 708-719

[20] Martin J.L.Turner, *"Rocket and Spacecraft propulsion: principles, practice and new development",* Springer-Verlag, 2008

[21] *ESPSS, Software Verification and Validation Plan,* Empresarios Agrupados

[22] *Description of Test Facility P2/M6,* Internal EADS document A5-NT_192_1016_MBBO

[23] I.E. Idelchik *"Handbook of hydraulic resistance,3rd edition*", CRC Press, 1996

[24] *Aestus Engine SN46/Pressure Regulator SN08 Analysis Report for the Combined Tests on the P2 Test Bench Steady State Investigations,* Internal EADS document A5-RE_1921_C_2013_MBBO

[25] *Test report Mechanical characterization of Propellant Feed Lines for EPS,* Internal EADS document A5-RE_19224_X_2001_ERNO

[26] *A Concise Summary of the Efffects of the Water Hammer on the EPS-Engine-Flexibles,* Internal EADS document A5-NT_1922_X_2010_ERNO

[27] *Impacts of Dissolved Gas in MMH on Engine Characteristics,* Internal EADS document A5-NT_1921_X_2110_MBBO